UNIVERSITY OF OKLAHOMA

GRADUATE COLLEGE

EXPERIMENTAL INVESTIGATION OF THE EFFECTS OF EXPOSURE TO PRESSURIZED HYDROGEN ON GENERAL USE POLYMER-BASED O-RING SEALS

A DISSERTATION

SUBMITTED TO THE GRADUATE FACULTY

in partial fulfillment of the requirements for the

Degree of

DOCTOR OF PHILOSOPHY

By ALFREDO BECERRIL CORRAL

Norman, Oklahoma

2026

Downloaded from SHAREOK. Persistent Handle URL: https://hdl.handle.net/11244/342576

EXPERIMENTAL INVESTIGATION OF THE EFFECTS OF EXPOSURE TO PRESSURIZED HYDROGEN ON GENERAL USE POLYMER-BASED O-RING SEALS

A DISSERTATION APPROVED FOR THE

SCHOOL OF AEROSPACE AND MECHANICAL ENGINEERING

BY THE COMMITTEE CONSISTING OF

Dr. Zahed Siddique, Chair

Dr. Yingtao Liu

Dr. Shreya Vemuganti

Dr. Pejman Kazempoor

Dr. Wilson Merchan-Merchan

©Copyright by ALFREDO BECERRIL CORRAL 2026

All Rights Reserved.

Acknowledgments

I would like to thank Dr. Zahed Siddique for his guidance and mentoring during my college career, for the opportunity to do research under his tutelage, and for his help in achieving my educational goals. His patience, kindness, and encouragement illuminated my academic path and allowed me to move forward. I would also like to thank Dr. Raghu Madhavan for his constant support during my research, as well as for providing his technical expertise and guidance allowing me to overcome many challenges. Likewise, I would like to extend a thank you to Dr. Wilson Merchan-Merchan for introducing me to the world of academic research and microscopy as well as for contributing his time and service to form part of my thesis committee. In the same way, I would like to thank Dr. Yingtao Liu, Dr. Pejman Kazempoor, and Dr. Shreya Vemuganti for providing their time and service to form part of my thesis committee.

I would like to thank Bethany Burklund for all her help during my research and her dedication to help students. I would like to thank Billy Mays and Greg Williams who helped me in any way they could to bring this research together. I would like to thank Nitesh Subedi for his technical expertise and help with research. Similarly, I would like to thank Ariful Islam, Monjur Bhuiyan, Brian Lopez, and Julie Ngo for their support and friendship.

I would like to thank my wife Katelyn Morgan for her unconditional support during my academic career. Her patience and optimism helped me prosper in my studies and research. I would also like to thank my father and my mother, who's support and knowledge inspired me during my graduate career.

Table of Contents

Acknowledgments iv

List of tables vii

List of figures viii

Abstract xiii

1. Introduction 1

1.1 Research motivation 1

1.2 Research Statement 10

1.3 Research objectives 22

2. Literature Review 24

2.1 Hydrogen storage and transport 24

2.2 Challenges in materials for hydrogen applications 38

2.3 Hydrogen assisted aging in polymers 48

2.4 Current approaches for characterization of hydrogen damage on polymers 49

2.5 Conclusion 54

3. Experiment design for the characterization of hydrogen damage on polymers 56

3.1 Material selection 58

3.2 Controlled exposure to high pressure hydrogen gas 64

3.3 Material characterization approach and methods 72

3.4 Conclusion 91

4. Experimental results and discussion 93

4.1 Tensile testing 93

4.2 Relaxation analysis 101

4.3 Hardness measurement 112

4.4 Material imaging 117

4.5 Conclusion 130

5. Concluding remarks and contributions 131

References 146

List of tables

Table 1: Mechanical properties of common polymers used for hydrogen [125] [126] [127]. 64
Table 2: Summary of the aging parameters employed. 71
Table 3: Summary of the calculated tensile strength and maximum deformation observed on FKM samples after exposure to hydrogen gas at different pressure levels. 95
Table 4: Summary of the calculated tensile strength and maximum deformation observed on NBR samples after exposure to hydrogen gas at different pressure levels. 97
Table 5: Summary of the calculated tensile strength and maximum deformation observed on NBR samples after exposure to hydrogen gas at different pressure levels. 99
Table 6: Comparison of the performance of materials exposed to low pressure 143
Table 7: Comparison of the performance of materials exposed to high pressure 143

List of figures

Figure 1: Utilization cycle of hydrogen as an energy carrier [8].....3
Figure 2: Pathways of hydrogen production from primary energy sources [8].....4
Figure 3: Currently used methods for hydrogen transport and short-term storage 6
Figure 4: Percentage distribution of current hydrogen uses per industry [22].....8
Figure 5: Schematic of hydrogen use as an energy carrier highlighting some of the main components vulnerable to hydrogen induced material degradation.....12
Figure 6: Schematic representation of hydrogen permeation and material degradation on pipelines with polymer liner.....16
Figure 7: Schematic representation of hydrogen permeation through polymer materials highlighting the three main phases of the process: Adsorption, diffusion, and desorption. 18
Figure 8: Schematic representation of the diffusion model for small molecules in polymer materials proposed by Pace and Datyner showing the movement of hydrogen molecules. 19
Figure 9: Currently used methods for storage and transport of hydrogen.....25
Figure 10: Volumetric density of hydrogen gas as a function of pressure for three different temperatures [8]. 26
Figure 11: Types of compressed hydrogen gas storage tanks. 28
Figure 12: Schematic representation of mechanisms for compressed hydrogen gas losses through sealing elemnts [9].....30
Figure 13: Volumetric density of hydrogen at three different temperatures showing gas and liquid phase [8]. 31
Figure 14: Isomeric concentration of molecular hydrogen as a function of absolute temperature [8]. 32
Figure 15: Schematic representation of the liquefaction cycle used in th eproductio of liquid hydrogen [70].....33
Figure 16: Illustration of the process employed in the utilization of magnesium as a solid carrier, highlighting the pressure and temperature necessary for the absorption and desorption of hydrogen gas. 36
Figure 17 : Class IV compressed hydrogen gas storage tank illustrating the use of polymer liner as well as other key components [61].....43

Figure 18: Schematic representation of polymer crosslinking showing the free binding sites before and the polymer network formed by molecular bonds after crosslinking. 44
Figure 19: Schematic representation of a polymer O-ring type seal highlighting the forces involved in creating the sealing effect used to contain pressure differential in components such as valves. 48
Figure 20: Hydrogen assisted polymer aging process highlighting the principal phases leading to changes in mechanical properties. 49
Figure 21: Schematic illustrating the experimental methodology used to compare the effects of exposure to high pressure hyfrogen gas on different polymer materials. 57
Figure 22: Diagram showing the dimensions in mm of the O-ring-214 specimens used. 59
Figure 23: Fluoroelastomers base chemical structure showing the C-F bond backbone that contributes to the material properties. 60
Figure 24: Molecular structure of EPDM showing the carbon backbone along the diene component. 61
Figure 25: Molecular structure of NBR highlighting the two copolymers used for the fabrication of the material. 62
Figure 26: Experimental system used for control exposure of material samples to high pressure hydrogen conditions. 66
Figure 27: Schematic diagram showing the main components and instrumentation used to control the hydrogen environment parameters for exposure of material samples. 68
Figure 28: Block diagram illustrating the control logic used to automate the pressure control system during exposure of material samples to high pressure hydrogen gas. 70
Figure 29: Summary of the methods used for characterizing material changes produced by hydrogen exposure on polymer sealing materials. 74
Figure 30: Experimental apparatus used to investigate the tensile behavior of the sample O-rings illustrating the main components. 77
Figure 31: Tensile strength and deformation at rupture measured for the materials investigated prior to hydrogen exposure. 79
Figure 32: Relaxation behavior of the materials investigated prior to hydrogen exposure for different deformations. 82
Figure 33: Bar chart comparison of the materials tested showing the tensile relaxation for different deformation levels before hydrogen gas exposure. 83

Figure 34: Durometer and stand used during the characterization of materials highlighting the main components of the system 84
Figure 35: Comparison of the shore A hardness measured for the materials analyzed prior to hydrogen exposure 85
Figure 36: Images obtained from cross section of the FKM O-rings analyzed prior to exposure to hydrogen gas. 87
Figure 37: Images obtained from cross section of the NBR O-rings analyzed prior to exposure to hydrogen gas. 88
Figure 38: Cross sections obtained from EPDM O-ring samples before exposure to hydrogen gas highlighting main chracteristics of the material morphology. 89
Figure 39: Schematic of the process used to analyze the quantity and distribution of the cavities present in the O-ring slices highlighting the main computational operations of the process. 90
Figure 40: Quantified voids for baseline condition of the materials investigated 91
Figure 41: Bar plot showing the tensile strength (A) and maximum deformation (B) calculated for FKM samples exposed to hydrogen gas at different pressures. 94
Figure 42: Comparison of the tensile strength and maximum deformation observed for NBR materials exposed to hydrogen gas at different pressure levels. 96
Figure 43: Comparison of the tensile strength and maximum deformation observed for EPDM materials exposed to hydrogen gas at different pressure levels. 98
Figure 44: Material comparison of the effects of hydrogen exposure on tensile strength (A) and maximum deformation (B) calculated for the materials tested. 100
Figure 45: Tensile relaxation at different deformation levels for the FKM material samples exposed to hydrogen gas at different pressure levels. 102
Figure 46: Fraction of force drop as a function of sample deformation for FKM samples exposed to hydrogen gas pressurized at different levels. 103
Figure 47: Comparison of the tension relaxation percentage for the different deformation levels as a function of the pressure the FKM-based material was exposed to. 104
Figure 48: Tensile relaxation at different deformation levels for the NBR material samples exposed to hydrogen gas at different pressure levels. 106
Figure 49: Comparison of elastic modulus 107
Figure 50: Comparison of the tension relaxation percentage for the different deformation levels as a function of the pressure the NBR-based material was exposed to. 108

Figure 51: Tensile relaxation at different deformation levels for the EPDM material samples exposed to hydrogen gas at different pressure levels. 109
Figure 52: Fraction of force drop as a function of sample deformation for EPDM samples exposed to hydrogen gas pressurized at different levels. 110
Figure 53: Comparison of the tension relaxation percentage for the different deformation levels as a function of the pressure the EPDM-based material was exposed to. 111
Figure 54: Comparison of the tension relaxation percentage for the different materials exposed to hydrogen environment at 55 bar and subjected to varying deformation levels. 112
Figure 55: Shore A hardness measured for the FKM material samples as a function of the exposure pressure 114
Figure 56: Comparison of the shore A hardness measured for the NBR samples exposed to different pressure levels..... 115
Figure 57: Measured shore A hardness for the EPDM based material samples exposed to hydrogen gas at different pressure levels. 116
Figure 58: Shore A hradness measurement normalized with respect to the baselline average for the three materials investigated as a function of the expossure pressure..... 117
Figure 59: Microscopic images obtained from FKM O-ring samples exposed to hydrogen gas at 55 bar 69 bar and 138 bar respectively highlighting the main defects observed. 119
Figure 60: Microscopic images obtained from FKM O-ring samples exposed to hydrogen gas at 345 bar 415 bar and 482 bar respectively highlighting the main defects observed..... 120
Figure 61: Results of the image analysis for quantification of voids for FKM material 121
Figure 62: Microscopic images obtained from NBR O-ring samples exposed to hydrogen gas at 55 bar 69 bar and 138 bar respectively highlighting the main defects observed. 123
Figure 63: Microscopic images obtained from NBR O-ring samples exposed to hydrogen gas at 345 bar 415 bar and 482 bar respectively highlighting the main defects observed..... 124
Figure 64: Results of the image analysis for quantification of voids for NBR material. 125
Figure 65: Microscopic images obtained from EPDM O-ring samples exposed to hydrogen gas at 55 bar 69 bar and 138 bar respectively highlighting the main defects observed. 126
Figure 66: Microscopic images obtained from NBR O-ring samples exposed to hydrogen gas at 345 bar 415 bar and 482 bar respectively highlighting the main defects observed..... 127
Figure 67: Results of the image analysis for quantification of voids for EPDM material..... 128

Figure 68: Comparison of the average cavity area (A) and cavity area fraction (B) observed on the different material samples exposed to hydrogen gas at different pressure levels. 129
Figure 69: Schematic representation of plasticizing effect on polymers produced by hydrogen gas infiltration. 132
Figure 70: Summary of changes measured for FKM material as a function of aging pressure. 138
Figure 71: Summary of changes measured for NBR material as a function of aging pressure. 139
Figure 72: Summary of changes measured for EPDM material as a function of aging pressure. 141

Abstract

The utilization of hydrogen as an energy carrier has become particularly attractive in the last decades. Hydrogen use as an energy carrier along with the use of renewable energy sources presents the possibility of developing energy infrastructure with minimum environmental impact by decreasing greenhouse gas emissions. Nevertheless, material interactions between hydrogen gas and polymer materials lead to changes in mechanical properties that can compromise the performance of components over time, leading to gas leakages and increasing concerns regarding the economic viability of hydrogen use as well as concerns about the inherent risks associated with technology. For these reasons, understanding material compatibility with hydrogen gas is exceptionally important since numerous components and systems across all aspects of hydrogen infrastructure are vulnerable to hydrogen assisted material degradation.

This study demonstrates that hydrogen-induced degradation in FKM NBR and EPDM under prolonged high-pressure exposure is governed not by monotonic strength loss, but by pressure-dependent competition between swelling-induced internal stress and hydrogen-assisted viscoelastic relaxation, which manifests most clearly under displacement-controlled tensile loading. An experimental system was designed and commissioned to safely conduct these experiments. The experimental system includes sensors for automated safety shutoff, remote controls, and data acquisition system. Specimens were exposed to gaseous hydrogen at pressures ranging from 55 to 482 bar for 200 hours at room temperature, followed by uniaxial tensile testing and hardness measurement. Raw force–time and deformation–time responses were analyzed alongside normalized force and deformation metrics to isolate pressure-dependent effects while accounting for specimen variability. Tensile strength was calculated, and results are reported as mean ± standard deviation. Similarly, material hardness was measured and reported as mean ± standard deviation. Additionally, material imaging and computational methods were used to characterize changes in morphology to the material as a consequence of exposure to pressurized hydrogen gas. These results showed that exposure of the selected polymer

formulations to a hydrogen environment pressurized at varying levels undergo structural changes at a molecular level through the effects of hydrogen dissolution and the subsequent depressurization. Two main effects were observed on the material samples analyzed: plasticization by gas infiltration and chemical aging through cross-link bond scission.

The results reveal that hydrogen exposure does not produce a monotonic degradation in tensile strength. Instead, all materials exhibit pressure-dependent and non-monotonic responses arising from competing mechanisms including swelling-induced internal stress, transient plasticization, and viscoelastic relaxation under displacement-controlled loading. NBR and EPDM retain tensile integrity across the investigated pressure range, though with altered stiffness evolution and increased variability at higher pressures, while FKM exhibits the highest susceptibility due to its highly permeable network. These findings highlight the importance of evaluating full tensile response histories, rather than peak strength alone, when assessing elastomer suitability for high-pressure hydrogen sealing applications.

CHAPTER 1: INTRODUCTION

1.1 Research motivation

One of the main technological challenges of this century is to satisfy the rising demands for energy that accompany population growth and urbanization [1]. Furthermore, climate change and the increase of people living in marginalized or poverty conditions have highlighted the need to diminish our reliance on energy production methods based on hydrocarbon combustion, particularly in developing countries [2]. Fuel combustion, whether used in power plants or automobiles, releases gases damaging to the environment such as carbon monoxide and nitrogen oxides, leading to increased greenhouse effects as well as acidification of freshwater bodies [3]. The continuous release of these pollutants can affect climate patterns around the world, leading to increased economic pressure on governments and citizens due to extreme weather events becoming more frequent. Hence, different ways to address fossil fuel dependence have gained traction in recent years as the unsustainability of petroleum and natural gas as the sole energy sources become more apparent. Nevertheless, currently available technologies such as photovoltaic panels and wind turbines are insufficient to satisfy increased energy demands. Examples of these are technological limitations such as low efficiency, dependence on weather, and the requirement of large amounts of land along with high installation costs that limit accessibility to solar energy [4]. Similarly, while wind turbines present a relatively low environmental impact, high maintenance costs due to environmental factors such as lighting strikes and collisions with birds along with the deforestation and soil erosion associated with wind farms limits the adoption of the technology [5]. Furthermore, the intermittent nature of these renewable energy sources means that energy storage devices must be included in the system to ensure energy is available when it is needed. Currently, rechargeable batteries are used to store energy produced by solar and wind farms. However, the production and disposal of these batteries still present environmental challenges derived from mining primary materials as well as the production of toxic byproducts and the requirement of specialized disposal facilities. In this way, by recognizing the limitations of

the different renewable energy sources available, we can appreciate the need of energy production systems that utilize multiple technologies rather than a single source.

In this regard, the utilization of hydrogen as an energy carrier has become particularly attractive during the last decades. The unique properties of hydrogen allow it to be a very attractive energy carrier due to its availability in the form of water, as well as its potential for low environmental impact [6]. Hydrogen possesses the lightest as well as smallest atom and is one of the most abundant elements in the planet as part of water, hydrocarbons, organisms, and many other substances. As pure hydrogen combines with other elements, such as oxygen, energy is released as part of the chemical reaction. Figure 1 shows a possible utilization cycle for hydrogen highlighting the potential for energy production with low environmental impact [7] [8]. Renewable sources of energy such as solar, eolic, or geothermal can be used to produce hydrogen gas, which can then be transported and stored until needed. Furthermore, the high availability of hydrogen and its capacity for low environmental impact stem from the idea that it can be produced from renewable resources and that the waste emission is a harmless byproduct, making hydrogen particularly attractive as a possible replacement for fossil fuels [9]. In this way, the development of hydrogen infrastructure represents a feasible solution for the current environmental challenges [28]. Nevertheless, most of the technology currently available for the production and handling of hydrogen gas cannot compete with fossil fuels in terms of cost, safety, and reliability [2].

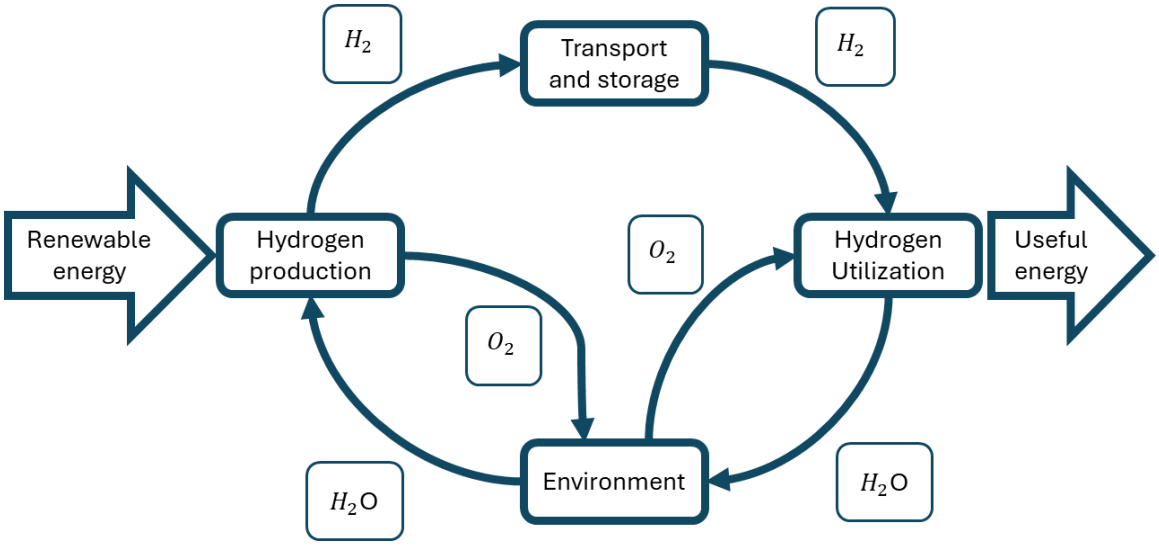


Figure 1: Utilization cycle of hydrogen as an energy carrier [8].

In this way, hydrogen infrastructure can be understood in three distinct sectors: hydrogen production and supply; hydrogen transport, storage, and distribution; hydrogen use and applications [10]. The first sector, production, refers to the technological and economic systems used to produce hydrogen as well as the infrastructure needed to supply it as primary material. Currently, traditional sectors such as refineries occupy this sector by producing hydrogen gas through steam methane reforming as well [10]. Nevertheless, social and political movements have pushed for the development of hydrogen production through renewable energies. Technologies related to this 'green hydrogen' aim to reduce environmental impacts and cut dependency on fossil fuels. However, this aspect of hydrogen usage has been underdeveloped due to the current availability and reliability of fossil fuels and traditional energy production systems [11].

The technology currently available for hydrogen production can be summarized in two main methods, as shown in Figure 2 [8]. Firstly, hydrocarbons and organic substances can be manipulated to extract hydrogen through fuel processing or reforming of the substances. This method, denominated steam reforming, is more well-developed and understood on an industrial scale [12]. However, this method still depends on the availability of fossil fuels and produces unwanted emissions. Similarly, hydrogen gas can be obtained from coal through a

gasification process and reforming. However, this method presents similar drawbacks due to the use of fossil fuels and high amounts of energy [12]. A more environmentally friendly option is production from the fermentation and pyrolysis of organic matter such as farming waste and wastewater [13]. In contrast, another method to produce hydrogen gas is the separation of water into oxygen and hydrogen through electrolysis [14]. This method offers a low environmental impact and is of particular interest as it presents a sustainable or renewable way to satisfy energy needs. Recent advances have resulted in the development of an electrolysis system that is able to operate with seawater without suffering significant degradation [15]. Nevertheless, technological development is necessary in order to allow electrolysis to be a cost-effective and reliable production method.

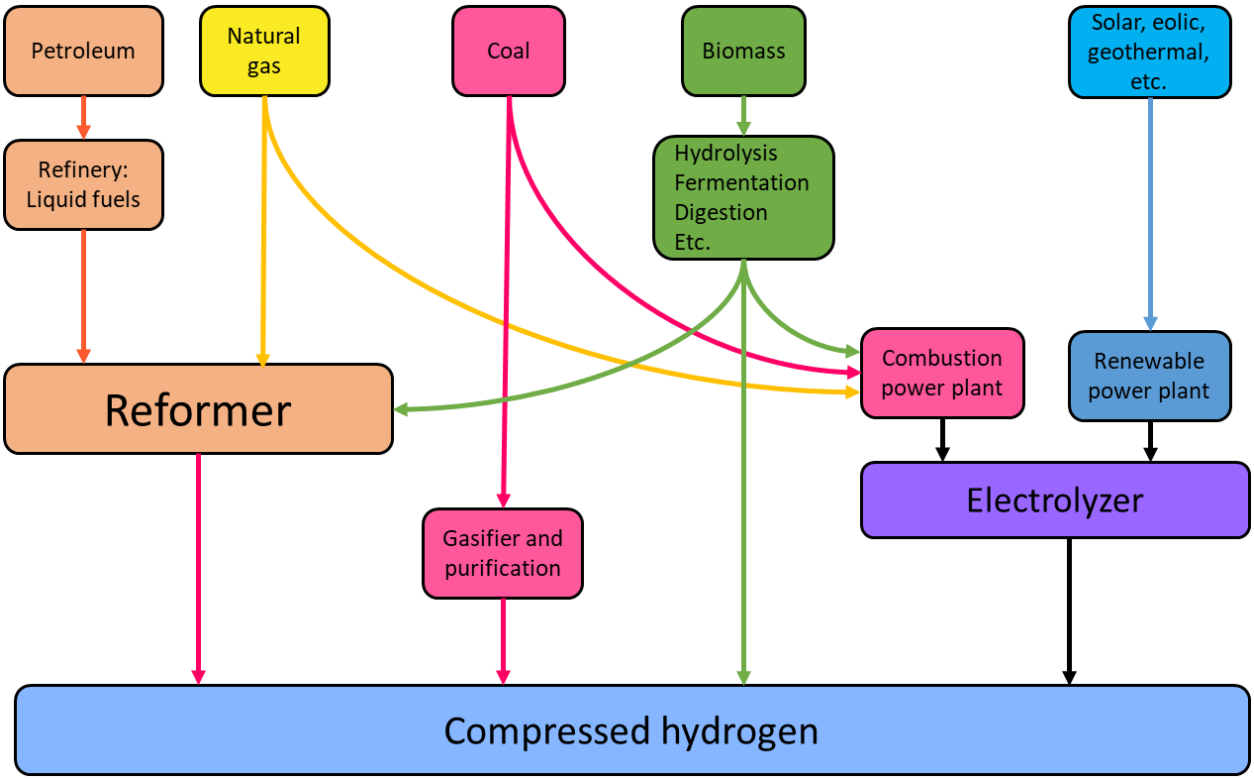


Figure 2: Pathways of hydrogen production from primary energy sources [8].

Given the different available hydrogen production methods, it is necessary to evaluate them from different viewpoints such as environmental impacts, health implications, as well as national and international economic impact. Currently. there are limited approaches that

would allow us to take into consideration all the factors related to developing hydrogen infrastructure as well as which specific technologies to invest in as the field expands. Still, several institutions such as MIT, SANDIA, ETH Zurich, among others have developed tools such as life cycle assessment methods to better understand the production, use, and waste generated by hydrogen as an energy carrier [8]. Similarly, the United States Government has launched the Hydrogen Fuel Initiative since 2003 to enhance national energy security and decrease environmental footprint through the development of technologies that will enable the use of hydrogen for energy purposes [16].

Similarly, there have been important advances in the way hydrogen is transported and stored. These hydrogen transport and storage technologies can be summarized as gaseous, liquid and solid. In the case of gaseous storage, high pressures are used to achieve energy densities that can compete with fossil fuels. The elevated storage pressures then necessitate specific safety requirements and regulations due to the specific characteristics of hydrogen gas such as its propensity to leak and its high reactivity in the presence of oxygen [17]. In the case of liquid storage, cryogenic temperatures are used to reduce the movement of hydrogen molecules, increasing density and facilitating transport. In a similar way, due to the low temperatures required for the liquefaction of hydrogen, specific technological challenges arise. These challenges include the development of insulation systems to prevent losses due to boil-off caused by environmental heat as well as the development of materials and seals used to safely transfer the liquid hydrogen [17]. Finally, storage of hydrogen in solid forms involves the use of metals and other compounds in the formation of hydrides, or hydrogen containing compounds, that can be processed to extract the hydrogen and use it as needed [18]. These solid carrier materials offer important advantages in safety and ease of use when compared to gaseous and liquid storage. However, further advances are required to achieve competitive energy densities as well as to enable the reutilization of the carrier material. Figure 3 presents a summary of the available hydrogen storage and transport technologies [19].

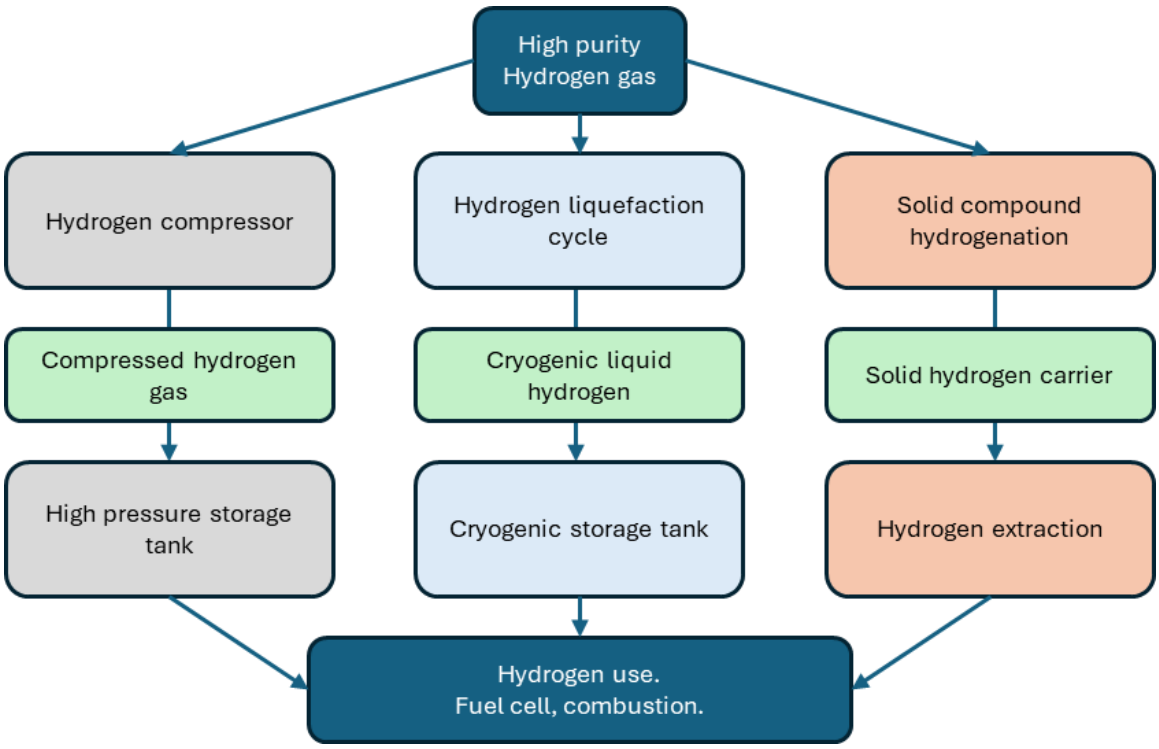


Figure 3: Currently used methods for hydrogen transport and short-term storage [17].

While there are different technologies for transporting hydrogen gas from source to consumer, several limitations still exist, impacting reliability and safety. It is important to understand how to develop feasible solutions for the adoption of hydrogen as an alternative energy carrier in everyday applications. Some of these limitations arise due to the material interactions between hydrogen gas and the components used to handle it. In the case of high-pressure tanks hydrogen molecules can interact with metallic components leading to what is denominated hydrogen embrittlement and a change in physical and mechanical properties [18]. The changes in material properties along with the operational cycle of charging and discharging then lead to safety concerns regarding the lifecycle of metallic components used in high pressure storage tanks. Similarly, polymer components exposed to hydrogen gas can be affected by hydrogen permeation into the polymer matrix. This could lead to the formation of blisters, the displacement of plasticizers and fillers, and compromise the performance of polymer liners and sealing components [18]. Furthermore,

these material interactions also affect other components, creating a limitation on the lifetime and performance of the auxiliary equipment such as valves, connections, and nozzles used to transfer the gas in and out of the tanks. Similarly, in the case of cryogenic liquid hydrogen storage, complex systems are required to maintain the low temperatures required for liquid hydrogen [20]. The complexity of these systems means that they contain various seals and valves used to manage flow and pressure. These components must then be fabricated using materials that are able to withstand cold operating conditions as well as the effects of interactions with hydrogen. In contrast, the material used for solid hydrogen storage must be able to withstand high temperatures along with thermal cycling [21]. In both systems, issues such as hydrogen embrittlement and permeation into polymer materials exist, along with the addition of extreme operating conditions. In this way, we can appreciate that *material compatibility is an essential aspect for developing systems for hydrogen transport and storage* regardless of the specific mechanism used.

Lastly, the third infrastructure sector for hydrogen as an energy carrier is its use and applications. In this regard, some of the current common applications of hydrogen gas include refinery and chemical production processes as shown in figure 4 [22]. In this case, others refer to use in food production, metallurgical processes, electronics and pharmaceutical manufacturing industries, among others. Nevertheless, while the use of hydrogen in the energy sector is currently negligible, many countries such as Canada, Sweden, and Oman have dedicated considerable amounts of resources to the development of environmentally friendly hydrogen energy infrastructure [23].

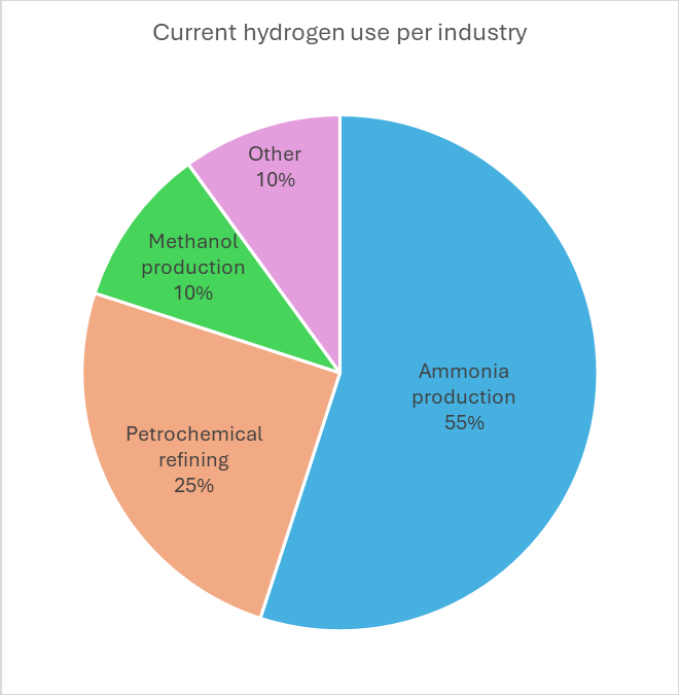


Figure 4: Percentage distribution of current hydrogen uses per industry [22].

Nevertheless, there have been developments in technologies related to energy applications. Some of the currently available systems designed specifically for hydrogen as an energy carrier are fuel cells and hydrogen combustion. Fuel cells are systems that utilize electrochemical reactions to generate electricity. In these systems, the energy released through the chemical reaction between hydrogen and oxygen gases is converted to electricity by using electrolyte materials and producing water and heat as byproducts [17]. One of the main advantages of fuel cells is the low environmental impact of the byproducts produced, as well as the potential to achieve highly efficient systems [24]. Furthermore, some electrolyte materials can also be used for separating water into hydrogen and oxygen through electrolysis [25]. In this way, the reversible nature of the chemical reaction between oxygen and hydrogen and the use of different electrolyte materials allows for the use of other renewable technologies such as photovoltaic cells to minimize environmental impacts from energy storage and use without the need of additional hydrogen production systems. Nevertheless, further development in hydrogen fuel systems to overcome current limitations such as high initial cost, degradation caused by heat generation, and chemical poisoning of

the electrolyte material catalyst used [26]. Similarly, hydrogen combustion has been researched as an alternative to fossil fuels due to the low environmental impact of the byproducts produced [27]. Nevertheless, material interactions between alloys and hydrogen gas present a limiting factor in the lifetime of the engine components. Furthermore, in both cases material degradation due to hydrogen increases the safety concerns of the systems and restricts their adoption as consumer technologies.

While hydrogen shows a promising alternative to fossil fuels, there are still many challenges to overcome to deploy hydrogen infrastructure for public use. Some of the main challenges for the deployment of this technology are derived from the unique physical and thermodynamic properties of the H_2 molecule. These properties include the composition, density, specific volume, specific heat, as well as compatibility with materials used in the processing equipment such as pipes, tanks, compressors, and valves [8] [9]. The current available technology for the use of hydrogen as an energy carrier cannot provide a solution that competes with fossil fuels in terms of reliability, safety, storage efficiency, and cost. In this way, significant technological and financial challenges still stand in the realization of hydrogen as a viable energy carrier. One of the main factors limiting current technology is the interaction between hydrogen gas molecules and materials used in the equipment for handling it [7] [8]. For example, changes to mechanical properties of metal alloys caused by hydrogen gas diffusion into the metallic matrix limit the types of materials that would perform adequately in the conditions required for transport and storage. Different material interactions unique to hydrogen molecules cause damage and degradation of properties in the materials components used. An example of this is the denominated hydrogen embrittlement that occurs when metallic alloys interact with hydrogen gas at high pressures [28]. Similarly, hydrogen gas exposure can affect polymer materials in the form of surface blistering and hydrogen induced crack propagation [29]. These types of material interactions are not sufficiently understood due to the specific mechanisms that govern them, impacting the economic viability of hydrogen as an energy carrier due to a relatively low service life of components and great production costs for hydrogen related equipment compared to the

currently available hydrocarbon infrastructure. However, great advances in understanding hydrogen gas interactions have been made to develop better understanding of material compatibility.

1.2 Research Statement

Hydrogen use as an energy carrier, along with the use of renewable energy sources. presents the possibility of developing energy infrastructure with minimum environmental impact by decreasing greenhouse gas emissions. This could be achieved by developing hybrid energy infrastructure that integrates renewable energy sources such as solar and wind to supplement more traditionally established technologies such as geothermal. The advantages of these renewable energy systems would then be further enhanced by using hydrogen as an energy carrier, limiting the environmental damage caused by mining of energetic materials such as lithium for the manufacture of batteries. Hence, the incorporation of hydrogen related technologies as part of energy infrastructure could facilitate the growth required to satisfy the rising energy demands while minimizing environmental impacts [30]. In this way, the development of hydrogen energy systems is recognized as an essential aspect of future clean energy. Nevertheless, material degradation caused by hydrogen gas on metallic alloys and polymers presents a limiting factor for adoption of hydrogen energy technologies due to safety concerns, elevated costs, and limited lifetime for essential components. The different mechanisms and phenomena related to hydrogen assisted material degradation such as hydrogen embrittlement in metallic alloys and hydrogen assisted crack propagation in polymers are not well understood [31]. Hence, developing a better understanding of how hydrogen assisted material degradation occurs would help bridge the gap towards accessible hydrogen technologies.

Additionally, understanding material compatibility with hydrogen gas is exceptionally important since numerous components and systems across all aspects of hydrogen infrastructure are vulnerable to hydrogen assisted material degradation. As previously mentioned, hydrogen embrittlement occurs when metallic alloys are exposed to pressurized hydrogen gas [32]. This effect is particularly worrying in components such as pipes used to

transport the gas from production equipment, such as electrolyzes or hydrocarbon reformers. In this case, material incompatibility would lead to changes to the mechanical properties of the materials, increasing the likelihood of hydrogen gas leaks creating safety concerns [33]. Furthermore, other interaction mechanisms such hydrogen induced crack propagation and reduced wear resistance can enhance the negative effects on other metallic components such as valves, reducing the useful life of components and increasing costs [34]. In a similar way, adverse effects are observed due to the interaction of hydrogen gas with polymer components such as the liners used in pipes and storage tanks. In the case of polymers hydrogen permeation leads to blistering and crack propagation, which can allow the hydrogen gas to escape [35]. These effects along with other factors such as pressure and temperature cycling create safety concerns as the system loses integrity and limit accessibility to hydrogen-related technologies. The effects of these material interactions are compounded when considering the enormous number of components involved in controlling and directing hydrogen gas from production to end use. Figure 5 presents a schematic showing examples of critical components vulnerable to hydrogen induced material degradation in the context of energy applications.

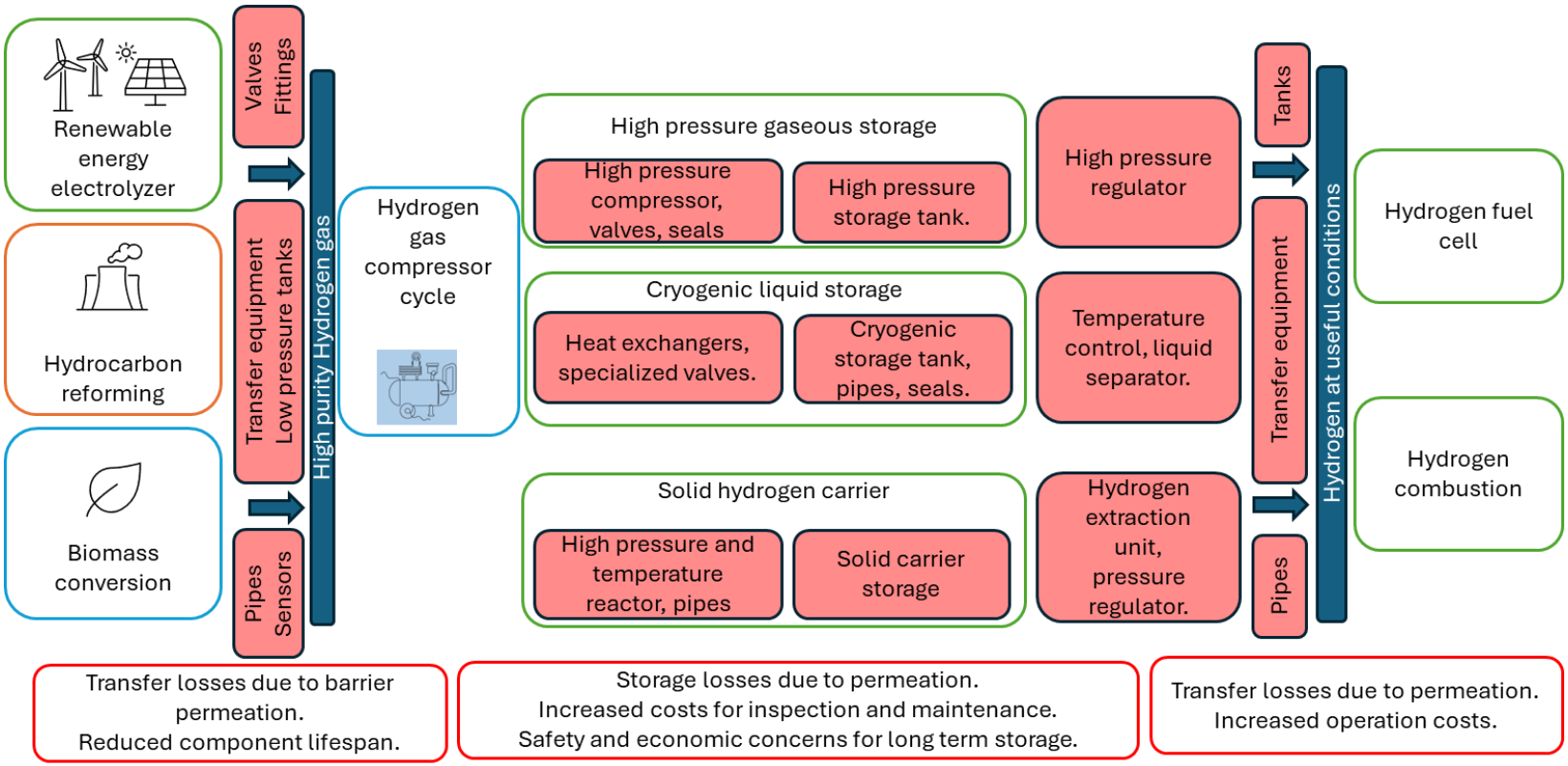


Figure 5: Schematic of hydrogen use as an energy carrier highlighting some of the main components vulnerable to hydrogen induced material degradation [36].

From this schematic we can appreciate the frequency in which material interactions associated with the use of hydrogen as an energy carrier could cause issues such as safety hazards, down time on equipment, and hydrogen losses. Material interactions with hydrogen can create vulnerabilities on critical components due to the range of conditions that hydrogen is present along with the variety of systems and component needed at each step of the process. For example, hydrogen embrittlement on pipes, fittings, and connections used to transfer hydrogen gas between devices can cause changes in the properties of the materials used. These physical and chemical changes along with the permeation of hydrogen and dislocation of the metallic matrix can then cause material defects to propagate, creating gas leaks and enhancing the risks associated with hydrogen [36]. Similarly, in the case of polymer components such as pipe liners and valve seals, hydrogen adsorption can lead to changes in mechanical properties as well as blistering and fracturing [37]. While these problems are well documented, there is no consensus on how these phenomena could be controlled due to the complexity of the processes involved and the microscopic scale at which they occur [38]. Hence, understanding how hydrogen gas interacts with materials is an important step in the realization of accessible hydrogen use as an energy carrier. Through research on the evolution of hydrogen induced degradation of commercially available materials and developing further insight into the mechanisms related, it would be possible to identify beneficial characteristics of materials destined for operation with hydrogen gas.

In this way, material compatibility with hydrogen gas remains one of the main challenges in the realization of hydrogen energy infrastructure. As previously explained, the changes in mechanical properties on metallic and polymer materials increase the likelihood of the formation and propagation of cracks [32]. The resulting material degradation then could result in pathways for hydrogen gas to escape into the atmosphere, creating the possibility of economic losses and safety risks [5]. These dangers arise due to the low ignition energy, high reactivity, high diffusivity, and colorless and odorless flames, which increase the risk of life and material loss [39]. This aspect of hydrogen use has been highlighted by several studies aimed at identifying causes of incidents related to hydrogen infrastructure. For

example, Alfasfos et al concluded that a significant proportion of hydrogen related incidents occurred during hydrogen storage due to a combination of material incompatibility and equipment failure [40]. Hence, ensuring material compatibility through the use of well understood and characterized materials becomes an essential step in the realization of hydrogen infrastructure.

Within this context, understanding the degradation mechanisms related to hydrogen and other material interactions becomes critical to overcome persisting challenges in commercial hydrogen use. Furthermore, the complexity of these degradation mechanisms and the influence of a multitude of factors such as fabrication defects, chemical structure, stress conditions highlight the need to develop material testing and characterization with specific applications in mind. One of the most notable components that is affected by hydrogen are pipe liners. These are polymer membranes used to cover the inside of pipes used to transport hydrogen between devices, separating the hydrogen gas from metallic components. In this application, polymer materials are used to prevent hydrogen embrittlement of the pipe, extending the service life of the ducts and preventing material degradation and the formation of cracks [41]. Nevertheless, these polymer liners are still vulnerable to hydrogen assisted material degradation meaning that they could develop cracks that allow hydrogen gas to interact with the metallic pipe as shown in figure 6. In this case, hydrogen molecules are adsorbed by the surface of the polymer liner. Following this, the hydrogen molecules diffuse through the polymer matrix, accumulating at gaps and imperfection, eventually reaching the interface between the polymer and the metal. The hydrogen then is desorbed from the polymer and adsorbed into the metal lattice, causing material degradation through hydrogen assisted phenomena such as embrittlement and crack propagation [37].While the negative effects of hydrogen have been documented through experimental analysis and numerical simulations, the evolution of material changes has not been thoroughly understood, specifically for long term exposure. Furthermore, factors other than hydrogen interactions such as pressure cycling and temperature changes enhance the possibility of material degradation. Hence, pipelines used for hydrogen transport must be inspected periodically to ensure the materials remain in adequate

condition, increasing maintenance costs. In this regard, further research on the interaction mechanisms between hydrogen gas and polymer materials is necessary to create models that would allow us to predict the evolution of hydrogen induced changes on materials.

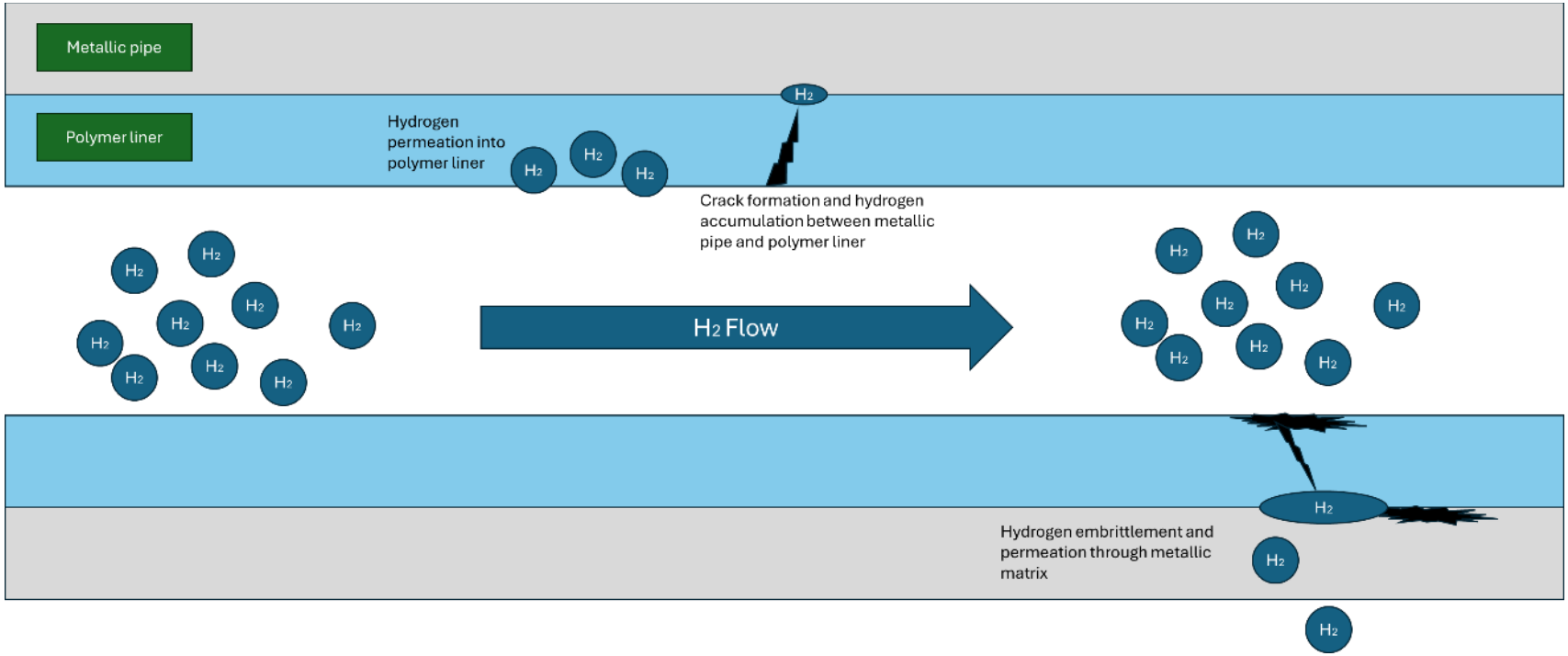


Figure 6: Schematic representation of hydrogen permeation and material degradation on pipelines with polymer liner [9].

Another challenge to overcome regarding hydrogen transport and storage is the escape of the gas through permeation of the container materials and barriers. As previously explained, the permeation of hydrogen gas into metals and polymers is one of the mechanisms related to hydrogen material assisted degradation. However, the ability of hydrogen molecules to diffuse through these materials also means that some of the gas can escape through devices such as storage tanks and transport pipelines [42]. These hydrogen gas leaks could then lead to economic losses during the storage and transport stages along with safety risks. While promising materials such as high-density polyethylene, ethylene propylene diene monomer, and polyamide 11 have been identified as candidates due to their chemical and mechanical properties, hydrogen permeation remains a challenge to overcome in material design [42]. The process of hydrogen permeation into polymer materials can generally be divided into three distinct phases described by solution and diffusion mechanisms as shown in figure 7. In the first phase, hydrogen molecules are adsorbed into the surface of the polymer material following the pressure gradient. Following this, the hydrogen diffuses through the polymer matrix, accumulating voids and imperfections. Lastly, hydrogen molecules are desorbed through the surface of the polymer following the pressure gradient [43]. In this way, due to the potential for polymer degradation due to rapid gas decompression along with the potential for gas leakage, hydrogen permeability becomes one of the main concerns for storage and transport infrastructure. Hence, hydrogen infiltration is highlighted as an important aspect for material design in hydrogen applications.

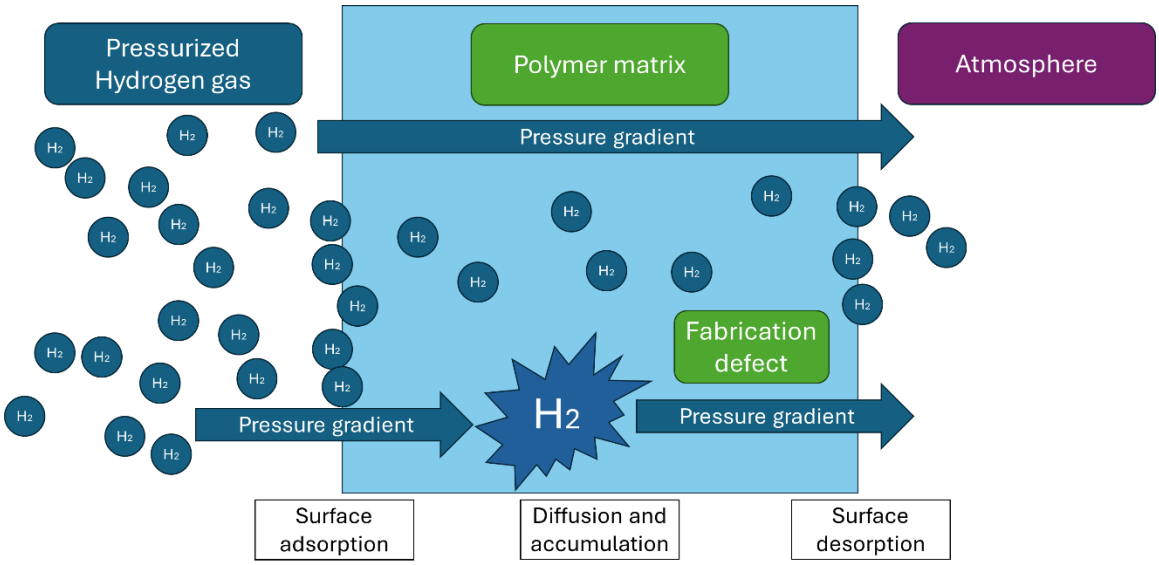


Figure 7: Schematic representation of hydrogen permeation through polymer materials highlighting the main phases of the process: Adsorption, diffusion, and desorption [7].

One of the main aspects that influences hydrogen permeation through polymers are the molecular structure and free volume, crosslink density, and the presence of voids and cavities. In general, polymer materials are composed of repeated units called monomers forming long chains with carbon atoms as a central backbone. Due to their structure, polymers materials can be designed with adequate properties for specific applications. Furthermore, molecular forces allow polymer chains to bind to each other forming complex networks through a process denominated crosslinking [44]. As explained by Barrer, when hydrogen molecules interact with the polymer during the diffusion process, the movement of the molecule and the subsequent transfer of energy results in the dislocation of the polymer chains, thus allowing hydrogen molecules to infiltrate the material [45]. Furthermore, Pace and Datyner proposed that the diffusion of hydrogen molecules could occur along the axis of the polymer chain as well as perpendicularly to it as illustrated in figure 8 [46]. Firstly, the hydrogen molecules are adsorbed on the surface of the polymer. Following this, the molecules can diffuse through space along the polymer chains, accumulating in gaps and causing dislocation of the polymer molecules. Furthermore, the release of energy from the molecules can result in result in movement along a different axis

[46]. In this diffusion model the space between the polymer molecules, denominated free volume, plays a critical role in hydrogen transport. Similarly, the crosslinking density of the polymer shapes the diffusion since it influences the degree to which the polymer chains can move relative to each other.

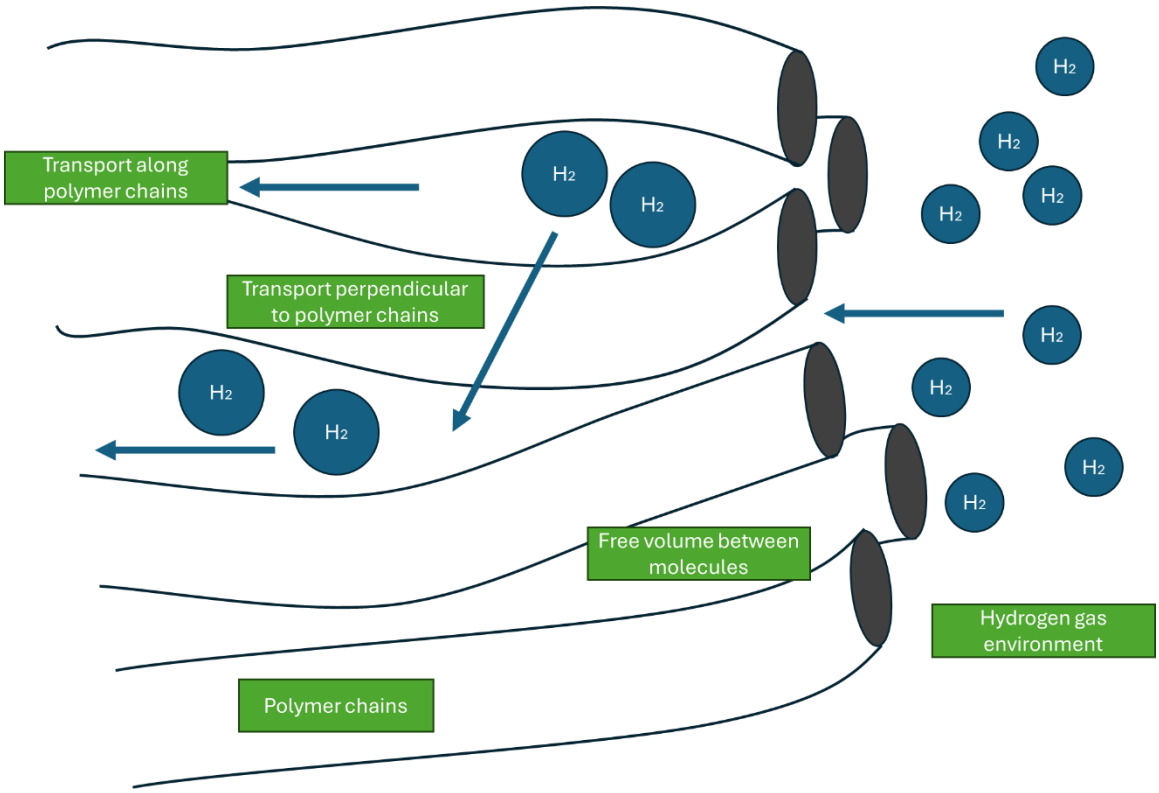


Figure 8: Schematic representation of the diffusion model for small molecules in polymer materials proposed by Pace and Datyner showing the movement of hydrogen [46].

While the molecular structure of polymers is one of the main factors that influence hydrogen permeability, there are other important factors to consider such as the presence of fillers and operating conditions such as pressure and temperature. In the context of polymers used for industrial applications, fillers refer to particle additives included in the manufacturing process of polymer components used to enhance properties such as tensile strength, wear rate, and coefficient of friction among others [47]. Multiple studies have been conducted to investigate the influence of polymer filler materials on hydrogen interactions. For example, Jung et al. concluded that the presence of fillers such as carbon black increase hydrogen solubility while decreasing the average diffusion coefficient of the polymer composite [48]. This effect can be attributed to the interstitial

properties along the boundary between the fillers and polymers as well as to the physical characteristics of the fillers themselves [49]. Similarly, the decrease in the average diffusion coefficient due to the inclusion of particles within the polymer matrix can be attributed to the reduction in free volume and the increase in crookedness of the path hydrogen molecules would follow [50]. It is important to note that the relationship between hydrogen solubility and diffusion depends on multiple factors such as type of filler and size of the particles. However, experimental studies show that the measured permeability of polymer materials tends to decrease as the filler concentration increases [48]. Additionally, the size of the filler particles included also impacts the solubility of hydrogen into polymer materials. In a study regarding the effects of carbon black particles, Yamabe et al. described a positive correlation between specific surface area of the filler particles and hydrogen solubility [51]. In this case, the Carbon Black (CB) particles are also able to adsorb hydrogen molecules. Hence, a higher specific surface area for the filler particles allows hydrogen molecules to infiltrate the polymer-CB composite more efficiently [50]. In a way similar to the examples presented, other studies have been conducted to evaluate commonly available polymers and filler material combinations for hydrogen use. Nevertheless, the number of polymer and filler materials as well as the development of new fillers means that further research is needed in order to characterize the synergistic and antagonistic effects that would improve current materials and technology.

Along with the material characteristics presented, operating parameters such as temperature and pressure heavily influence the permeation of hydrogen gas through metals and polymers. Example of these are the effects observed when polymers are exposed to high pressures. Under high pressure conditions the material is deformed and experiences negative strain effectively being compressed [52]. In a molecular scale, this means that the carbon chains that form the polymer matrix can be dislocated and affecting the free volume fraction of the material, thus changing the permeation behavior of hydrogen molecules. In this regard, multiple studies have characterized two different pressure-dependent diffusion processes in rubber. At pressures lower than 10 MPa, the relative size of the hydrogen gas molecule and the space between polymer chains allows Knudsen diffusion to dominate the transport mechanics [53]. In this process, the hydrogen molecules are transported along the pressure gradient colliding with the polymer chains but rarely interact with each other [54]. In contrast, at pressures higher than 10 MPa the reduced free volume means that bulk diffusion dictates the permeation behavior through the polymer matrix [53]. In this case, the hydrogen molecules cannot travel through the polymer free volume as easily. Instead, the hydrogen molecules

spontaneously move, occupying small gaps through the polymer structure through a concentration gradient [55]. Similarly, temperature has significant effect on the diffusivity and permeation of hydrogen through polymer materials. In this case, elevated temperature is translated to elevated kinetic energy per molecule. The increased molecular movement caused by elevated temperatures enhances hydrogen permeability through increased solubility and diffusivity [43]. While the basic principle behind the influence of operating parameters on material interactions with hydrogen gas is well understood. The wide variety of fillers and matrix material combinations creates unique scenarios that influence the permeation process due to synergistic interactions that improve material performance as well as antagonistic mechanisms that cause the opposite effect. Hence, further research on the behavior of commonly used, well characterized materials could provide further insight into material properties that result in beneficial for hydrogen transport and storage devices.

From analyzing the current challenges in the realization of hydrogen energy infrastructure we can appreciate the importance that material compatibility holds. While hydrogen production and use technologies such as electrolyzer units and fuel cells have made significant advances to increase efficiency and longevity, several challenges remain in the development of technology that can connect these two sectors [40]. Currently, this bottleneck is caused by significant knowledge gaps in the way materials interact with hydrogen. These interactions cause negative effects such as hydrogen assisted material degradation and hydrogen permeation creating safety concerns and limiting the accessibility and reliability of hydrogen related technologies [32]. In this regard, different studies have been conducted to characterize material response to hydrogen exposure. Some of these studies have been aimed at measuring the change in mechanical properties of the material investigated as well as to understand the mechanisms involved in hydrogen assisted material degradation. Examples of these are the experiments carried out by Theiler et al. which demonstrated blistering of polymer materials along with a decrease on mechanical properties [56]. Similarly, Jung et al. investigating the hydrogen permeation through polymer materials and concluding that filler materials can result in reduced permeation [48]. Nevertheless, an increase in hydrogen solubility due to adsorption on filler particles and pressure dependency on the permeation behavior of hydrogen highlights the need of further research to develop materials adequate for hydrogen service [49].

Additionally, affordability and availability are crucial aspects of hydrogen use system and materials. While developing materials that present optimum characteristics for long term performance in hydrogen service is important, the integration of these materials should not limit the capacity of hydrogen technologies to compete with current energy systems. In this regard, multiple institutions have set development goals highlighting the need for low-cost and reliable materials. Specifically, the U.S. department of energy outlines the need to improve the long-term performance of hydrogen related equipment such as storage tanks and seals by developing novel materials [57]. In this regard, investigating the hydrogen compatibility of available polymers resulted in beneficial results, identifying promising materials. Examples of prospective materials for hydrogen use include Ethylene Propylene Diene Monomer (EPDM) and Nitrile Butadiene Rubber (NBR) [58], [59]. These commonly used and commercially available materials result are of particular interest due to their mechanical and chemical properties as well as their ability to be combined with filler materials to enhance their properties. Nevertheless, as previously explained further research is needed to understand how the properties of these polymer materials change over time as a result of hydrogen exposure. Furthermore, the endless material combinations and the development of novel filler materials and fabrications processes increase the need to understand the underlying mechanisms behind hydrogen induced material degradation as it applies to polymers to develop cost-effective materials.

1.3 Research objectives

Given the need to appropriately characterize hydrogen induced damage, this research focuses on investigating the changes caused to commercial polymer sealing materials by exposure to hydrogen gas. This study is in line with the development goals established by the US DOE as well as other organizations for storage and transport of hydrogen [60]. The wide variety of available materials used for the fabrication of seals as well as the specific challenges related to hydrogen service creates the need to establish common processes to characterize hydrogen assisted material degradation. Moreover, the need for economically feasible solutions to allow hydrogen use as an alternative energy carrier able to compete with established technologies means that currently available materials could be attractive candidates for the development of hydrogen specific materials. In this regard, this research aims to characterize the changes in mechanical properties caused as a result of exposure to pressurized hydrogen gas on commercial polymers. Additionally, the characterization

of the changes in material morphology are investigated in order to supplement the findings. With this consideration, the main objectives of this research are summarized as follows:

1. Investigate the effects of hydrogen exposure on mechanical properties commercial polymer compounds commonly used for sealing components
2. Image and characterize the changes to material morphology caused by hydrogen exposure to commercial polymer compounds.
3. Investigate the pressure dependent behavior of hydrogen assisted material degradation for polymer exposed to different pressure levels
4. Investigate the differences in the presentation of hydrogen induced material degradation on different materials exposed to identical conditions

CHAPTER 2: LITERATURE REVIEW

As briefly shown in Chapter 1, hydrogen energy infrastructure encompasses a variety of systems focused on production, transport, storage, and use applications. While these systems have diverse roles in the way they interact with hydrogen, they can all be vulnerable to the adverse effects of interactions with hydrogen gas. In this regard hydrogen transport and storage is one of the aspects of hydrogen infrastructure currently limited by material development and a poor understanding of the mechanisms involved. The following section presents a summary of the different technologies related to hydrogen transport and short-term storage. Additionally, the material interactions with hydrogen and the main challenges are discussed. Lastly, the approaches currently employed by scientists to determine polymer material comparability with hydrogen gas are described.

2.1 Hydrogen storage and transport

Once hydrogen gas is produced, it becomes necessary to transport and store it for use as necessary. Furthermore, for hydrogen as an energy carrier to be successful, it must be able to compete with the currently dominating fossil fuels in terms of cost, storage efficiency, reliability, and safety. One of the most evident challenges with the use of hydrogen as an energy carrier is its energy density. In atmospheric pressure and ambient temperature, hydrogen gas has a density of 0.08238 Kg/m^3 and an energy potential of approximately 120 MJ/kg, depending on the system used [8]. These properties imply that, when compared to available fuels such as gasoline with a density of $743kg/m^3$ and an energy density of 44 MJ/kg, hydrogen has a much higher energy content per weight but much lower when compared in terms of volume [16]. In this way, some of the main challenges in the transport and storage of hydrogen arise from the need to achieve and maintain high storage efficiency. This in turn, implies need for the development of application specific handling equipment such as compressors, valves, seals, pipes, and tanks that account for the unique attributes of hydrogen as well as the need for a cost-efficient solution [8]. Some of the current approaches to storing hydrogen include High pressure storage vessels, cryogenic liquid hydrogen storage, and solid hydrogen storage materials as shown in figure 9. Each of these methods presents different advantages and disadvantages, but they have shown promising results.

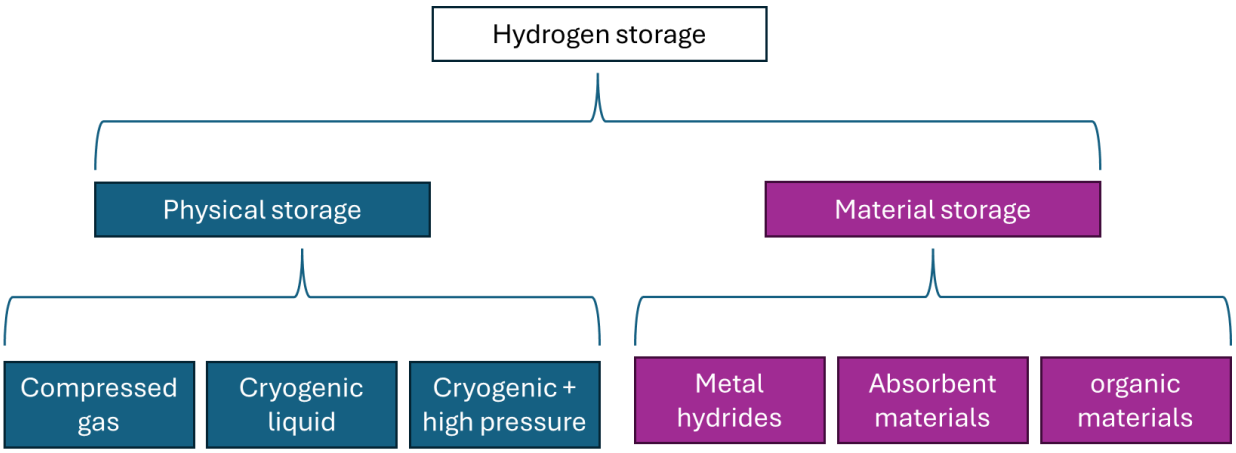


Figure 9: Currently used methods for storage and transport of hydrogen.

The storage systems for compressed hydrogen gas consist of multiple valves, regulators, piping, thermal management systems, and high-pressure vessels constructed specifically for this application [16]. In the case of stationary applications, these storage vessels often involve large systems designed to prevent losses due to permeation of materials and ensure safe operation [8]. In contrast, in the case of transport applications such as in vehicles, the space and weight allowed for fuel is much more restricted. In this regard, different institutions such as the United States DOT has set different goals for hydrogen storage systems to be used in vehicles based on the performance of currently available fossil fuel systems [61]. These goals are focused on energy storage capacity, refueling time, and vehicle performance and provide guidelines on the target weight and volume of portable hydrogen storage vessels.

2.1.1 High pressure hydrogen tanks

As previously mentioned, one of the main challenges in hydrogen storage is matching the energy density of currently available fossil fuels. One of the available solutions for this problem is to use high pressure storage to increase the density of the hydrogen gas. As shown in figure 10, a density of 20 Kg/m^3 is achieved at approximately 300 bar, while 40 Kg/m^3 is reached at 700 bar [8]. In turn, these changes in the storage pressure of the hydrogen gas would provide an energy density increase from 9.88 MJ/m^3 at normal conditions to 2400 MJ/m^3 and 4800 MJ/m^3 at 300 bar and 700 bar respectively, allowing hydrogen to compete

with fossil fuels. In this regard, compressed hydrogen gas transport and storage represents the most stablished technology [9].

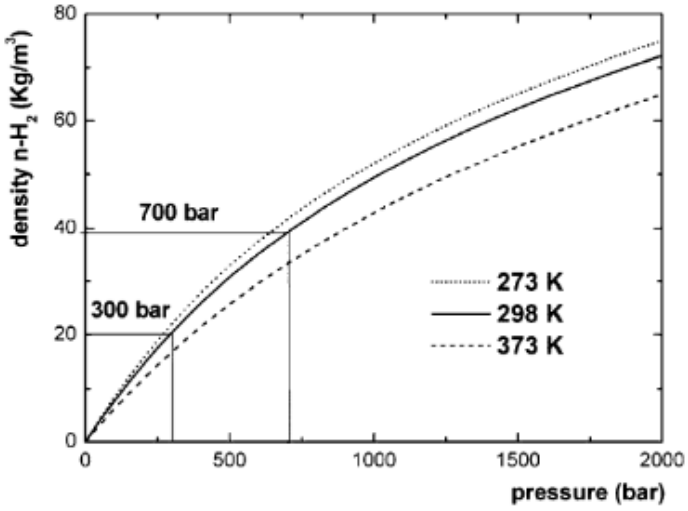


Figure 10: Volumetric density of hydrogen gas as a function of pressure for three different temperatures [8].

Given the need to compete with the energy density of fossil fuels, hydrogen transport and storage systems must then be able to withstand high pressure and relatively high stress cycles, as well as the previously mentioned hydrogen embrittlement and hydrogen-induced cracking which can be exacerbated by high pressures [62]. For this reason, the materials and design of storage vessels must consider the fracture mechanics accentuated by hydrogen gas as well as the high hydrostatic loads. In the case of hydrogen embrittlement, the dissolution of hydrogen molecules into the metallic matrix causes a decrease in the ductility of the material through the formation of hydrides [62]. Furthermore, in high-pressure and high-temperature conditions, hydrogen molecules can enter the vessel or pipe material causing microscopic cracks and voids [63] [62]. Both mechanisms affect the performance of the materials used for handling hydrogen gas and limit the useful life of components.

Another important aspect of compressed hydrogen to consider are the risks and hazards associated with the high flammability and low ignition energy of hydrogen [9]. The increased risk of explosions means that the systems designed must be able to prevent the formation

of leaks. In the case of high-pressure pipelines this is achieved by the use of a multi-materials approach in the form of a metallic pipe and a polymer liner [9]. The combination of a load bearing metallic component, and a polymer layer allows the design to sustain the required pressures for transport while avoiding hydrogen induced material degradation that could lead to failure. In this way, the use combination of different materials provides a cost-effective approach that enhances the longevity and safety of pipelines used for the transport of hydrogen gas [9].

Different fabrication and quality standards for hydrogen gas storage vessels have been developed around the world. These standards describe the material properties, operating pressures, fatigue cycles, allowable defects, among other properties and are aimed to ensure safety and reliability of storage systems. Example of these standards are the AME section VIII and the ISO Natural Gas Vehicle standards used for hydrogen vessels designed for pressures up to 100 MPa (15,000 psi) designed in the United States [16]. In general terms the storage systems designed for use with hydrogen must be able to satisfy the following requirements:

- Material compatibility with hydrogen gas
- Ability to withstand elevated pressure
- High resistance to fatigue failure
- Minimize losses to the environment
- Resistance to external damage
- Addition of reliable safety measures

As shown in figure 11 there are four main types of hydrogen storage tanks currently available. These tanks are differentiated by the materials used as well as the construction of the vessel: type I is an all metal tank, similar to those used in inert gases for industrial applications; type II is a metal tank lined polymer fibers in the hoop direction; type III tanks are made of metal with a polymer fiber lining fully covering the interior surface; type IV storage tanks also have fiber lining covering the interior but are constructed with polymer material [64].



Figure 11: Types of compressed hydrogen gas storage tanks [17].

An example of these tanks is the tube trailers currently used to transport compressed hydrogen gas. These storage vessels are typically fabricated of a specialized AISI 4130X steel designed to withstand the effects of hydrogen interaction as well as high fatigue cycles [63]. These storage tanks are designed with a seamless construction that minimizes stress concentrations. Furthermore, special heat treatments and testing are necessary to ensure that the appropriate mechanical properties are achieved on the material. Hydrostatic tests are performed to measure volumetric changes on the vessel, formation of cracks or defects, or the presence of leaks [63]. The development of these standards and testing procedures is necessary to ensure safety, given the nature of hydrogen gas and the elevated pressures at which it is stored.

While different standards and materials for hydrogen storage and transport have been identified, the progressive degradation of metals due to interactions with hydrogen are still a limit factor in the realization of hydrogen infrastructure [65]. Hence, in an attempt to overcome this limitation, composite vessels consisting of different layers of metals and polymers have been developed [66]. Overall, these vessels consist of a metallic shell and a load bearing polymer liner used to decrease the effects the hydrogen interactions with alloys. While polymers do not react chemically with hydrogen, gas molecules can diffuse and occupy cavities or defects. The internal accumulation of hydrogen in the material can

cause mechanical damage if the pressure is reduced faster than diffusion would allow in a process known as rapid decompression failure [65]. Similar failure can occur within polymers used with hydrogen equipment in the form of seals for valves and connections among others. Additionally, current storage vessels and systems designed for the transport of compressed hydrogen gas are vulnerable to losses due to leakage through sealing components [9]. This leakage occurs due to the molecular size of hydrogen and the high pressures required. Figure 12 shows a schematic representation of the different mechanisms in which hydrogen leaks can develop [9]. The elimination of this type of loss represents a challenge in the development of material resistance to permeation and degradation due to stress cycling. While the modes of failure for hydrogen equipment is well known, further research is needed to understand the mechanisms through which they occur and how to prevent them [14], [15].

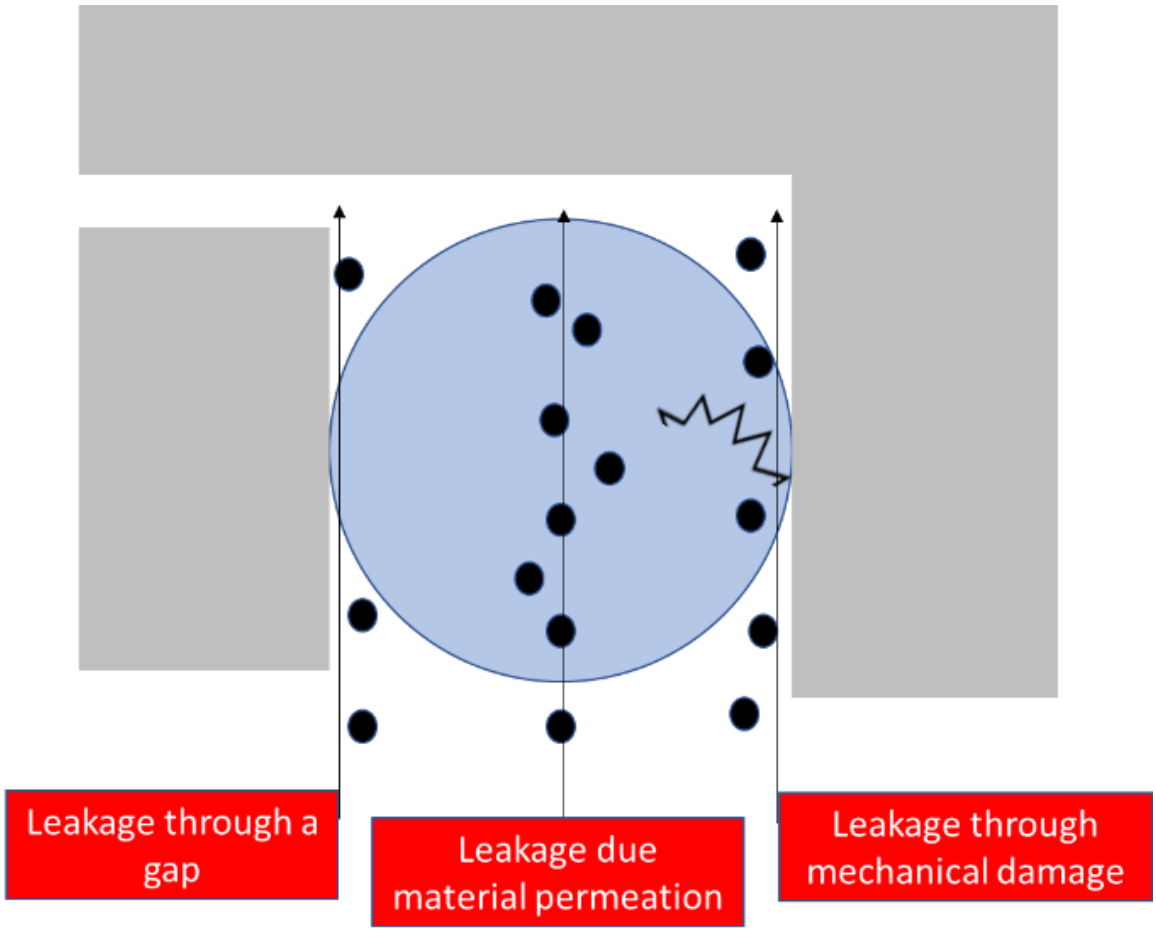


Figure 12: Schematic representation of mechanisms for compressed hydrogen gas losses through sealing elemnts [9].

For these reasons, one of the main technological challenges related to the storage of hydrogen gas in high pressure vessels are the material interactions with molecular hydrogen. In the case of metals, the permeation of gas molecules causes both physical and chemical changes leading to decrease in mechanical properties [9]. Similarly, the interactions between polymer materials and hydrogen gas lead to limited component life and increase hydrogen leakage over time [7]. Different material interactions relevant to the storage of hydrogen are further described in section 2.2. The effects of hydrogen exposure are then further enhanced by pressure cycling as part of the discharge and refilling process leading to material fatigue as well as the possibility of rapid decompression [67], [68]. In this way, current technology available for high pressure hydrogen gas storage and transport are not

able to satisfy the needs of the population to compete with fossil fuels. Further understanding and development of materials is needed to eliminate hydrogen loss over time as well as to achieve cost effective storage vessels.

2.1.2 Cryogenic hydrogen storage

An alternative to compressed hydrogen gas for transport and storage is the use of liquid hydrogen. By reducing the temperature of the pressurized gas, it is possible to change the phase into that of a liquid. As shown in figure 13, at low temperatures hydrogen can achieve a density of 80 Kg/m^3 at relatively low pressures of 100 bar [8]. This aspect of liquid hydrogen makes it of particular interest since it would help increase the storage efficiency of hydrogen energy systems. Nevertheless, the low temperatures used, and the thermodynamic properties of hydrogen create a different set of engineering challenges to overcome.

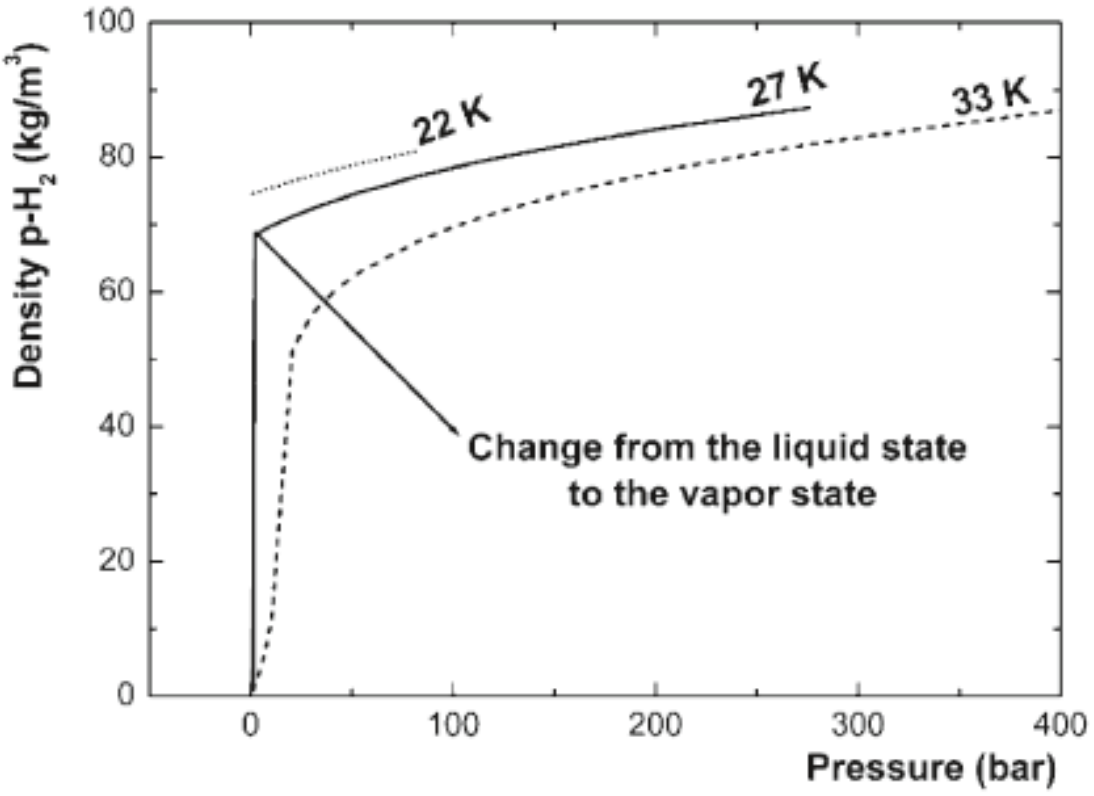


Figure 13: Volumetric density of hydrogen at three different temperatures showing gas and liquid phase *[8]*.

Hydrogen gas exists in two isomeric forms with different spin states in the proton of each atom. These forms are denominated ortho-hydrogen and para-hydrogen. Figure 14 shows the concentration of para-hydrogen as a function of temperature, as well as a representation of both isomers [69]. At the cryogenic temperatures required for the formation of liquid hydrogen, there is a higher concentration of para-hydrogen. In this way, the change in temperature required affects properties such as boiling temperature, and exothermic para-conversion, which in turn must be considered during the design of components and systems [8]. Furthermore, the success of liquid hydrogen transport and storage depends on the development of a liquifying cycle that is able to operate at a cost-effective rate, as well as adequate storing methods to maintain cryogenic temperatures.

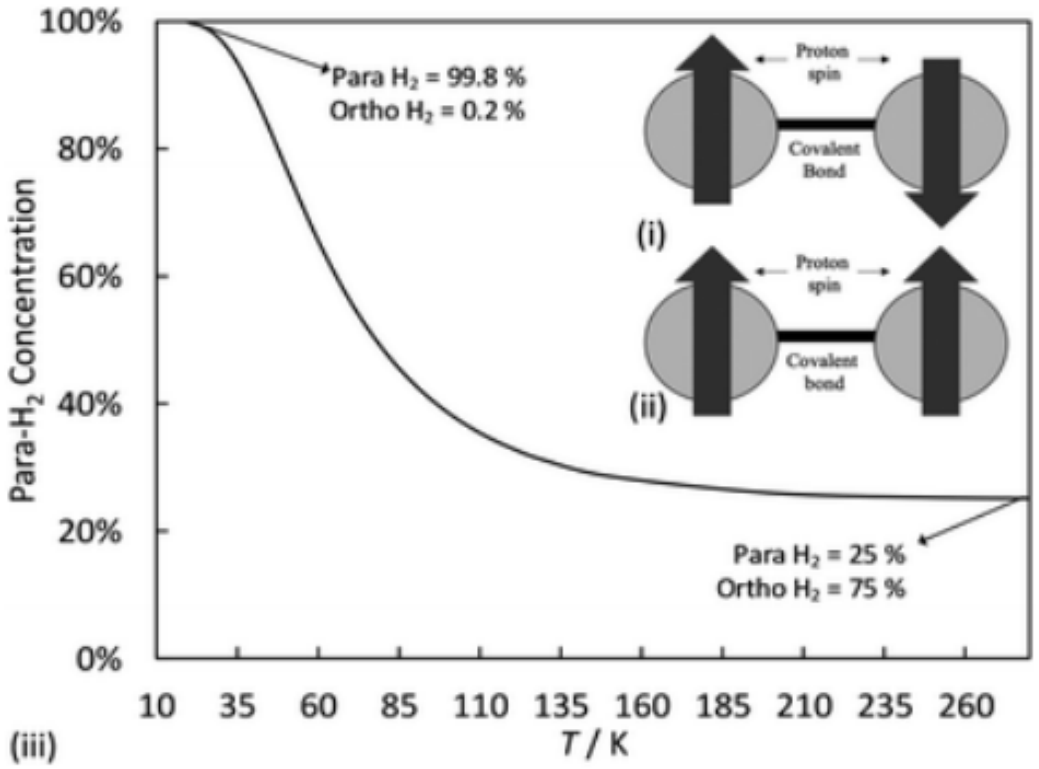


Figure 14: Isomeric concentration of molecular hydrogen as a function of absolute temperature *[8]*.

The industrial liquefaction processes currently available use a combination of cooling mechanisms and the adiabatic expansion of hydrogen gas to achieve a change in phase. Some of the main components that are used in this process include compressors, heat exchangers, turbines, expanders, intercoolers, valves, among others [8]. Figure 15 shows a schematic representation of the liquefying cycle currently used [69]. As part of the liquifying cycle, hydrogen gas is pre-cooled to a temperature of 80K, incorporating an adsorption filter to remove contaminants that could freeze and damage equipment. Following this, a low temperature refrigeration cycle is used to decrease the temperature of the gas, continuing the change from ortho-hydrogen to para-hydrogen during the process with the help of catalysts to assist the conversion. Finally, an adiabatic expansion of the gas is used to allow for condensation to form, obtaining liquid hydrogen that can then be stored [69]. All these components interact directly or indirectly with the hydrogen gas and thus are susceptible to the previously mentioned hydrogen embrittlement and hydrogen-induced cracking. Damage to these components would decrease the efficiency of the process or could lead to catastrophic failure. For this reason, appropriate material selection and design specifications are required in the development of hydrogen liquefier plants.

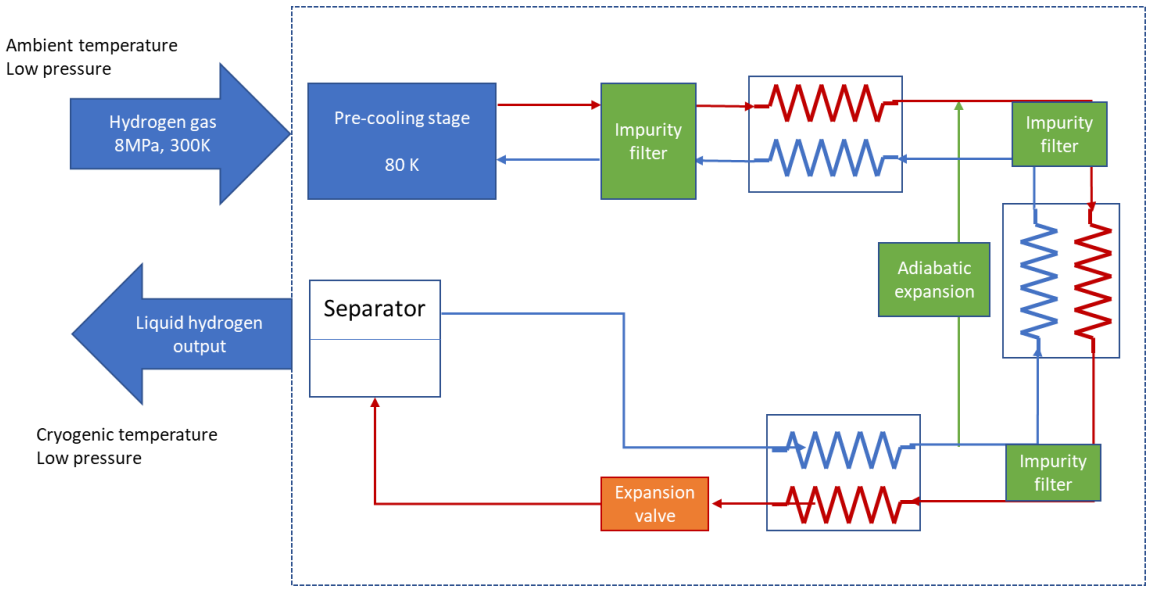


Figure 15: Schematic representation of the liquefaction cycle used in th eproductio of liquid hydrogen *[69]*.

The liquid hydrogen produced has a high volumetric density and is free from impurities. Nevertheless, the low temperatures of 20-30 K must be maintained during storage in order to prevent increased pressure and losses due to evaporation [8]. Furthermore, the design of cryogenic storage vessels for hydrogen must take into consideration the possibility of losses due to evaporation. Increases in temperature or splashing of the contained liquid can cause the hydrogen to change phase into gas, which increases the likelihood of permeation and fugitive emissions during transfer between tanks [69]. This type of loss caused by the low boiling point of liquid hydrogen account for the greatest challenge in the use of liquid hydrogen due to the unavoidable continuous loss observed in currently available systems accounting for a loss of up to 0.4% of the stored hydrogen [70]. Unless large amounts of energy are used to maintain low temperatures, cryogenic storage of hydrogen still requires advances in the design of materials tailored for cryogenic applications as well as improvement in the design of storage vessels and transfer equipment.

As previously discussed, the cryogenic storage vessels must be able to minimize heat input due to radiation and conduction. These vessels typically have a double wall construction with the inner vessel suspended by supports engineered to minimize heat transfer, separated from an outer vessel by layers of insulated material and evacuated of all gases [71]. In the case of liquid hydrogen, the low temperature can have a synergistic effect with the degradation caused by hydrogen interactions, further increasing the potential for damage and failure of the storage vessel [72]. For this reason, the material selection must take into consideration the compatibility with cryogenic temperatures as well as low susceptibility to damage from hydrogen with adequate strength and stiffness. Some of the most currently used metallic materials include austenitic stainless steel such as AISI 4130X, aluminum alloys, nickel-copper alloys, and composite materials [69]. While cryogenic storage of hydrogen provides a clear advantage in the storage density, further development of the technology is needed to achieve a competitive solution. The different challenges presented by the low temperature as well as the thermo-physical properties of hydrogen as well as the need for cryogenic equipment and specialized personnel present significant

disadvantages for the deployment of liquid hydrogen storage [71]. Nevertheless, the possibility of high storage density shows promising options for hydrogen infrastructure if the necessary materials and design characteristics are further researched and developed for the market.

2.1.3 Solid hydrogen carriers

An alternative to gas and liquid storage of hydrogen is the use of solid materials. To achieve this, different materials such as metal hydrides are used to capture hydrogen molecules that can be released and used when needed. These engineered nanomaterials take advantage of different intermolecular forces to allow for absorption and solution of hydrogen gas [12]. To achieve high storage density, porous materials such as intermetallic alloys composites are exposed to hydrogen gas, which reacts with the metal substrate forming solid metal hydride compounds [73]. Then, the hydrogen is released from the hydride structure by applying heat through an endothermic process. This storage method takes advantage of variations in the charge distribution of hydrogen molecules and solid substrates to bind them together through physisorption or through a reversible chemical reaction [70]. For this reason, materials such as metallic alloys or other structures with large specific surface areas make ideal storage materials. An example of the suitable materials used for solid hydrogen storage is Magnesium. This metal shows the capacity for reversible hydrogenation and dehydrogenation while also being relatively cheap and readily available. Furthermore, magnesium hydride relatively high storage capacities in the form of a gravimetric hydrogen density of 7.6 weight % and a volumetric density of 110kg m^{-3}, allowing it to compete with methods such as high pressure gas tanks and cryogenic storage [74]. Figure 16 shows a schematic of the use of solid hydrides as a means for hydrogen storage and transport as presented by Stampfer et al in 1960 [75].

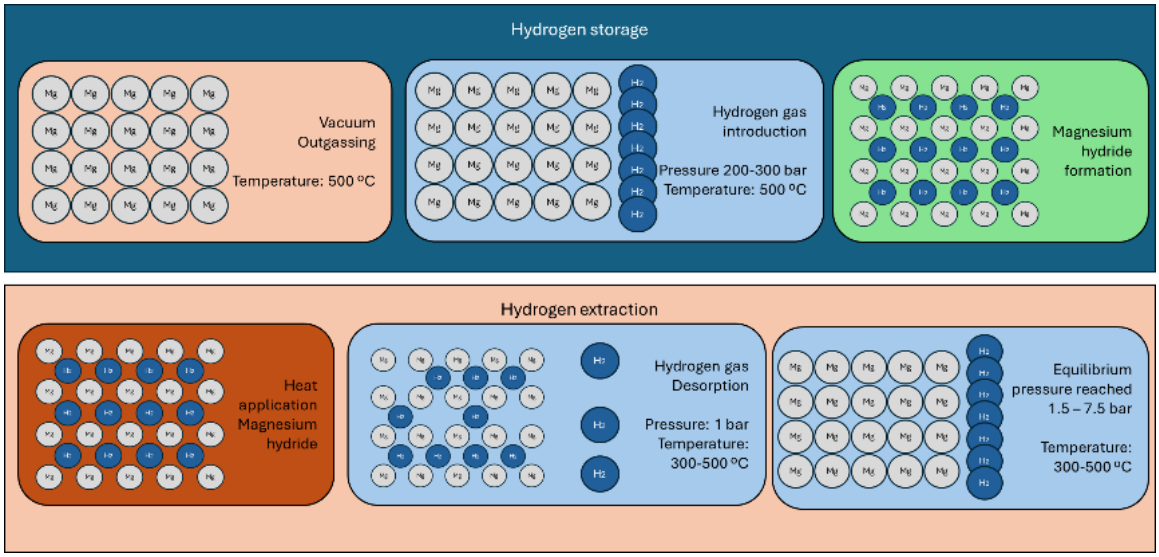


Figure 16: Illustration of the process employed in the utilization of magnesium as a solid carrier, highlighting the pressure and temperature necessary for the absorption and desorption of hydrogen gas.

In this case, the crystal structure of Mg presents a hexagonal close-packed (hcp) lattice which is changed through the inclusion of hydrogen atoms and the application of pressures higher than 3.9 kbar into β-MgH_2 that possesses an orthorhombic structure similar to that exhibited by α-PbO_2 [76]. The process through which the hydride compound is formed can be explained as a series of steps: Firstly, Van der Waals forces between the metal and the hydrogen aid the permeation of gas into the metal lattice through physisorption; following this, chemisorption causes the formation of bonds between metal and hydrogen atoms; then the hydrogen occupies interstitial sites forming α-MgH_2; finally, the hydrogen atoms impregnate the Mg crystal lattice, forming β-MgH_2 leading to the disappearance of α-MgH_2 resulting in a metal hydride that can then be used to transport hydrogen [76]. This reaction is reversible and can be utilized to reduce the possibility of hydrogen losses during transport as well as the possibility of component failure due to material interactions with H_2.

However, it is important to note that the reversible storage capacity of magnesium is heavily dependent on the preparation methods used as well as the use of additives and catalysts. For example, recent advances have shown that catalyst doping by introducing metals such as Titanium, Vanadium, and iron can reduce the dissociation energy of hydrogen molecules

[77]. The modified kinetics of the MgH_2 system along the transition metal catalyst then results in lower temperatures, and hence less energy, needed to complete the storage and extraction of molecular hydrogen. In this way solid hydrogen storage technology offers many advantages over the previously discussed storage methods such as a large storage, an efficient hydrogenation and dehydrogenation cycle, and the lack of direct interaction between hydrogen and the storage vessel, enhancing the overall safety of storage systems [21], [78].

Nevertheless, one of the main disadvantages of this method for hydrogen storage and transport is that both the absorption and desorption processes require significant amounts of energy to be carried out. For this technology to be viable, low absorption and desorption temperatures are needed, as well as a cost-effective life cycle due to the degradation of the substrate over time. In this way, the greatest challenges are the development of materials with an improved life cycle and a reduced cost. Some of the most promising materials currently available are made of microporous metallic structures such as hydrides or alanates. These materials have shown a volumetric hydrogen density of 115 Kg/m^3 and a hydrogen-to-metal ratio greater than 2 [70]. Furthermore, this method of hydrogen storage still presents many technological challenges and drawbacks, it is of particular interest due to its increased safety as well as the possibility of working along with fuel cells to minimize energy consumption and utilize waste heat [73]. Nonetheless, the high cost and low availability of some of the materials developed still represent a limiting factor in this technology. For these reasons, further research is needed to develop low-cost materials that are not affected by the desorption temperatures along with an increased capacity for a reversible absorption reaction [21].

2.1.4 Conclusion

From this literature review we can conclude that the utilization of hydrogen as an energy carrier has gained traction in the last few years due to the possibility of lowering costs as well to address global warming and other adverse effects of the pollution that accompanies the combustion of hydrocarbons. However, several technological challenges still stand in the way for hydrogen to be an economically competitive option in terms of storage efficiency,

safety and reliability. These challenges are introduced because of the material interactions of metallic alloys and polymer materials with pressurized hydrogen gas. Phenomena such as hydrogen embrittlement in alloys, hydrogen induced crack propagation, and hydrogen induced surface blistering in polymers limit the available materials and decrease the service life of components, increasing the operational cost for hydrogen infrastructure and decreasing its reliability. In this regard, material science has made great advances to bridge the gap, example of this is the multi-materials approach used for the construction of pipelines and storage tanks using a combination of polymers and metals [9]. Hence, by gaining a better understanding of the materials interactions involved in the storage and transport of hydrogen it would be possible to develop better technologies and systems to satisfy the future needs of people.

By reviewing the different methods used to transport and store hydrogen it is possible to identify the current technological challenges to overcome. For both gas and liquid storage, there is a constant loss due to ineffective seals and material permeation [79]. Furthermore, material interactions with hydrogen lead to embrittlement of alloys and decrease in mechanical properties, thus limiting the useful life of storage tanks and connections used for transport. While these effects are avoided in the use of solid carriers, the equipment used to store the hydrogen gas is still vulnerable. Additionally, solid storage is currently underdeveloped as a technology due to its elevated costs and lack of scalability for use in industry.

2.2 Challenges in materials for hydrogen applications

Hydrogen gas has many specific characteristics that distinguish it from other gases. The main difference being the size of the molecule compared to other gases used in industrial applications. The hydrogen molecule has a size of 2.8 Angstrom while other gases such as Carbon dioxide and nitrogen have relatively larger molecules with 5.5 and 3.3 Angstrom respectively [80]. This characteristic of the molecule means that hydrogen gas tends to escape through small openings and gaps that molecules larger such as propane would not be able to traverse. Furthermore, its low number of electrons makes hydrogen molecules

chemically reactive, leading to chemical changes in the materials used in the fabrication of storage vessels and auxiliary equipment for handling hydrogen [81]. For these reasons, it is important to develop a precise understanding of the mechanisms in which hydrogen gas molecules interact with different materials, as well as how these effects can be mitigated.

By analyzing the current technological challenges limiting the expansion of hydrogen energy infrastructure we can appreciate the lack of knowledge and development in adequate materials. This is most visible in the case of transport and storage, where hydrogen embrittlement and material permeation present a significant limiting factor for vessels and sealing components. One of the most challenging aspects of these interactions is that the degradation of material properties presents itself through a time dependent process along with damage caused by other factors such as temperature and chemical reactions [19]. This process controlled by time is denominated aging, and it can be differentiated in two main types according to the main driving mechanism. In this context, physical aging describes reversible changes in secondary bonds along the polymer chain [28]. This type of change is related to the effects of internal stresses and other physical factors acting on the material. In contrast, chemical aging refers to the irreversible changes caused by the formation or breakage in the primary bonds at the molecular level, changing the structure of the material [44]. In the case of hydrogen applications, the aging produced by material interactions with the gas limits the service life of components and creates further challenges in the form of safety and economic concerns due to the high flammability of hydrogen gas.

Given the negative effects associated with hydrogen gas, it is important to understand the evolution of the changes caused by hydrogen gas on the materials used to store and transport it. For polymer materials, one of the main concerns regarding aging is the change in mechanical properties that could affect the capacity of the material to maintain an adequate seal. Nevertheless, it is important to note that not all materials react in the same way. For example, studies have shown that the use of additives such as carbon nanoparticles and plasticizers affect the way in which degradation caused by hydrogen gas presents on polymers [66]. Hence, by developing a better understanding of the changes produced by hydrogen exposure in different materials, it would be possible to identify which

material characteristics result beneficial for components designed intended for hydrogen service.

2.1.1 Metallic materials

In the case of metals, one of the most notorious material interactions is that of hydrogen embrittlement. In this process, dissociated hydrogen atoms permeate metallic alloys causing the formation of hydrides. Different atomic forces such as weak van der Waals forces and covalent bonding facilitate the processes of physisorption and chemisorption [28]. In this process, denominated adsorption, the hydrogen concentration is dependent on the partial pressure of the hydrogen gas, as well as the temperature, and the characteristic of the material. Following this, competing mechanisms of formation of molecular hydrogen trapped in cavities as well as diffusion through the bulk material lead the absorption of hydrogen [28]. These mechanisms thus result in the accumulation of gas in grain boundaries, dislocation, and other defects such as precipitates and inclusions within components. Furthermore, the introduction of hydrogen into the material matrix causes irregular stress distributions as well as the dislocation of granules [28]. These chemical and mechanical changes cause imperfections in the material that ultimately affect the useful life of components used in hydrogen infrastructure. This degradation of mechanical properties observed in metallic alloys due to interactions with hydrogen gas is commonly denominated Hydrogen Embrittlement [82]. Hence, interaction between hydrogen and metals presents unique challenges when compared to other substances.

Material degradation in the presence of hydrogen gas has been investigated and described since [83]. Nevertheless, the physical mechanisms that contribute to the changes in physical properties are not completely understood. In this way, hydrogen embrittlement of metallic alloys has continued to be the cause of component failure, limiting the use of hydrogen as an energy carrier [28]. Although it is understood that hydrogen gas affects materials through processes such as hydrogen embrittlement, the mechanisms through which these changes occur are not well understood. An example of this process can be observed in the interaction between hydrogen gas and commercial steel alloys, where degradation of the mechanical properties of materials promotes the formation and

propagation of cracks [78]. The high-pressure working conditions and the repetitive load cycling on handling components along other characteristics of the system such as temperature, chemical composition of the alloy, and its microstructure heavily influence the solubility of the hydrogen gas. This effect is higher on materials such austenitic steels with a fcc structure due to the size of the interstitial sites as well as the increased ductility observed for this type of metals [28]. In this way, along with the risk of flammability and reactivity of hydrogen gas, its capability to permeate and degrade metallic alloys introduces unique issues when developing systems for transport and storage [84].

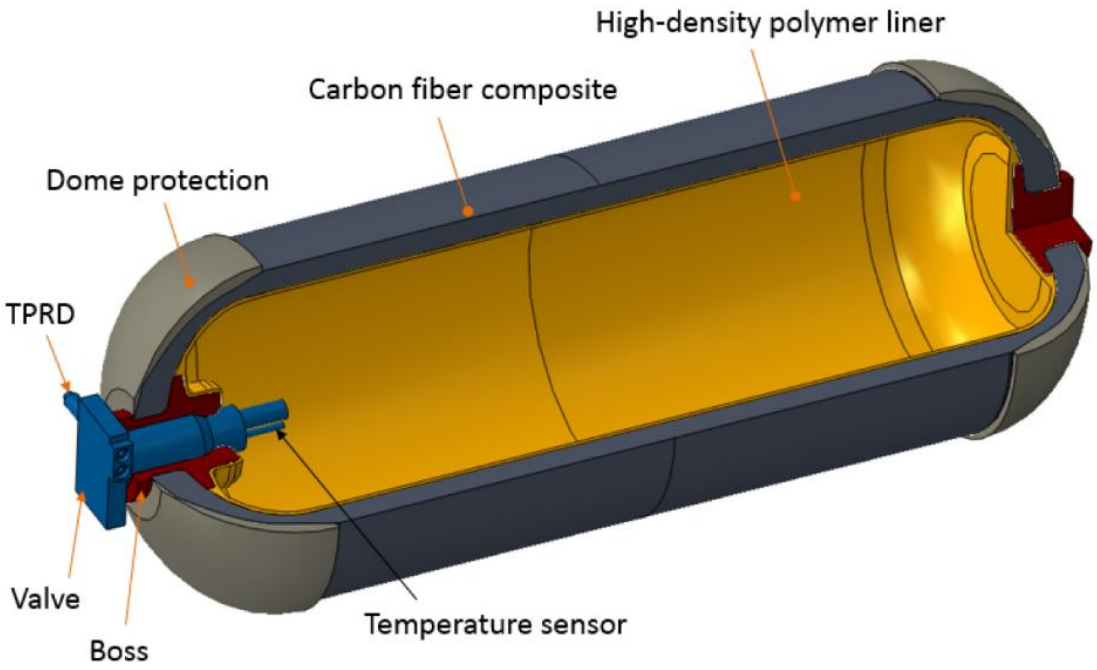
Different explanations for the detrimental effect of hydrogen gas on metals have been experimentally confirmed. In the case of materials that produce hydrides, hydrogen gas is diffused into cracks due to the increased pressure and chemical potential of the substances [78]. This diffusion of hydrogen into the material causes the formation of hydrides, which have different mechanical properties compared to the original material, such as being generally more brittle [63]. These differences in mechanical properties along with the higher volume of formation generate stress conditions that propagate the crack, allowing the process to repeat [85]. Similarly, in the case of materials that do not form hydrides such as iron and nickel, brittle failure can occur after exposure to a hydrogen environment at high pressure [86]. This type of failure is generally caused by the formation and aggregation of internal voids caused by the diffusion of hydrogen molecules into the metal matrix and is denominated as Hydrogen-Induced Cracking [62].

In this way, the interaction between metallic alloys and hydrogen tends to cause degradation of mechanical properties over time. For example, in the case of high tensile steel alloys used for compressed hydrogen storage tanks, the combination cyclical mechanical stress along with chemical changes due to hydrogen embrittlement leading to the formation and propagation of cracks severely limits service life for components due to safety concerns on material failure. This degradation mechanism has been related to the microstructure of the alloys, where the size of the metal crystal grain has a direct impact on susceptibility to hydrogen effects. Specifically, it has been demonstrated that alloys with larger grain structure, and larger gaps between grains, are more susceptible to hydrogen entrapment,

leading to decrease in tensile strength and other negative impacts, when compared to alloys with smaller grain structures [87].

2.1.2 Polymer materials

While metals have many uses within hydrogen applications, as illustrated by class IV hydrogen storage tanks shown in figure 17, hydrogen embrittlement of alloys presents a limit to what can be achieved through their sole use. In this case, material limitations for metals are overcome by using polymer material to separate the gas from the tank shell, preventing hydrogen embrittlement. Similarly, the valve used and its respective fittings also make use of polymer materials for sealing barriers. Therefore, polymers and composite materials have gained traction as promising materials to overcome the current challenges presented by hydrogen induced degradation [7]. Hence, development of appropriate polymer materials with characteristics that allow for a longer service life and increased reliability are a key step in the progress of hydrogen use as an energy carrier.



TPRD = Thermally Activated Pressure Relief Device

Credit: Process Modeling Group, Nuclear Engineering Division. Argonne National Laboratory (ANL)

Figure 17 : Class IV compressed hydrogen gas storage tank illustrating the use of polymer liner as well as other key components [60].

Polymers are materials composed of interconnected carbon chains or macromolecules denominated polymers. These materials have a large capacity for plastic deformation at room temperature, allowing them to return to their original shape after being deformed [88]. These molecules are attached to each other through covalent or ionic bonds between, creating interconnected networks that compose the bulk of the material, as shown in figure 18 [89]. This structure allows each chain to stretch when a mechanical load is applied without causing permanent changes. When the external force is removed, intermolecular forces return the polymer chains to their original position, allowing for a highly reversible strain response [89]. Furthermore, the molecular structure of these materials provides erosion resistance and low chemical reactivity. These characteristics, along with their relatively low cost, make polymer materials ideal for the development of components for hydrogen handling and storage.

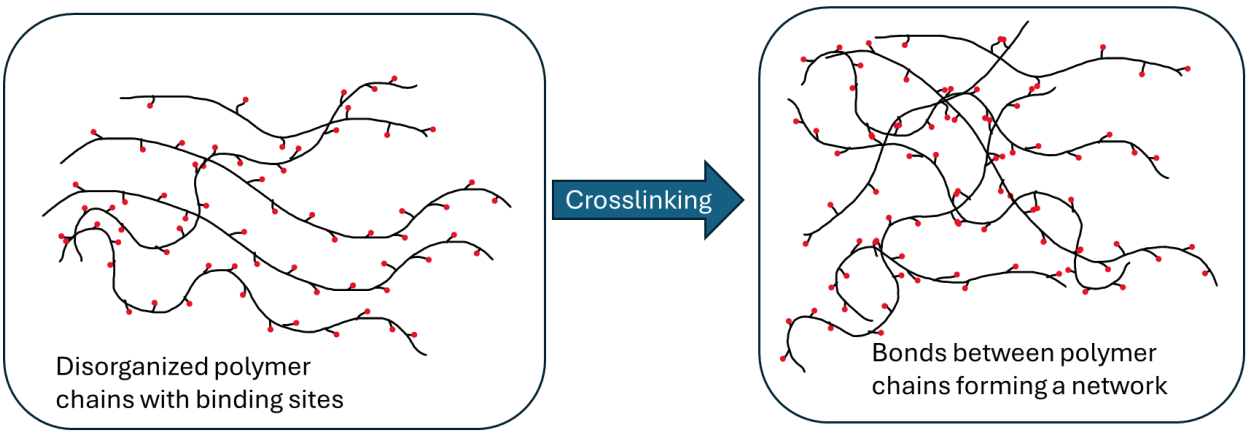


Figure 18: Schematic representation of polymer crosslinking showing the free binding sites before and the polymer network formed by molecular bonds after crosslinking.

For these reasons, polymer materials are commonly selected for the fabrication of critical components such as sealing components, valves, and liners for pressurized gas storage tanks. In these applications the tribological properties of the materials are particularly important [90]. For example, in the case of stem seals for valves, it is important to mitigate fugitive emissions to achieve cost effective hydrogen storage and transport. Hence, aside from hydrogen compatibility, the materials selected must be able to satisfy a variety of requirements depending on the specific characteristics of their application. In the case of materials used for seals, the sealing performance and the frictional characteristics are influenced by the inclusion of plasticizers and fillers within the polymer matrix [91]. In this way, it is important to understand the molecular structure of polymer materials in order to understand limitations of currently available materials as well as to develop new materials.

Furthermore, while the mechanical properties of polymers such as flexibility and chemical resistance make them ideal candidates for applications such as sealing components and storage tanks liners, repeated exposure to high pressure cycling can alter the properties of the material. The degree to which this hydrogen induced degradation presents itself depends on many factors such as operating conditions and molecular structure of the material. In this way, the different molecular structures presented by polymers mean that material degradation could present itself differently at similar operating conditions for different

polymers. For example, materials with a higher degree of free volume are more susceptible to swelling due to hydrogen diffusion into the polymer matrix [92]. In this way, the material degradation of polymers is closely related to their molecular structure as well as the presence of filler materials and additives. Hence, further research to understand how hydrogen permeation and its subsequent damage is related to material structure.

Therefore, in the case of non-metallic materials such as polymers used in the fabrication of sealing components, operation with high pressure hydrogen gas presents unique challenges due to the specific material interactions that take place. Polymer materials used for sealing components such as High-Density Poly-Ethylene (HDPE) Nitrile Butadiene (NBR) are commonly used in the fabrication of liners for storage tanks and transport pipes as well as gaskets and seals in valves and other components [93]. The structure of polymer materials can be described as a series of carbon chains entangled and bound due to different molecular interactions [94]. The degree of unification then affects the overall properties of the material as well as its resistance to hydrogen gas permeating the damage occasioned. In the case of materials such as HPE and NBR, denominated elastomers, these carbon chains are chemically bonded, or cross-linked, creating loose three-dimensional flexible networks that allow for deformation [94]. The characteristics of this polymer network give elastomers their ability to deform when forces are applied and then revert to an initial state when the load is removed [95]. While these versatile materials present many beneficial properties for sealing components, the loose carbon networks can be infiltrated by hydrogen gas, particularly at high pressures. The saturation of cavities within the material can then lead to cavitation and blistering when the pressure is removed from the component, creating an imbalance between the gas stored inside the material and its surroundings in a process denominated Rapid Gas Decompression (RGD) [96].

In the case of components exposed to high pressure, RGD failure present itself when suddenly exposing components to atmospheric pressure, causing the initiation and propagation of cracks along the material as well as changes in volume [29]. The RGD failure process can be explained as two separate stages: permeation and depressurization. Initially, the material is infiltrated by gas particles, enhanced by high pressure and high temperature

causing swelling of the component. Furthermore, the plasticization of the polymer matrix applies strain to the different polymer chains, limiting flexibility, increasing free volume, and ultimately decreasing the glass transition temperature [29]. During this stage, the introduction of gas into the matrix and the accompanied stresses affect the mechanical and thermal properties of the material. These changes continue until an equilibrium condition is reached between the internal and external gas pressure. In this case the permeation and solubility of hydrogen is mainly determined by the material characteristics, amounts and types of fillers used [97].

In the second stage of component failure, the sudden reduction in the forces applied to the component initiates a complex process in which the pressure gradient causes a three-dimensional state of pneumatic tension through the component, which facilitates the formation of voids and cavities. Following this, the adiabatic expansion of the gas cools the polymer creating a temperature gradient in the component. In this way, the dissolved gas influences the polymer through these two mechanisms create a gradient of physical and mechanical properties creating internal stresses and eventually rupture of the polymer chains [29]. The formation of these voids and the rupture of polymer chains then lead to the initiation and propagation of cracks, and the failure of the sealing component.

Furthermore, other processes related to the high pressures used in transport and storage of hydrogen gas can also induce a level of damage during the handling of pressurized gas. When elastomers are exposed to a fast drop in pressure, the imbalance between the gas solute in the matrix and the exterior of the material can lead to a type of failure denominated Rapid Gas Decompression (RGD) failure [98]. While this process is similarly complex and is governed by a multitude of factors, the characteristics of hydrogen gas tend to enhance the effects of RGD due to the increase permeation into the polymer matrix.

In the case polymers, polymer degradation or aging can be caused by a multitude of environmental factors such as temperature, presence of chemical substances, ultraviolet light exposure, among others. As a result of the interactions with these factors, the properties of the polymer material can be altered in the form of changes in hardness and

tensile strength, changes in elastomer structure, and the formation of cavities within the matrix that would lead to decreased sealing performance [99]. In the case of hydrogen storage this degradation is particularly important, as the loss of stability in the polymer coupled with the application of depressurization cycles could lead to gas leakage and present the possibility for accidents [100].

Hence, in the case of handling compressed hydrogen gas, it is expected that the polymer materials will undergo degradation as part of their service operation. For example, routine operations such as pressure cycling during loading and unloading of storage vessels could expose components to RGD, increasing the hazardous nature of compressed hydrogen gas operation. In this way, considering the interactions between hydrogen gas and the materials used for handling it is of critical importance. Incorrect material selection would lead to unexpected failure and short useful life for hydrogen infrastructure, reducing its competitivity [78] [85]. For this reason, the identification and development of materials with adequate properties is necessary for the realization of hydrogen infrastructure. In this way, it is highlighted that the development and characterization of materials with optimal properties is a required step in advancing hydrogen technology.

In this way, material compatibility remains one of the main challenges in the realization of hydrogen usage as an energy carrier at a commercial level. Regardless of their nature, metals, polymers, and composite materials are all affected by hydrogen induced degradation in one way or another [28]. This degradation occurs because of complicated molecular interactions that result in altered mechanical and physical properties in the materials used to handle and store hydrogen gas. These changes in properties can lead to unexpected failure of components such as seals, thus increasing the risks associated with hydrogen gas [7]. Examples of this are the previously described hydrogen embrittlement and RGD that could lead to premature failure in components such as high-pressure storage tanks. Hence, developing a better understanding of the material interactions related to hydrogen gas is a necessary step in the development of a reliable hydrogen energy infrastructure.

2.3 Hydrogen assisted aging in polymers

Polymer materials are commonly used as O-rings and other types of seals in different types of valves and components used in the oil and gas industry due to their chemical and mechanical resistance as well as their elasticity [101]. These polymer seals operate under various forces such as the pressure of the fluid they contain as well as compressive and tensile forces included as part of the seal design. For example, in the case of O-ring type seals, compressive forces are used to deform rubber sealing components, generating a sealing effect due to the internal reaction forces in the polymer material as shown in figure 19 [102]. Hence, properties such as the elastic modulus and maximum deformation of the material are of important consideration when designing polymer sealing components. Furthermore, understanding how interactions with fluids such as pressurized hydrogen gas affect these properties over time as the material age is particularly important to ensure that the stresses and deformations applied during use do not exceed the capacity of the material. In this way, understanding hydrogen induced material degradation, or aging, of polymers becomes an important step for the development of systems for hydrogen use as an energy carrier.

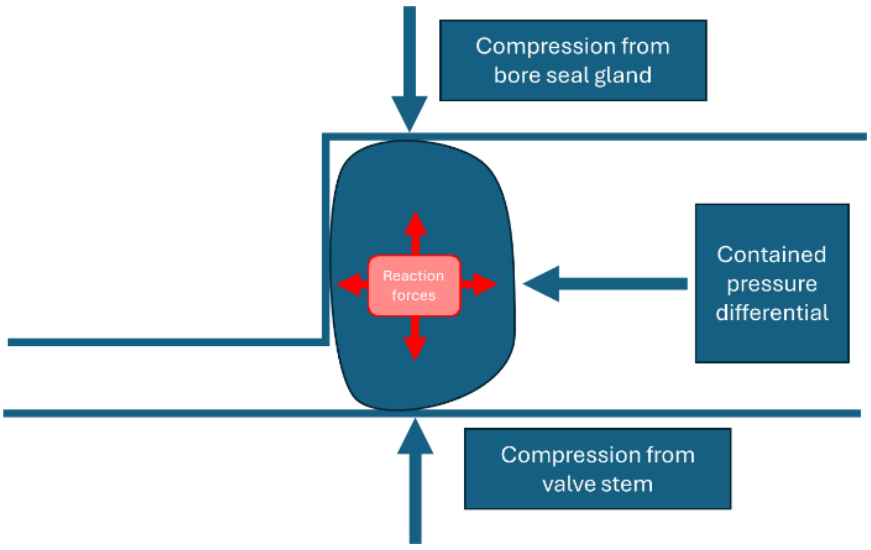


Figure 19: Schematic representation of a polymer O-ring type seal highlighting the forces involved in creating the sealing effect used to contain pressure differential in components such as valves.

While the material degradation is the result of different processes related to interactions with hydrogen gas, the main problems arise due to permeation into the polymer matrix. Figure 20 shows a schematic of the aging process [92]. In the case of polymers, the free volume between the carbon chains creates conditions that allow increased hydrogen transport leading to accumulation, swelling of the material and ultimately changes the mechanical properties of the polymer. Furthermore, the accumulation of hydrogen gas inside the polymer matrix presents the conditions that lead to rapid gas decompression damage in the form of blisters and cracks. The degree to which the material is affected by these processes is heavily related to the molecular structure, crosslinking density, crystallinity, and the inclusion of fillers and plasticizers. Hence, further research is necessary to understand which material properties would be beneficial for hydrogen operation.

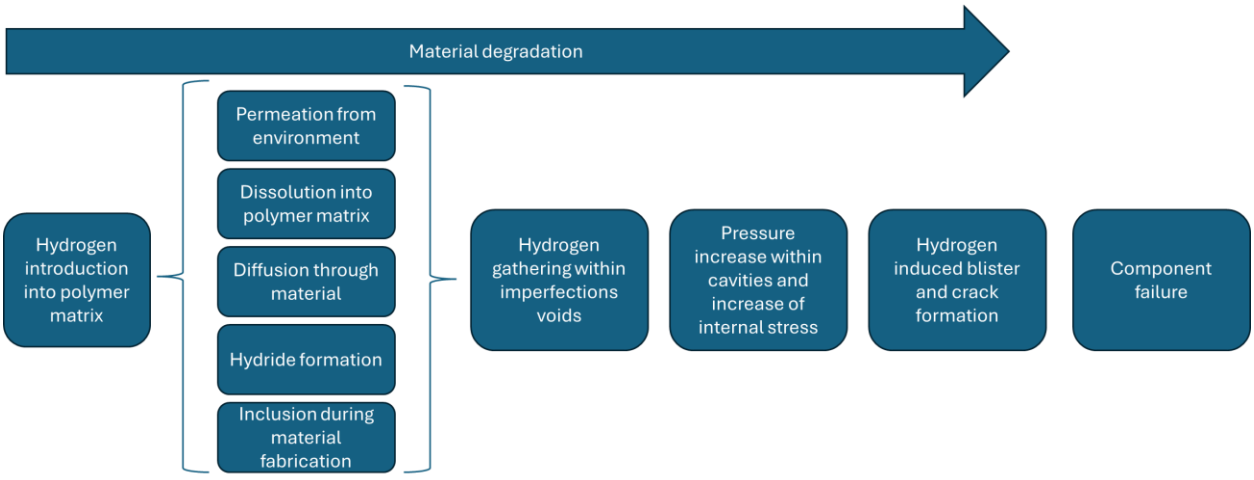


Figure 20: Hydrogen assisted polymer aging process highlighting the principal phases leading to changes in mechanical properties.

2.4 Current approaches for characterization of hydrogen damage on polymers

As previously discussed, there are different driving mechanisms behind the material degradation observed in polymers exposed to hydrogen gas. While different explanations for each of these mechanisms have been explored, a comprehensible model for the overall effects of the interactions between gaseous hydrogen and polymers has not been sufficiently developed [103]. One of the main challenges when analyzing and characterizing

the damage caused by hydrogen gas interactions is the microscopic nature of the damage, particularly the mechanical interactions between the hydrogen gas and the material at crack tips [104]. Hence, one of the most adopted approaches for the characterization of material changes under hydrogen environment is through empirical observations. While multiple methods have been developed, the general research scheme can be summarized as the characterization of baseline properties, followed by material exposure to hydrogen gas, and a final characterization of material changes and comparison of mechanical properties.

In these studies, as demonstrated by Zaghdoudi, the material samples were exposed to hydrogen gas at varying pressure levels and for different time durations in order to better understand the evolution of the changes in material properties [67]. Hence, the different levels of exposure allow the investigation of material suitability for different operating conditions. Furthermore, this type of study allows for a better understanding of the material changes over time as it interacts with the hydrogen molecules, allowing for better identification of material and components service life for practical applications such as hydrogen refilling stations.

Once the materials are exposed to hydrogen, the mechanical properties of samples are determined, and the degradation is assessed using different microscopy techniques such as SEM and Micro-CT to identify changes in the morphology of the material [28] [103]. Microscopic imaging of the materials gives insight into the morphological changes on the material that result from interactions with hydrogen gas. Specifically, through imaging, it is possible to quantify and characterize the formation of fractures, cavities, and agglomerations of filler particles due to hydrogen permeation [65]. The data obtained from imaging studies can then be used to identify the mechanisms that contribute to the degradation of material properties. These observations provide useful information that allows scientists to determine the rate and level of degradation for materials exposed to hydrogen gas. Furthermore, by using microscopy techniques to measure the size and distribution of cracks and other effects, it is possible to develop and validate mathematical models for the interactions between hydrogen molecules and other elements.

Another example of studies conducted to investigate the changes in mechanical properties of polymer materials was conducted by Theiler et al. In this study, two different acrylonitrile butadiene rubbers were exposed to high-pressure hydrogen environment to measure the changes in hardness, compression set, and tensile behavior [56]. As detailed by the author, the studies were performed in accordance with established testing standards such as ANSI CHMC 2:19. This standard describes the testing methods used for evaluating the material compatibility of polymers for applications with high pressure hydrogen gas [105]. In this case, the use of established standards is particularly important to ensure that results can be replicated as well as to guarantee their validity. Furthermore, established testing standards provide a common basis to compare the performance of different materials. Following material preparation, the polymer samples were exposed to high purity hydrogen to pressures up to 100 MPa at a temperature of 120 C for varying durations [56]. In this way, conditions like what could be encountered in real life hydrogen systems can be replicated. Furthermore, by outgassing the samples during the initial preparation steps and high purity gas, the author ensures that there are no additional chemical interactions that could affect the results. Finally, a series of tests were performed to characterize the changes in mechanical properties of the polymers selected. These tests included density measurements, tensile testing, dynamic mechanical analysis, hardness measurement, compression set calculation, and scanning electron microscopy imaging [56]. The numerous tests performed provide valuable insight into the changes produced by hydrogen exposure and allow comparison of different properties.

For instance, by measuring changes in density, hydrogen dissolution and material swelling [85]. In this regard, Theiler et al. reported a decrease in density for both material types following exposure to hydrogen gas [56]. In this way, the author shows evidence of the infiltration of hydrogen gas into the polymer matrix. Similarly, by comparing tensile strength and the thermos-mechanical properties of the rubber, it is possible to measure the degree of degradation caused on the material. In this respect, the author measured a decrease in the glass transition temperature as well as a significant reduction in the maximum elongation and maximum tensile strength [56]. Additionally, both materials showed an

increase in compression set after exposure to hydrogen [56]. Understanding these results and how they relate to permanent changes in the polymer structure is crucial as polymer components are crucial for ensuring safety and are exposed to a wide range of conditions. For example, an increased compression set could compromise the ability of gaskets and O-rings to create an adequate seal leading to premature failure. Similarly, a decrease in tensile strength over time due to hydrogen exposure could mean that the operating conditions overcome the limits of the material, also causing premature failure. Hence, being able to predict how these properties change over time, and to what extent these changes can contribute to component failure, is paramount to ensure safety and reliability of hydrogen systems. Finally, through microscopic imaging of the samples, the author obtained important information regarding topography changes. Specifically, in this study the polymers exhibited the displacement of the polymer matrix along with the formation areas with an increased concentration of filler particles [56]. These results are similarly important since they provide evidence of migration of components and separation of phases within the polymer composite showing evidence of material degradation because of hydrogen exposure.

These results follow the trend set by other studies such as the study performed by Miaomiao Yang et al. aimed to evaluate the potential to reduce hydrogen induced degradation in NBR through the addition of novel vulcanization additives [59]. As previously explained, the microstructure of polymers including the presence of fillers and cross link density heavily influence hydrogen dissolution and diffusion [106]. Similarly, it has been shown that hydrogen molecules tend to accumulate at voids such as filler-polymer interfaces and regions of low cross-link density when polymers are exposed to high pressure hydrogen gas [51]. In this context, the interstitial properties of the filler particles and polymer aggregates become extremely important. Materials such as zinc oxide (ZnO) particles are commonly used as catalysts to increase cross-link density through vulcanization [107]. Vulcanization refers to the process in which chemical additives and heat are used to promote the formation of molecular bonds between polymer chains, forming cross-linked networks [108]. In this way ZnO particles are added during the fabrication process to improve the mechanical

properties of polymers such elasticity and aging resistance [102]. Nevertheless, in the case of hydrogen applications, ZnO creates a vulnerability in the polymer composite due to hydrogen accumulation at interstitial sites, eventually leading to blistering and crack propagation [59]. To overcome this limitation, alternative vulcanization additives have been investigated. These materials include nano-ZnO particles and zeolitic imidazoltane framework-8 (ZIF-8) which show promising characteristics for hydrogen applications such as high specific area, and multiple interaction sites that offer stronger bonding to the polymer matrix [109]. Hence, this study presents Metal-Organic Framework materials as an alternative to overcome current limitations in polymers designed for hydrogen applications.

To quantify the effect of the vulcanization additive, multiple material samples with different ZnO and ZIF-8 concentrations were manufacture by Yang et al. [59]. Hence, by fabricating the polymer compound the author ensures complete knowledge of the composition and limits the possibility of introducing unknown materials and interactions. Furthermore, by adding materials sch as silica, steric acid, and sulfur the materials created for this study resemble commercial formulations used in industry. Following the fabrication of the materials, samples were exposed to high purity hydrogen gas at a pressure of 70MPa for a duration of 24 hours [59]. In this case, the pressure and exposure time selected reflect the operating conditions of short-term hydrogen storage devices such as high-pressure tube trailers and ensure the dissolution and diffusion of hydrogen molecules through polymer samples. Following this, the pressure vessel was evacuated at a controlled depressurization rate, and the samples were analyzed to characterize the changes caused by hydrogen exposure. X-ray computed tomography and imaged in order to measure and characterize the size and distribution of internal voids before and after hydrogen exposure. In this case, the properties of x-rays and the absorption behavior of the materials were used to discern between the polymer matrix and the metal additives [59]. By using this imaging technique, the author categorizes the information obtained through imaging and allows the use of computational methods to calculate the size and distribution of voids in the matrix. This is particularly important since the analysis must avoid the inclusion of artifacts caused by differences in material phases, ensuring that only the areas of interest are counted. Through

this analysis the author concluded that ZnO particles showed relation to a significant fraction of the blisters and voids caused when compared to ZIF-8 particles [59]. In this way, the study provides evidence suggesting that the substitution of ZnO for alternative materials with the ability to create a stronger bond with the polymer matrix can result in increased resistance to hydrogen induced degradation. Furthermore, by using computational techniques and image analysis software the author was able to quantify the material degradation on both material types, thus providing an objective basis for comparing the performance of the materials.

Additionally, Yang et al. characterized changes to mechanical properties of the polymer samples. By measuring changes to properties such as tensile strength and hardness the author compared the effects of changes in the polymer structure due to hydrogen exposure. Through this analysis the author concluded that the inclusion of the MOF material ZIF-8 resulted in better retention of mechanical properties compared to ZnO [59]. In this regard, the improved interstitial bond of ZIF-8 seemed to influence the mechanical performance of the polymer supporting the results obtained through imaging. In this way, the process of exposing material samples to hydrogen gas under different conditions can be used to identify how hydrogen aging presents itself during the service life of components. This knowledge results crucial for the design of systems for handling hydrogen as well as for the development of safety standards and inspection procedures to ensure safety and reliability. Furthermore, by using this approach it is possible to observe how the damage on different materials changes over time, allowing for the development of predictive models, which can then be used for maintenance and safety guidelines.

2.5 Conclusion

As previously explained, one of the main challenges for the realization of hydrogen use as an energy carrier is material compatibility. By reviewing the different technologies and methods used for the transport and storage of hydrogen we can observe a pattern of physical and economic limitations. Example of these issues are the permeation leaks and losses through sealing elements in storage tanks. In these case, the effect of hydrogen embrittlement in

metallic components and the permeation through polymer materials becomes an essential problem to overcome. However, it is important to note that the negative effects of hydrogen assisted material degradation affect all of the components involved such as compressors, pipelines, and valves. Furthermore, the effects of hydrogen exposure on metallic materials and polymers are described in order to understand the underlying mechanisms. In this case, the permeation of gas molecules into the material structure, either through diffusion through the interatomic space of metallic lattices or through the free volume of polymers, are identified as the main factors driving hydrogen assisted material degradation. In this way, the importance of material compatibility for the development of hydrogen related technologies is highlighted.

CHAPTER 3: EXPERIMENT DESIGN FOR THE CHARACTERIZATION OF HYDROGEN ASSISTED DEGRADATION ON POLYMERS

Given that the degradation of material properties is a complex process influenced by multiple parameters such as temperature, pressure, and material imperfections, it would be beneficial to gain deeper insight into how this damage evolves over time. Moreover, given the high storage pressures and the cyclical nature of hydrogen storage systems, RGD failure and the mechanisms that govern it are of particular importance for the development of hydrogen use infrastructure. After analyzing the work of other scientists and identifying common aspects of the research methods employed, an experimental system to expose materials to high pressure hydrogen gas and evaluate changes on mechanical properties was developed. Figure 21 shows the schematic of the experiment methodology utilized. The obtained material samples were inspected and analyzed to establish baseline parameters. Following this, the material samples were exposed to hydrogen gas at varying pressures. The information gained from comparing the effects of continuous pressure conditions would be useful for evaluating the performance of materials according to different types of applications and components for hydrogen infrastructure.

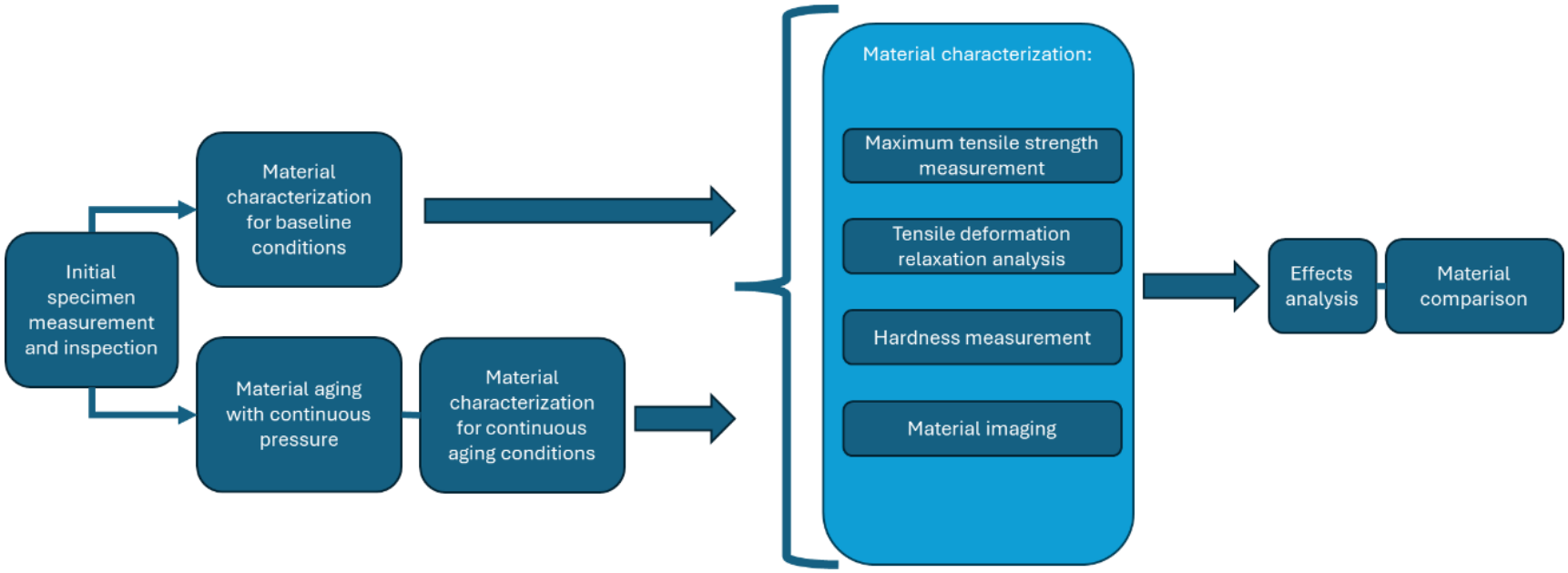


Figure 21: Schematic illustrating the experimental methodology used to compare the effects of exposure to high pressure hyfrogen gas on different polymer materials.

As previously discussed, one of the main objectives of this experimental design is to compare the effects of hydrogen exposure on commercial elastomers. Examples of these materials are EPDM and NBR as investigated by Theiler et al. and Yang et al. respectively. These materials are commonly used in the fabrication of sealing components and pipe liners due to their physical and chemical properties as well as due to their wide adoption in different industries [9]. Moreover, these materials are well characterized and have been studied due to their promising behavior when exposed to other fluids aside from hydrogen gas. The parameters selected for the controlled hydrogen exposure and material aging were based on different components and applications related to hydrogen storage and transport as described in chapter 2. Specifically, testing pressures ranged between 55 bar and 482 bar to reflect conditions such as those encountered by storage tanks, transport pipes, and dispensing valves in currently available hydrogen supply facilities [110]. The material samples used for this study were obtained from commercial suppliers such as Parker Hannifin Corp in the form polymer O-rings. This was done to ensure that the test results provide information useful for real-world industrial applications by reflecting the behavior of materials used for industry rather than idealized formulations. In addition, changes to mechanical properties were measured as a means of establishing an objective comparison of the effects of hydrogen exposure on the selected materials. Based on the previous work of scientists, the tensile strength and hardness of the materials was analyzed. Furthermore, the tensile relaxation behavior of the samples was investigated to determine changes to the behavior of the material. Lastly, microscopic imaging of the sample cross section was performed to characterize the changes to the morphology of the material due to hydrogen effects. The data collected was then analyzed through a statistical model to evaluate the impact of operating conditions and material differences on relative degradation.

3.1 Material selection

Three different materials were selected to compare the effects of exposure to hydrogen gas at high pressure: FKM fluoroelastomer, Acrylonitrile Butadiene Rubber (NBR) and Ethylene Propylene Diene Monomer (EPDM). The three different polymer compounds were selected as common representatives of materials used in the production of seals for multiple

industries. In this regard, these are well understood materials that have been developed for handling different types of chemical substances such as hydrocarbon fuels and acids, having been tested and proved over time in industrial applications. The materials were purchased as commercially available O-rings with a nominal hardness rating of 75A and size 214 with dimensions as shown in Figure 22.

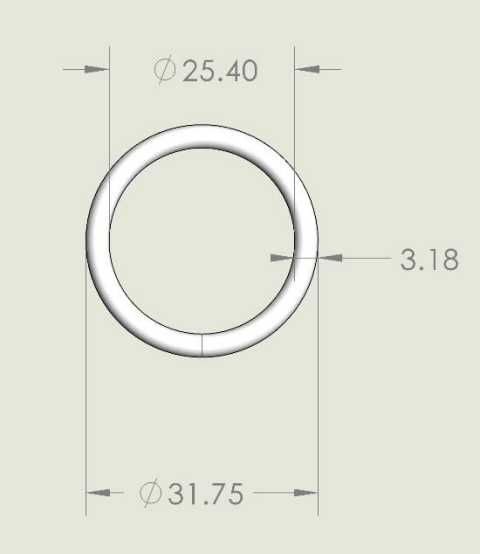


Figure 22: Diagram showing the dimensions in mm of the O-ring-214 specimens used.

Fluoroelastomers are attractive materials due to their capacity to withstand high temperatures in conjunction with their chemical resilience, being able to tolerate aggressive chemicals such as acids, fuels, and petroleum-based lubricants [111]. Fluorocarbon-based rubber (FKM) compounds are typically utilized in the aeronautical industry due to their exceptional chemical and thermal resistance and recently has drawn significant interest from the hydrogen community for various hydrogen applications, however there exists little data evaluating its hydrogen compatibility [112]. The molecular structure of FKM polymer is primarily composed of chains of carbon and fluorine along with other specific monomers such as hexafluoropropylene and tetrafluoroethylene selected depending on the application as shown in figure 23 [113]. The relative sizes of carbon and fluoride atoms, as well as the ratio between both elements, results in a material with low free volume and high cohesiveness, giving fluoroelastomers positive characteristics that aid in hydrogen

resistance. Furthermore, crosslinking methods such as peroxide and bisphenol curing aid in the formation of additional bonds that increase the mechanical properties of the material [113]. Overall, these characteristics allow the material to exhibit beneficial properties for the handling of pressurized hydrogen gas due to resistance to gas dissolution and rapid decompression damage [67]. Nevertheless, material degradation and other characteristics of the interactions with pressurized hydrogen gas still present challenges, particularly at elevated pressure. In this case, the specific material tested was Viton 75A provided by DuPoint-Dow. This material has an industrial designation of ASTMD2000-01 M6HK810 A1-10 B38 C12 C20 EF31 EO88 F15 detailing the material type as commercial FKM compound with specific mechanical properties such as hardness, tensile strength, resistance to swelling, among others [114].

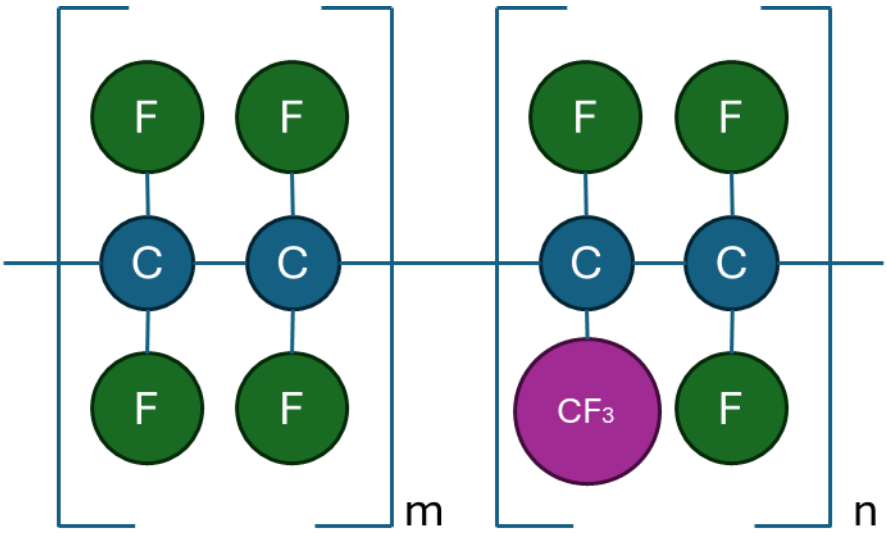


Figure 23: Fluoroelastomers base chemical structure showing the C-F bond backbone that contributes to the material properties.

Similarly, Ethylene Propylene Diene (EPDM) rubber has shown promising characteristics for the operation with pressurized hydrogen gas, particularly its properties at low temperatures and sealing capacity [58]. Nevertheless, EPDM still presents the typical limitations for operation in the form of blistering and gas leakage. This material is composed primarily by

repeating units of ethylene and propylene. In this case, the molecule contains a stable carbon chain as the backbone along with ethylene norbornene or dicyclopentadiene as the diene component that introduces unsaturated sites beneficial for polymer crosslinking as shown in figure 24 [115]. This molecular structure results particularly beneficial due to its saturation, providing the material with exceptional resistance to aging due to ultraviolet radiation and ozone [116]. In this case, the specific material selected was EO603-70 provided by Parker Haniffin Corp with an industrial designation ASTM D2000 M4CA710 A25 B35 EA14 [117].

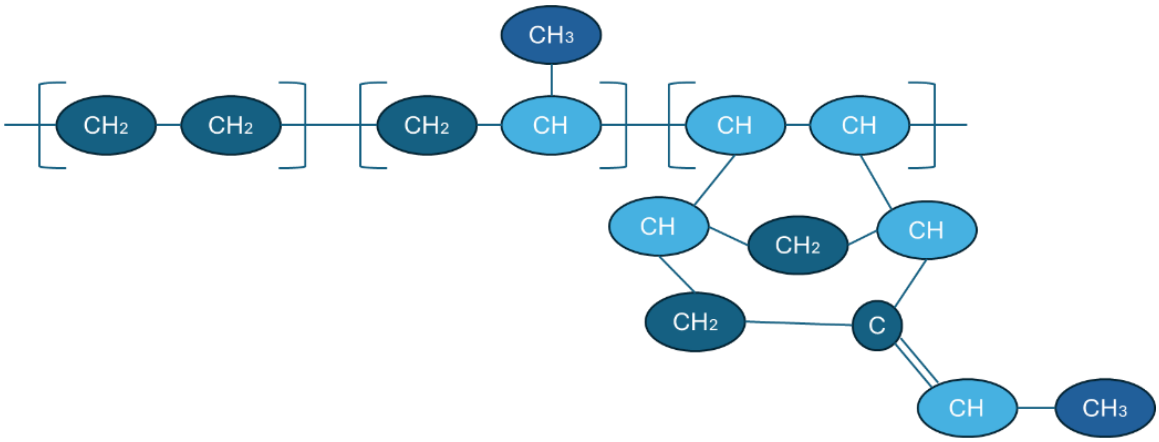


Figure 24: Molecular structure of EPDM showing the carbon backbone along the diene component.

In contrast to fluoroelastomers, EPDM has a relatively long and flexible chain structure that results in a higher fraction of free volume within the polymer matrix. While these characteristics of the molecular structure result in a material with higher crosslinking and resistance to environmental degradation, it is more susceptible to hydrogen permeation and the consequent RGD damage. Specifically, the non-polar network formed by the inclusion of the diene component provides resistance against bond cleaving, giving the material good resistance to chemical changes and mechanical damage. However, free volume created along with the non-polar nature of the matrix, allows for higher hydrogen solubility and transportation within the material through diffusion, leading to an increased likelihood of cavity formation and volumetric swelling when exposed to high pressure hydrogen gas [50].

Another property derived from the polymer structure is the relatively low tensile strength and high maximum deformation, nevertheless this beneficial characteristic of the material ca also be altered by hydrogen induced degradation of the cross-linked network as well as the formation of blisters within the polymer matrix. Nevertheless, the mechanical and chemical properties of EDPM materials can be enhanced through the use of filler particles such as Carbon Black and Metal-Organic Framework particles [48].

A third material that was analyzed was Nitrile Butadiene Rubber (NBR) due to its common use in the fabrication of sealing components such as O-rings and piston seals. This material has especially high resistance to abrasion and tearing coupled with a relatively low manufacture price and adequate resistance to solvents and oils [118]. This material is formed by the copolymerization of acrylonitrile and butadiene. In this molecule, shown in figure 25 carbon atoms serve as a backbone with the acrylonitrile group determining the polarity and mechanical properties of the material. In this molecule, the charges of the nitrile groups (CN) along the molecule create attraction forces that increase the stability of the matrix and reduce mobility of the polymer chains. Furthermore, this molecular structure results in a matrix with relatively low free volume, which in turn results in low gas permeability. The specific material used was NBR70 with an industrial designation of ASTM D2000 M2BG714A14B14EA14EF11EO14 provided by McMaster Carr.

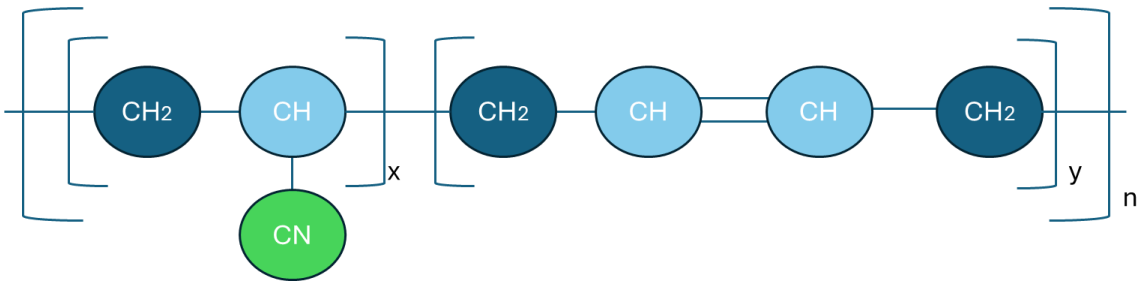


Figure 25: Molecular structure of NBR highlighting the two copolymers used for the fabrication of the material.

An important characteristic of this material is that the ratio between the monomers can be changed to affect the material properties [119]. In the case of higher concentrations of

acrylonitrile, NBR tends to have a higher resistance to gas permeability while increasing the elastic modulus and the glass transition temperature of the material. In this regard, NBR shows a relatively higher tensile strength when compared to EPDM at the cost of a lower maximum elongation. On the other hand, lower concentrations of acrylonitrile are more flexible, sacrificing chemical resistance. Nevertheless, the presence of polar sites along the molecular structure tends to increase hydrogen sorption and accumulation within the matrix during pressurization and depressurization [50]. This can result in the propagation of blisters caused by RGD as well as swelling of the material and decomposition due to stress related effects [120]. While improvements to the material and a better understanding of the mechanisms that govern hydrogen induced degradation are necessary, these qualities make NBR a promising material for hydrogen service.

While the different characteristics of the materials presented have made them attractive options for the fabrication of components and seals designed for pressurized hydrogen gas service [48] [49]. Nevertheless, further research is needed to develop materials with less propensity to failure through material degradation and hydrogen permeation [59]. Table 1 presents a summary of the main mechanical properties of these materials. From comparing some of the basic mechanical properties of the material, it is possible to identify key differences such as density and elongation percentage at break. While the measured hardness has a relatively close value for the three material samples, their ability to stretch presents a stark difference. Similarly, the measured compression set varies for the materials, highlighting key differences in the way they respond to mechanical factors. Thus, by comparing these materials, it would be possible to identify key characteristics that allow them to withstand the effects of pressurized hydrogen gas.

Table 1: Mechanical properties of common polymers used for hydrogen [121], [122], [123].

Material	**Hardness (shore A)**	**Elongation at break (%)**	**Tensile strength (MPa)**	**Specific gravity (g /cm3)**	**Compression set (%)**
FKM	75	175	14	1.85	22
NBR	73	238	14	1.22	9.9
EPDM	75	418	11.8	1.31	13.9

3.2 Controlled exposure to high pressure hydrogen gas

As previously described, storage vessels for hydrogen gas are designed to handle pressures up to 700 bar [8]. This aspect of their operation creates the conditions for hydrogen induced material degradation on elastomer components such as storage tank liners and valve seals. Additionally, parameters such as exposure time, temperature, and pressure heavily influence the solubility and diffusivity of hydrogen gas through polymer materials [31]. Furthermore, due to the high pressures used for storage and transport of hydrogen gas and the exposure to charging and discharging cycles at varying decompression rates, Rapid Gas Decompression (RGD) failure can further enhance the damage observed on sealing components [29]. With these aspects in mind, as well as limitations of the equipment available, the samples selected were exposed to pressures ranging from 55 to 482 bar for a period of 200 hours to simulate operating conditions. This pressure range represents both the typical conditions for the use of gaseous H2 as well as its storage in high pressure tanks [9]. Hence, this pressure range is sufficient to analyze pressure dependent changes in polymer materials induced by interactions with hydrogen gas. Similarly, the exposure period was selected based on the previous work of scientists to ensure that hydrogen was able to permeate the material and generate significant changes [48]. To achieve this, a stainless-steel high-pressure vessel fitted with control valves, pressure and temperature sensors, and gas detection units were utilized. Figure 26 shows a schematic of the system used to expose the material samples to high pressure hydrogen gas, highlighting the main components. This experimental system used current standards on hydrogen equipment such as those

developed by ASTM International, as well as recommendations from hydrogen equipment manufacturers in order to ensure safety and reliability. This system included the capacity to flush the reactor vessel with nitrogen gas to prevent contamination of the material samples. Additionally, a remote-control system was implemented to prevent physical interaction between the researchers and the pressurized reactor vessel. The safe operation of the aging system was assured through the use of pneumatic and solenoid valves as well as hydrogen detection equipment. Extensive preparations and design considerations were taken into consideration to ensure that the experimental system would be able to provide consistent results while maintaining the safety of researchers and the equipment as the main priority. To this end, the component selection and installation for the experimental system were made based on recommendations from manufacturers. Components such tubing, fittings and valves made from annealed AISI 316 stainless steel alloy were selected due to their resistance to the damaging effects of exposure to hydrogen gas [70]. These components were rated for operation with pressures up to 4,000 bar and represent a cost effective for the realization of this study. For this application, conical metal-to-metal seals were employed for transport and control of the hydrogen gas between components. These components were carefully inspected after each experiment to maintain safety and prevent leakage of hydrogen gas due to degradation of the materials.

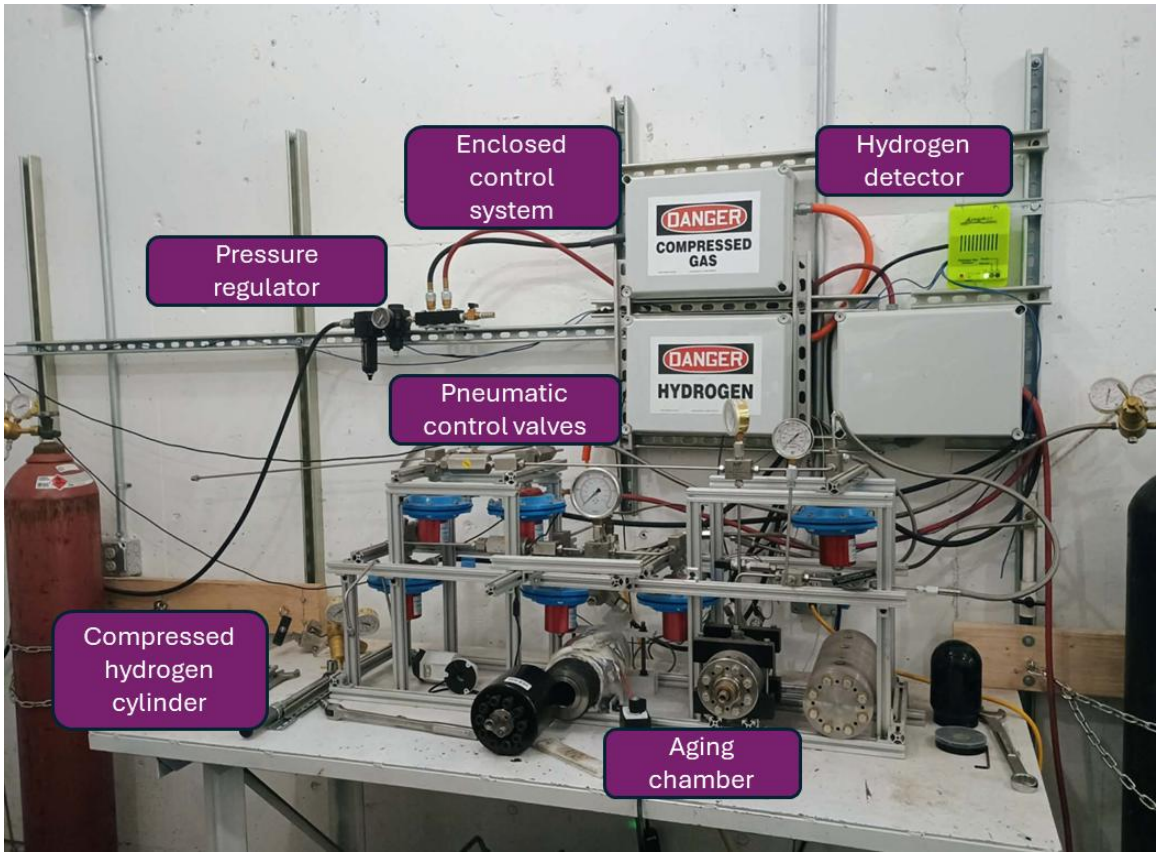


Figure 26: Experimental system used for control exposure of material samples to high pressure hydrogen conditions.

High purity Hydrogen gas supplied from a compressed gas cylinder to prevent the ingress of contaminants or foreign substances. The gas was supplied at a pressure of 70 bar to an air driven pressure booster used to control pressure conditions to which the material samples were exposed to. A set of pneumatic control valves allowed for flushing of the aging chamber with nitrogen gas followed by introduction of hydrogen. This flushing step was crucial to prevent ignition of hydrogen gas due to the presence of oxygen [32]. Similarly, the use of pneumatic valves allows remote operation with the intention to isolate the operator from the system as well as reducing the risk of sparks and heat related to electronic control devices, ensuring safety [28]. Furthermore, the valves, pressure lines, and pressure vessel are designed to withstand pressures up to 4,000 bar due to their annealed stainless-steel construction and the utilization of high-pressure metal-to-metal seals to prevent gas leakage while aging the test samples. The selection of materials for the construction of the

experimental system was based on compatibility with hydrogen gas. Similarly, metal-to-metal sealing barriers were selected due to their ability to withstand high pressures under static conditions [124]. All of the components were inspected before and after exposing the material sample to hydrogen gas in order to ensure safety. Figure 27 shows a schematic of piping and instrumentation integrated as part of the controlled hydrogen exposure system.

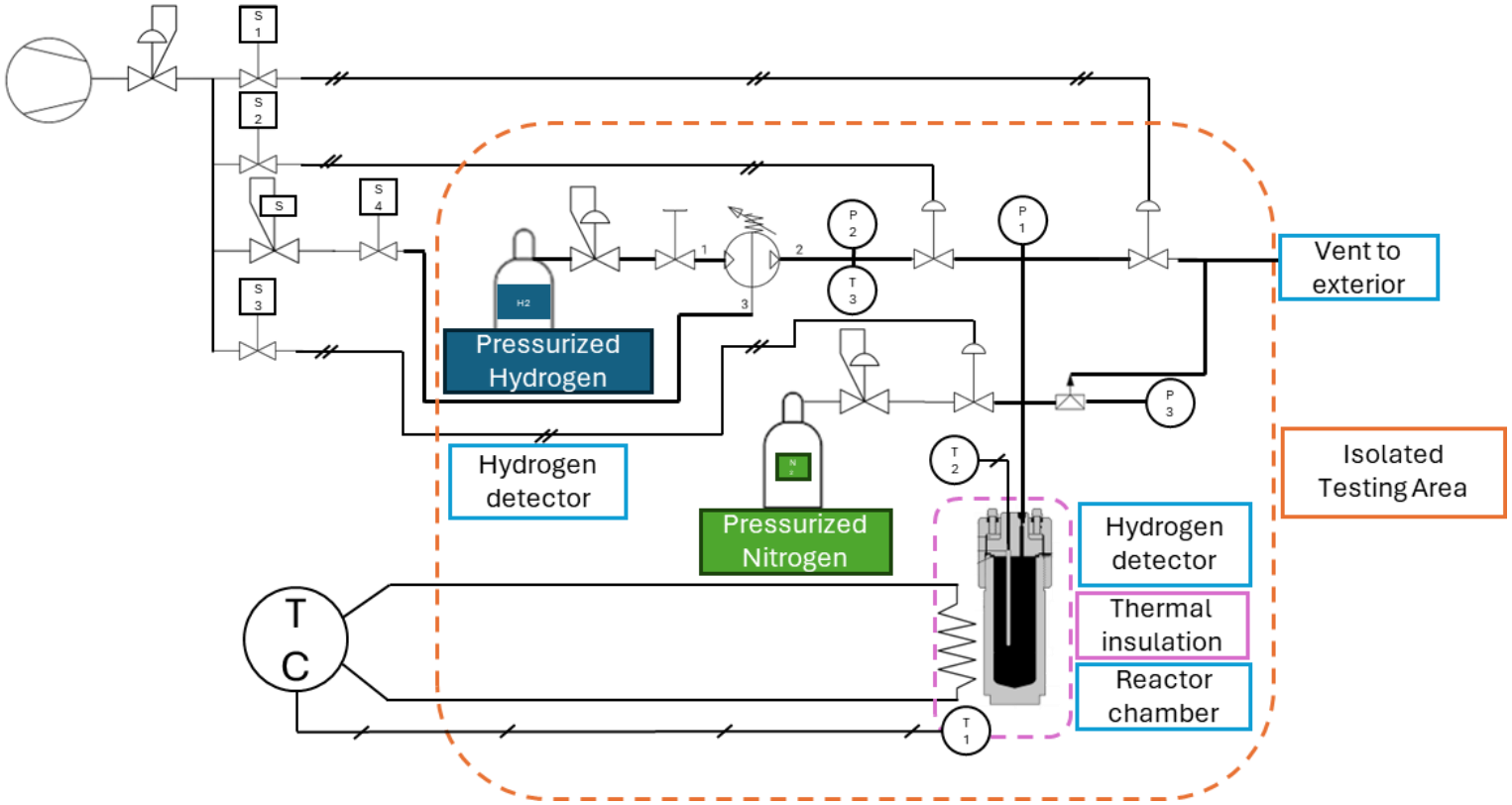


Figure 27: Schematic diagram showing the main components and instrumentation used to control the hydrogen environment parameters for exposure of material samples.

The aging chamber counted with separate ports for hydrogen gas inlet and for temperature measurement. Similarly, a safety rupture disk and a venting system to allow gas to escape out of the building were included. To ensure safety, a hydrogen detection system was installed to monitor the gas concentration next to the testing system as well as inside the building. In case of detecting a significant gas leak, the pressurized gas would be vented to the exterior of the building, and the components would be isolated from each other. Furthermore, the pneumatic control of the system allows for remote operation and limits the generation of heat and sparks associated with electronic components, thus allowing for safe operation during the hydrogen exposure phase of the experiment. After the chamber was filled with hydrogen, an air driven pressure booster was used to elevate the internal pressure of the aging chamber according to the test matrix. Pressure was automatically monitored and maintained through the use of electronically controlled solenoid valves and pressure regulator. These control components were programmed to increase the hydrogen pressure in case the vessel pressure fell more than 4 bar below the prescribed point, accounting for gas leaks during the aging period. An electric heater and a PID controller were used to ensure the temperature conditions were identical between experiments. Figure 28 shows a schematic of the control logic implemented for the hydrogen aging exposure system used to control the exposure conditions of the material samples. The automatic control logic was programmed using the LabView environment provided by National instruments. This software was used to integrate the different sensors described for data acquisition along with an electronic control interface. In this way, the experimental system allowed for the monitoring, control, and recording of data during the exposure of polymer samples to hydrogen gas.

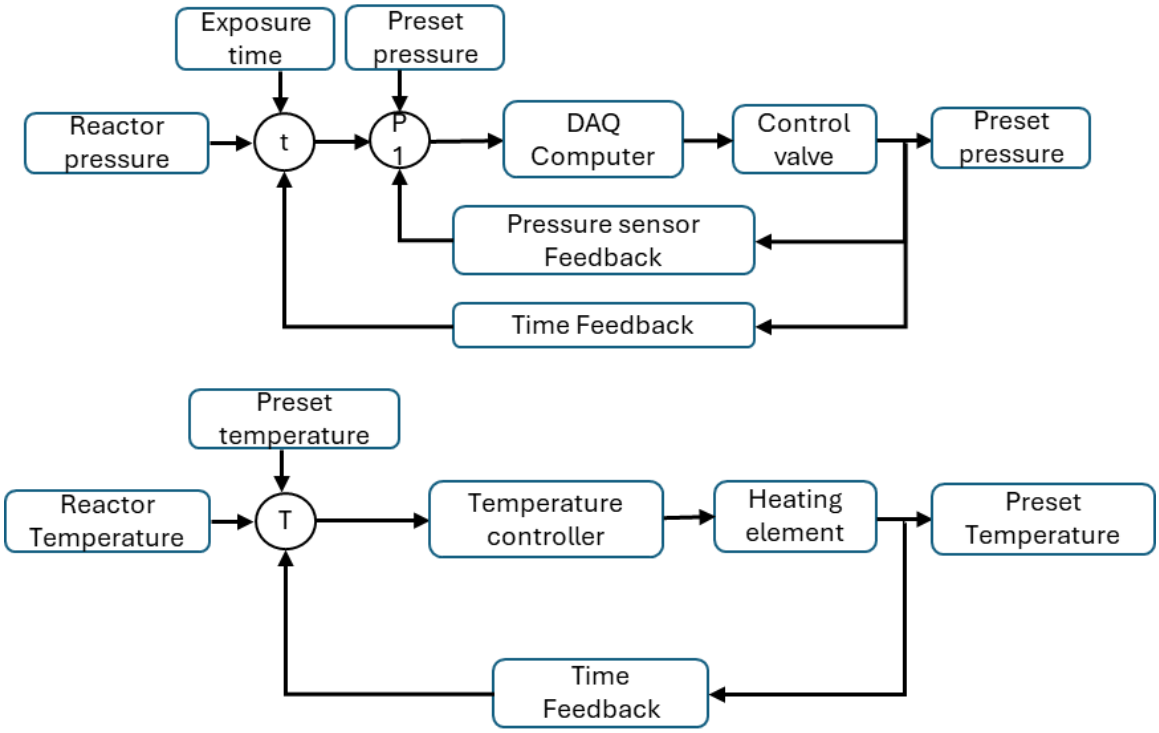


Figure 28: Block diagram illustrating the control logic used to automate the pressure control system during exposure of material samples to high pressure hydrogen gas.

Through the investigation of current industrial standards and practices on the handling of hydrogen gas, the experimental system was able to provide a safe and reliable way of performing this study. Through the use of suitable materials and components, the experimental system was able to operate at a wide range of pressures. Similarly, the effect of temperature-driven variations was minimized by the implementation of an automatic heating control system. Furthermore, the implementation of a remote-control system guaranteed the safety of researchers when handling the high-pressure aging of material samples. Dangers to the users were minimized by isolating the system, mitigating the hazards associated with hydrogen as well as the risks presented by pressurized gases. In addition, the application of an automated control logic for the monitoring of the exposure pressure ensured consistency between experiments along with enhanced reliability by correcting the losses in pressure expected due to hydrogen permeation through the reactor vessel and control valves. Lastly, the adoption of preventive maintenance practices ensured

the continued function of the system without encountering incidents that could compromise the safety of the research team or the test equipment.

Prior to exposure to hydrogen gas, the material samples were subjected to an initial inspection and preparation to ensure eliminate the effects of visible manufacturing effects on the data collected. Following this, the aging fixture and sample holder were cleaned using alcohol and allowing time for it to evaporate. This step was crucial to prevent the ingress of contaminants that could influence the behavior of the polymer samples as well as to prevent damage to the reactor vessel. The aging of the test specimens was performed by exposing the material samples to continuous pressure for 200 hours. For this, the vessel was charged, and the hydrogen gas was allowed to permeate into the samples for 200 hours followed by a single depressurization event. These tests were performed at an ambient temperature of 25 C. Table 2 shows the experimental matrix completed highlighting the different parameters to which the samples were subjected.

Table 2: Summary of the aging parameters employed.

Material	**Group**	**Exposure pressure (bar)**	**Temperature (C)**	**Duration (hours)**
FKM *NBR* *EPDM*	1	55	25	200
	2	69		
	3	138		
	4	345		
	5	415		
	6	428		

After the material samples were exposed to the pressured hydrogen gas, the changes in mechanical properties were measured and used to compare the degree of degradation caused by the absorption and desorption of the hydrogen gas into the polymer matrix. The changes to mechanical properties were quantified through tensile testing, tensile relaxation analysis, and hardness measurement. Additional analysis of changes in sample morphology

was performed using optical microscopy. In this analysis, the number of circular voids and cavities, as well as their size and distance from the edge of the sample was measured. The following section describes in detail the measurements and calculations used to characterize the changes to the materials after hydrogen exposure.

3.3 Material characterization approach and methods

As described in Chapter 2, exposure to hydrogen gas can alter the mechanical behavior of polymers through different correlated mechanisms. One of the most prominent effects observed is material swelling caused by hydrogen permeation and absorption into the polymer matrix. In this case, the hydrogen molecules diffuse through the polymer network occupying the free volume between carbon chains. Following this, the pressure gradient causes internal stress and the macroscopic expansion of the material. Then, during depressurization, these internal stresses can overcome the intermolecular forces holding the polymer network leading to the formation of voids and cracks [29]. In addition, the presence of hydrogen molecules though the polymer network can lead to decrease attraction between polymer chains, causing a plasticizing effect and facilitating molecular mobility [53]. In this way, exposure to hydrogen gas can lead to physical changes such as changes in density, crosslink reorganization, phase separation, and changes in hardness following decompression.

In this regard, the aim of the measurements performed on the material specimens was to establish a systematic evaluation of the changes to the materials due to hydrogen exposure. To achieve this, aspects such as tensile deformation behavior, mechanical response, and material morphology were investigated and characterized following the exposure of different polymer materials to hydrogen gas pressurized to different levels. Furthermore, this study aims to compare the level of hydrogen induced degradation of different materials exposed to comparable conditions. This information would then be used to establish a link between material characteristics and the degree to which these property changes occur. To quantify the effects of hydrogen exposure, different properties of the obtained samples were measured before and after aging under pressurized hydrogen gas, establishing a basis for

quantifying changes to the condition of the tested materials. These tests included tensile testing to measure stress at different deflection points, the relaxation of the material for a given deflection, as well as the ultimate tensile stress. Similarly, a 5mm slice was obtained from the O-rings specimens and used to measure the hardness of each material for the tested conditions. Finally, light microscopy was used to characterize the morphology of a typical cross section of the sample allowing to quantify the presence and distribution of vacancies within the polymer matrix. Figure 29 shows a summary of the methodology used for the characterization of the materials tested.

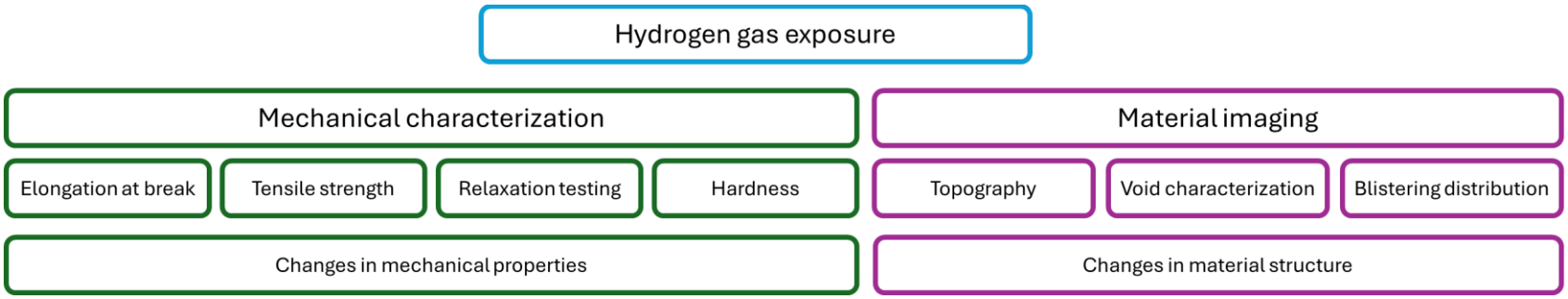


Figure 29: Summary of the methods used for characterizing material changes produced by hydrogen exposure on polymer sealing materials.

Through tensile testing, it was possible to quantify and compare the changes in the stress response when the materials are deformed. The elongation at break and tensile strength of the material samples was measured and characterized. Similarly, the material relaxation under a specified deformation was investigated. Changes to the tensile behavior of these materials are particularly important for barrier applications such as O-rings as the sealing mechanism relies on a known deformation response of the material [94]. Hence, the changes to the tensile behavior of the materials analyzed caused as a result of hydrogen exposure can be analyzed in a systematic way to compare the degree of material degradation of the samples exposed to pressurized hydrogen gas. Additionally, by analyzing the measured hardness of the material samples investigated it was possible to compare the wear resistance before and after hydrogen exposure. This is particularly important in applications where motion along sealing elements is involved such as in valve stem seals. Consequently, the information obtained would then be applied within the context of polymer selection and development to improve the current understanding of failure modes in sealing components specifically designed for hydrogen service.

The observed changes in deformation response would then be explained through hydrogen assisted aging mechanisms such as matrix displacement, filler redistribution, and structural changes in the materials. In this way, imaging of slices obtained from the material specimens enables another way to quantify the change occasioned by hydrogen gas accumulation within the material. Specifically, the topography of the material can be characterized by analyzing the distribution of imperfections and voids within the polymer matrix. These imperfections can then be characterized as blisters caused by hydrogen dissolution and diffusion through the polymer followed by rapid depressurization. Lastly, the size and distribution of these structural changes can be quantified to compare the degree of material degradation. Thus, the information obtained through material imaging can be used as supporting evidence to explain changes in mechanical properties.

3.3.1 Tensile strength testing

One of the most noticeable effects of exposure to high pressure hydrogen in elastomer materials is the formation of voids and blisters [59]. In addition, the displacement of the

polymer matrix due to the permeation of hydrogen molecules can cause changes to the mechanical properties of the material such as elastic modules and ultimate tensile stress [56]. These changes affect how the material would respond to external forces and must be taken into consideration when designing materials specifically for use with hydrogen gas. Hence, as a way of comparing the effects of hydrogen exposure and depressurization, measurements of the elastic modulus, relaxation setting, and ultimate tensile stress were performed on the samples. These measurements were taken in accordance with the ASTM D1414 standard that describes the tensile testing for O-rings [125]. Figure 30 shows the testing apparatus used illustrating the servomotor and linear actuator, the load cell, and the spool motor that constitute the main components of the machine. A servomotor outfitted with a linear actuator was used to control the strain applied to the polymer specimens. A load cell transmitter was used to measure the force applied to cause the deformation. A specimen holder consisting of two spools was then used to secure the O-rings during testing.

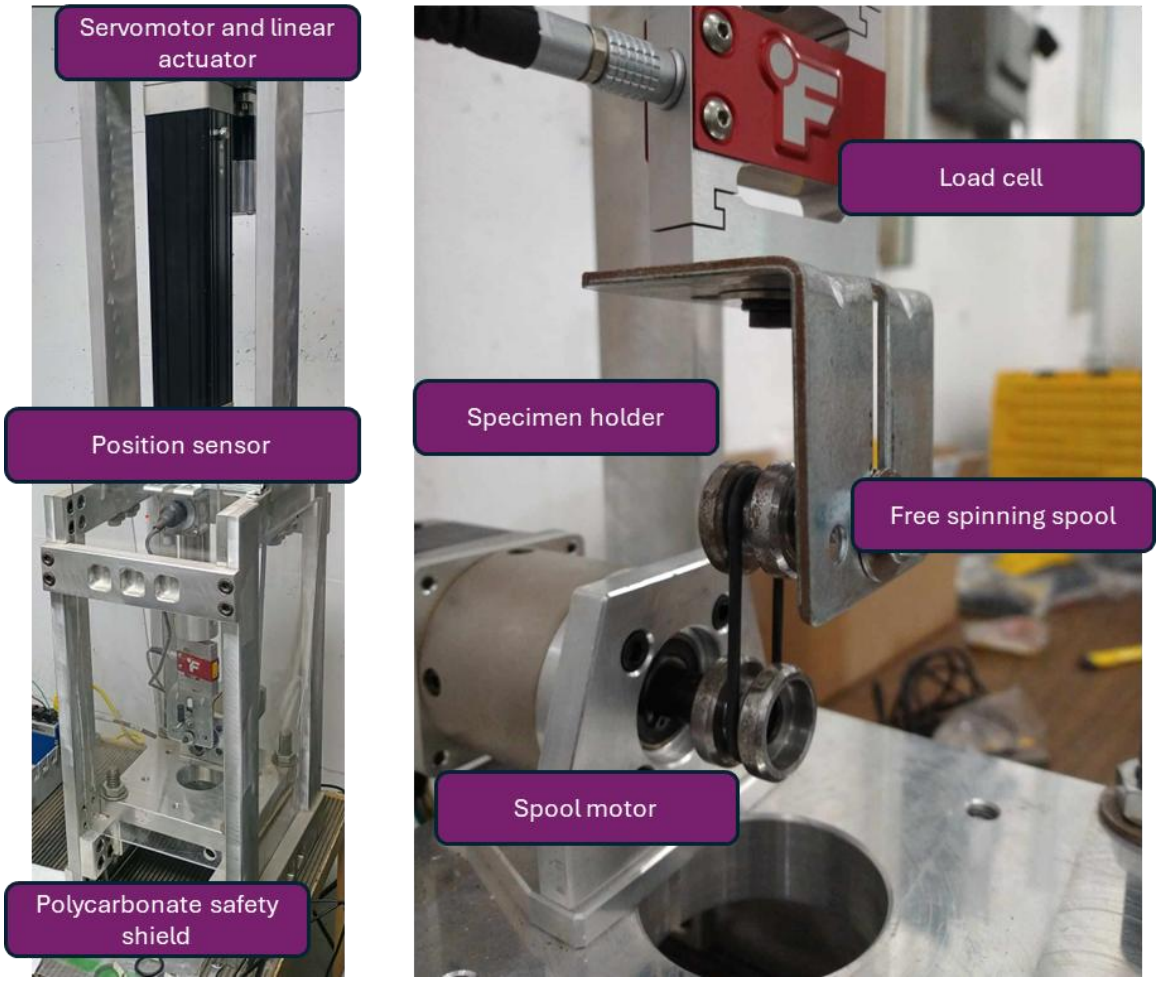


Figure 30: Experimental apparatus used to investigate the tensile behavior of the sample O-rings illustrating the main components.

For these measurements, the sample and room temperature were maintained at 23±2°C in order to eliminate temperature effects from the measurements. Similarly, the spools used to hold the samples during testing were designed with a diameter of 50 mm to be placed at an initial distance of mm, minimizing the initial stress on the samples. Additionally, the top spool was fitted with a radial bearing while the bottom spool was mounted on a motor programmed to rotate one revolution per 150mm of travel to minimize uneven stress in the sample due to deformation of the polymer. These components were controlled through a computer interface allowing for automatic data collection.

The specimen was measured at four different points to characterize the cross section and then it was loaded to the testing mechanism. The initial specimen preload was measured and ensured to be less than 0.1 N, similarly, the initial deformation was set to be less than 0.2 mm. Following this, a continuous strain rate of 0.5 mm/s was applied to the material specimen until rupture of the polymer O-ring occurred. The raw data obtained from the tensile testing procedure consisted of force and deformation data along with time. This data was then processed to remove artifacts associated with the methodology such as initial zero or negative values corresponding to the sample preload. Similarly, data recorded after specimen breakage was eliminated from the analysis. Following the preprocessing stage the data was trimmed at the maximum force value to characterize specimen rupture. The maximum force measured and deformation at the moment of rupture were recorded for each specimen tested. Following this, the tensile strength of the material was calculated using the cross-sectional area as shown on equation 1 to account for the total area of the sample. Similarly, the elongation at rupture was calculated using the initial inner diameter of the O-ring specimen as shown on equation 2 [125].

$$T = \frac{F}{0.785}\, w^2 \tag{1}$$

Where:

F = Force at specimen rupture

W = Axial thickness for O-ring sample

$$Ultimate\ elongation\ \% = \left[\frac{(2D+G-C)}{C}\right] 100 \tag{2}$$

Where:

D = Distance between the center of the spool at specimen rupture

G = Circumference of the sample holder spool

C = Inside circumference of the O-ring prior to deformation

Multiple specimens were tested for each aging regime in order to provide statistical significance. The material response was then presented as the mean value measured for a given specimen condition. Similarly, variability within specimens was quantified through the standard deviation calculated within the sample. Figure 31A shows the baseline tensile strength, and Figure 31B shows the deformation at breakage measured for the selected materials prior to exposure to hydrogen gas.

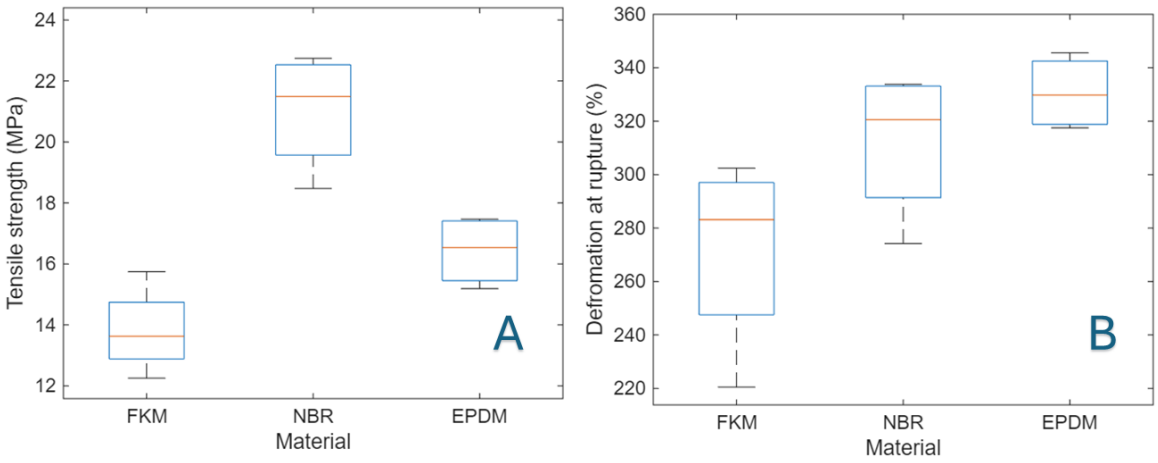


Figure 31: Tensile strength and deformation at rupture measured for the materials investigated prior to hydrogen exposure.

3.3.2 Tensile relaxation analysis

While the tensile strength and maximum deformation of polymers are important characteristics, the deformation properties before failure of the material are critical for the sealing performance of components such as gaskets and O-rings. Specifically, the reaction force that causes the sealing effects is dependent on the elastic modulus and structure of the material. Changes to the behavior of the material due to hydrogen exposure could cause changes to the stiffness of the polymer, thus affecting the sealing performance. In addition, changes to material properties could cause seals to be extruded into gaps, further compromising the sealing effect and potentially leading to leakages [102]. Hence, understanding the deformation behavior outside from the limits becomes important for the design of polymer components for service with hydrogen gas.

To this end, the relaxation of the material under a known deformation was investigated. To achieve this, a fixed deformation of 10 mm was applied to the specimen, measuring the tensile response of the material and allowing time for relaxation of the specimen until a continuous force value was observed. This was repeated at even intervals of 10 mm to characterize changes to material response as a function of hydrogen exposure and deformation level. The data obtained was divided according to the specimen deformation to allow comparison between different aging pressure effects. Furthermore, to allow better comparison, the force, deformation, and time data measured was normalized with respect to the rupture point of the specimen. The normalization of the data allows us to ignore the absolute magnitude and testing time without affecting the deformation and failure response, highlighting the pressure related aging effects using a dimensionless basis appropriate for all materials. Equations 3 through 5 show the mathematical operations employed to process the data. Similarly, equations 6 and 7 show the operations used to calculate the mean and standard deviation of the values measured.

$$F_{normalized}(t) = \frac{F(t)}{F_{max}} \quad \text{Eq (3)}$$

$$\delta_{normalized}(t) = \frac{\delta(t)}{\delta_{max}} \quad \text{Eq (4)}$$

$$t_{normalized}(t) = \frac{t}{t_{max}} \quad \text{Eq (5)}$$

Where:

$F(t)$ and $\delta(t)$ represent the force response and measured deformation as a function of time.

F_{max} and δ_{max} are the maximum force and deformation measured at specimen rupture.

t_{max} represents the time of specimen rupture at which F_{max} and δ_{max} are measured.

$$\overline{x} = \frac{1}{n}\sum_{i=1}^{n} x_i \quad \text{Eq (6)}$$

$$\sigma = \sqrt{\frac{1}{n-1}\sum_{i=1}^{n}(x_i - \overline{x})^2} \quad \text{Eq (7)}$$

Where:

$\overline{x}$ denotes the mean value

σ indicates the standard deviation

As previously discussed, the way the material responds to a prescribed deformation is closely related to its structure. This is particularly true for polymer-based materials and includes aspects of the macrostructure, such as the presence of cavities and cracks, as well as the microstructure in the case of molecular crosslinks. In this way, being able to predict how materials respond to forces and deformations is crucial for the design of polymer components, particularly in applications such as hydrogen service where there are high risks involved. In this way, by characterizing how a material reacts to known deformations can provide useful information. Furthermore, by characterizing how this reaction changes as a consequence of exposure to hydrogen gas it is possible to better understand the constraints for the application of different materials depending on their specific function. Figure 32 shows a summary of the relaxation behavior for the materials investigated prior to exposure to hydrogen gas. From this analysis we can learn how the material behaves when a load is applied to it. The relaxation of the specimen can then be understood within the context of the polymer matrix structure and the internal forces holding the material together. Then, changes to material relaxation can then be explained through structural changes within the polymer such as the introduction of internal stresses and altered molecular bonds.

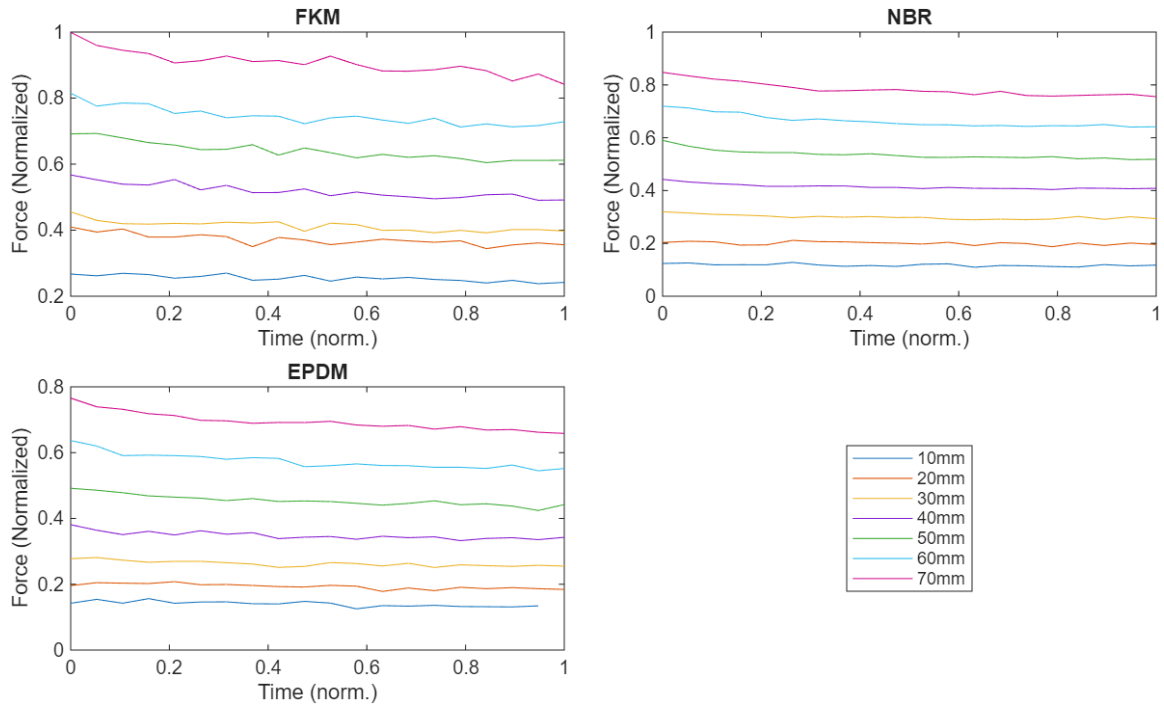


Figure 32: Relaxation behavior of the materials investigated prior to hydrogen exposure for different deformations.

The change in force measured during the relaxation period at each deformation level was then recorded and used to compare the effects of hydrogen exposure for the different materials. The maximum and minimum force measured at each deformation level were used to calculate the change in force due to relaxation of the material. The calculated force change was then normalized with respect to the calculated tensile strength of each specific material hydrogen exposure condition as shown in equation 8.

$$F_{relax} = \frac{F(t=0) - F(t=30)}{F_{max}} * 100 \qquad \text{Eq (8)}$$

Where:

F_{relax} indicated the Force relaxation

$F(t = 0)$ denotes the force at the start of the relaxation period

$F(t = 30)$ signifies the force measured at the end of the relaxation period

F_{max} means the tensile strength calculated for the material aging condition

Figure 33 shows a summary of the baseline tensile relaxation behavior observed for the materials prior to hydrogen exposure. In this case, each bar represents the change in the measured force as a result of material relaxation, normalized with respect to the maximum force measured for each material at each deformation level. From this figure we can appreciate that the tension in the NBR material tends to decrease by a smaller percentage compared to the FKM and EPDM materials for most of the deformation steps except for the cases where 50 mm and 60 mm were applied. Similarly, we can observe the different trends between the materials. While FKM appears to have a relatively consistent relaxation percentage, NBR and EPDM show an increase as the deformation magnitude increases.

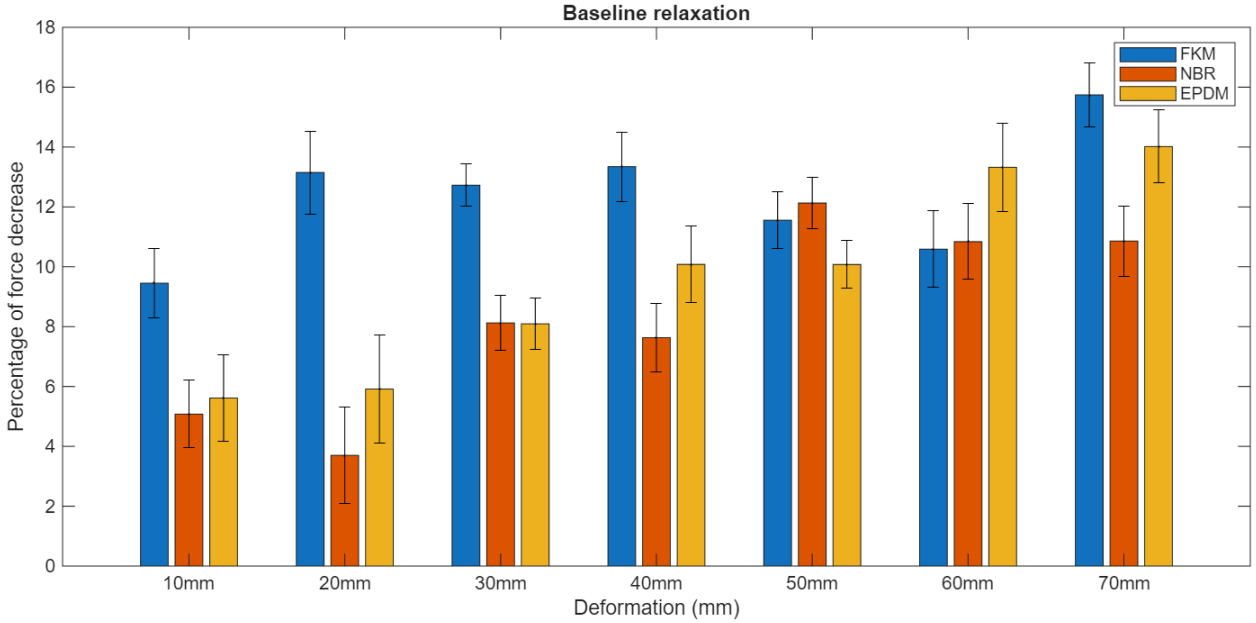


Figure 33: Bar chart comparison of the materials tested showing the tensile relaxation for different deformation levels before hydrogen gas exposure.

3.3.2 Hardness measurement

In a similar way, hard measurement of the material samples was performed in order to investigate changes to wear resistance due to hydrogen exposure and structural changes. These measurements were performed according to the Standard Test Method for Rubber Property – Durometer Hardness published by ASTM international. The test is based on the response of the material to indentation by a tip with a specific shape and a known hardness

[126]. In this case, a type A indenting tip was used in order to maintain consistency with the data provided by the material samples manufacturers. Figure 34 shows the durometer apparatus used to characterize the materials investigated in this study.

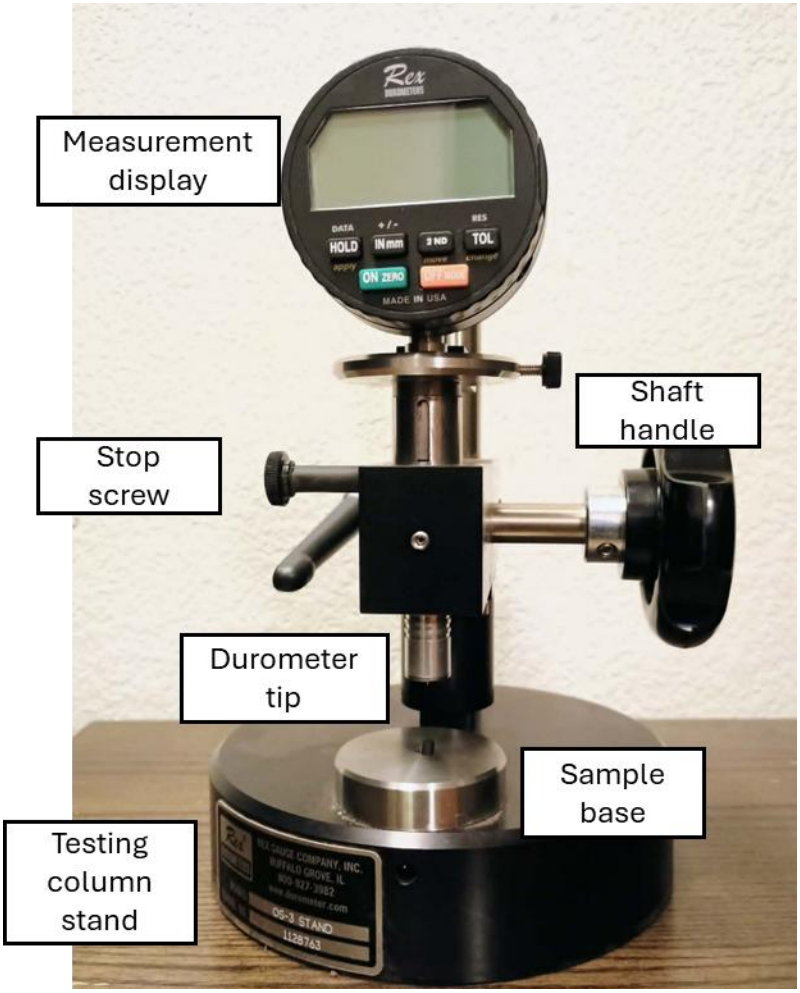


Figure 34: Durometer and stand used during the characterization of materials highlighting the main components of the system

Once the measuring apparatus was prepared, five slices with a thickness of 6mm were cut from the tested sealing elements at random positions within the circumference. The specimens were inspected and measured in order to ensure consistency. Following this the polymer slices were placed on the durometer stand and aligned with the pressing tip. The scale of the instrument was then zeroed, and the presser tip was lowered, compressing the material. The material hardness at the slice cross section was then measured and recorded

at the time of indentation. The hardness was then presented as the calculated mean obtained from the multiple specimens tested for each aging condition. Additionally, the standard deviation for each aging regime was calculated to illustrate variability. Figure 35 shows a summary of the baseline hardness for the investigated materials measured prior to exposure to hydrogen gas.

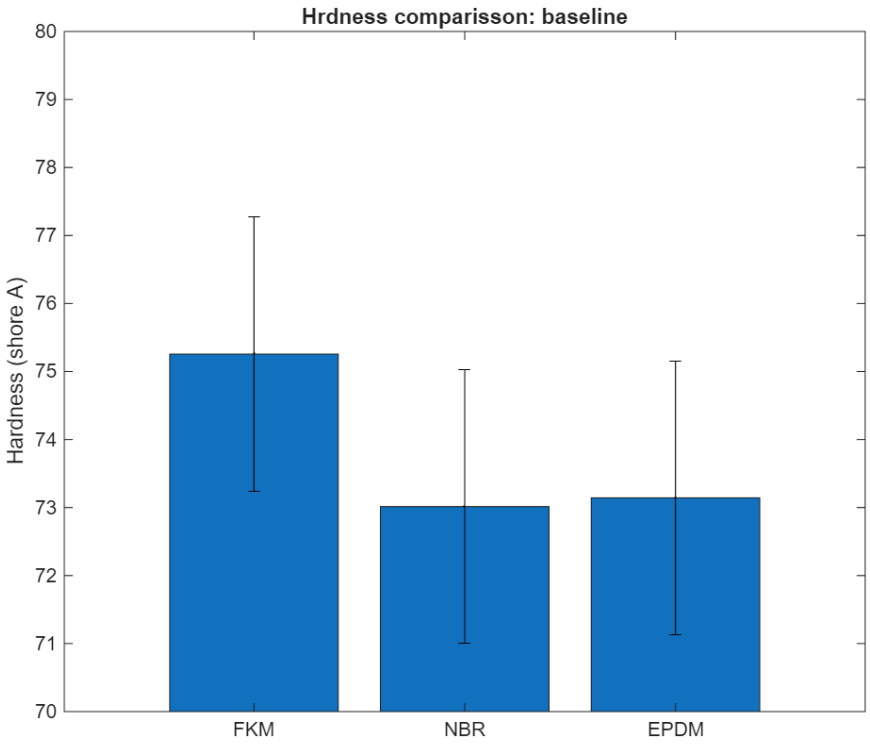


Figure 35: Comparison of the shore A hardness measured for the materials analyzed prior to hydrogen exposure

3.3.3 Material imaging

Additionally, material imaging was performed to characterize changes on the material as a result of hydrogen exposure. To achieve this, five slices with a thickness of 2 mm were obtained from the polymer O-rings. The slices obtained from the material were imaged using a VHX 7000 ultramicroscope at a magnification of 110X. The samples were scanned near the outer diameter and image processing software was used to identify different aspects of the material structure and topography. For this analysis, the microscope uses a light source to provide illumination of the samples. The light is then reflected from the surface of the

material specimen, and it is captured by photoreceptor elements. The illumination light was provided at an angle from the polymer slices, reflecting from the flat surface of the disk. However, the incidence angle of the light creates shadows where cavities and other protrusions are present. This allows the irregularities on material such as cavities to be identified in the image as dark spots. Material samples from each of the materials selected were obtained and imaged prior to exposure to hydrogen gas to establish an understanding of the baseline condition. Figure 36 shows images of the cross sections obtained from FKM O-ring samples that exemplify different characteristics of the material. One of the main aspects of this material is the high concentration of filler particles. Furthermore, some of the voids observed have angular geometric shapes similar to the filler crystals. This suggests that these imperfections were formed when the O-ring was sliced to observe the cross section.

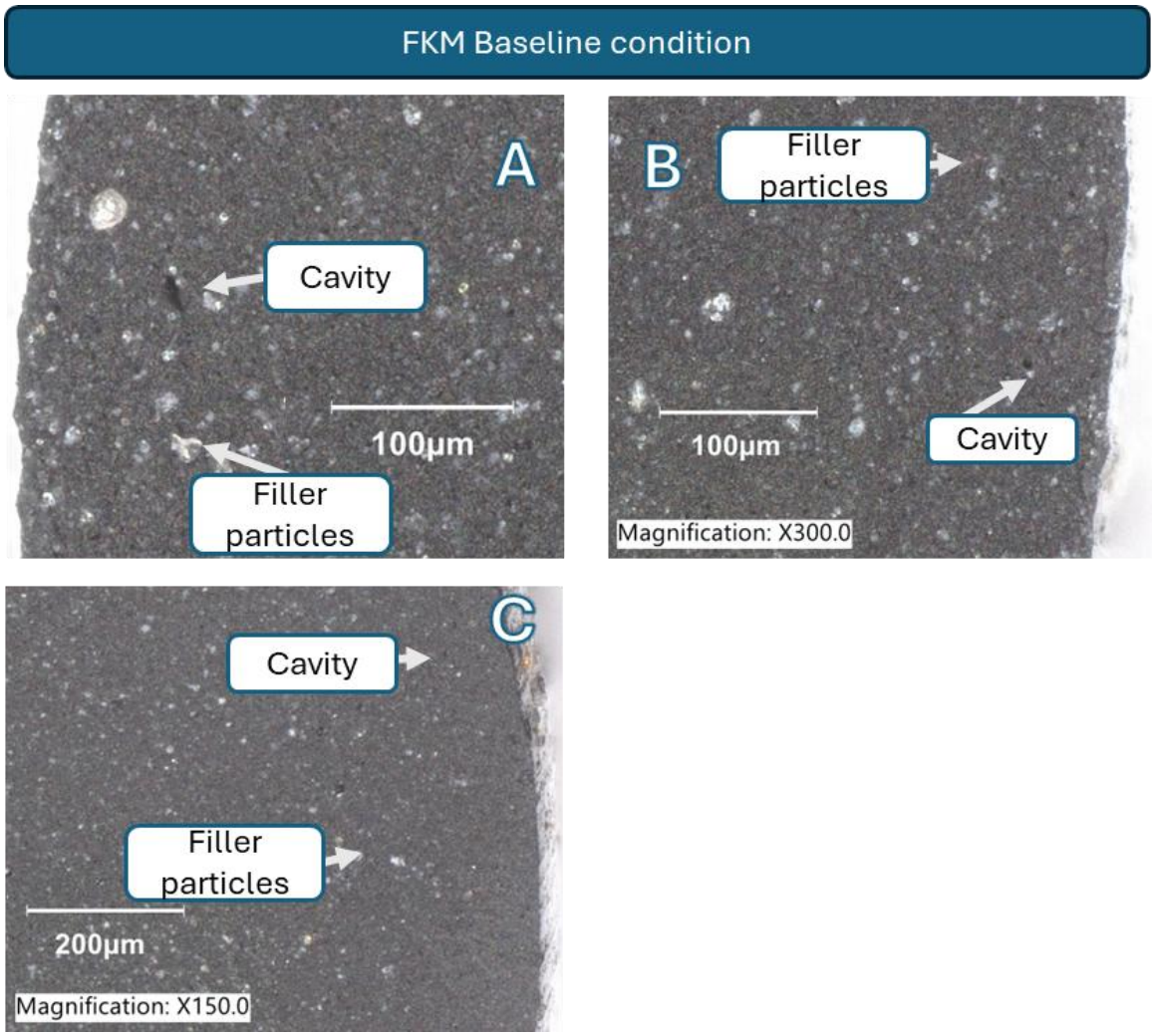


Figure 36: Images obtained from cross section of the FKM O-rings analyzed prior to exposure to hydrogen gas.

Following this, Figure 37 shows examples of the baseline conditions for cross section samples obtained from the NBR O-rings analyzed. In this case, Figure 37A shows cavities through the polymer matrix in a small number. Similarly, filler particles in the form of crystals are present in the material. However, a different material phase is observed in this case due to the separation between acrylonitrile and butadiene that compose the material. In contrast, Figure 37B shows a typical cross section of the material without abundance of fillers, cavities, or other imperfections. Lastly, Figure 37C shows a cross section of the NBR based O-rings in which larger depressions or cavities can be observed. These features show

a circular outline but do not display a shadow due to differences in depth when compared to other features.

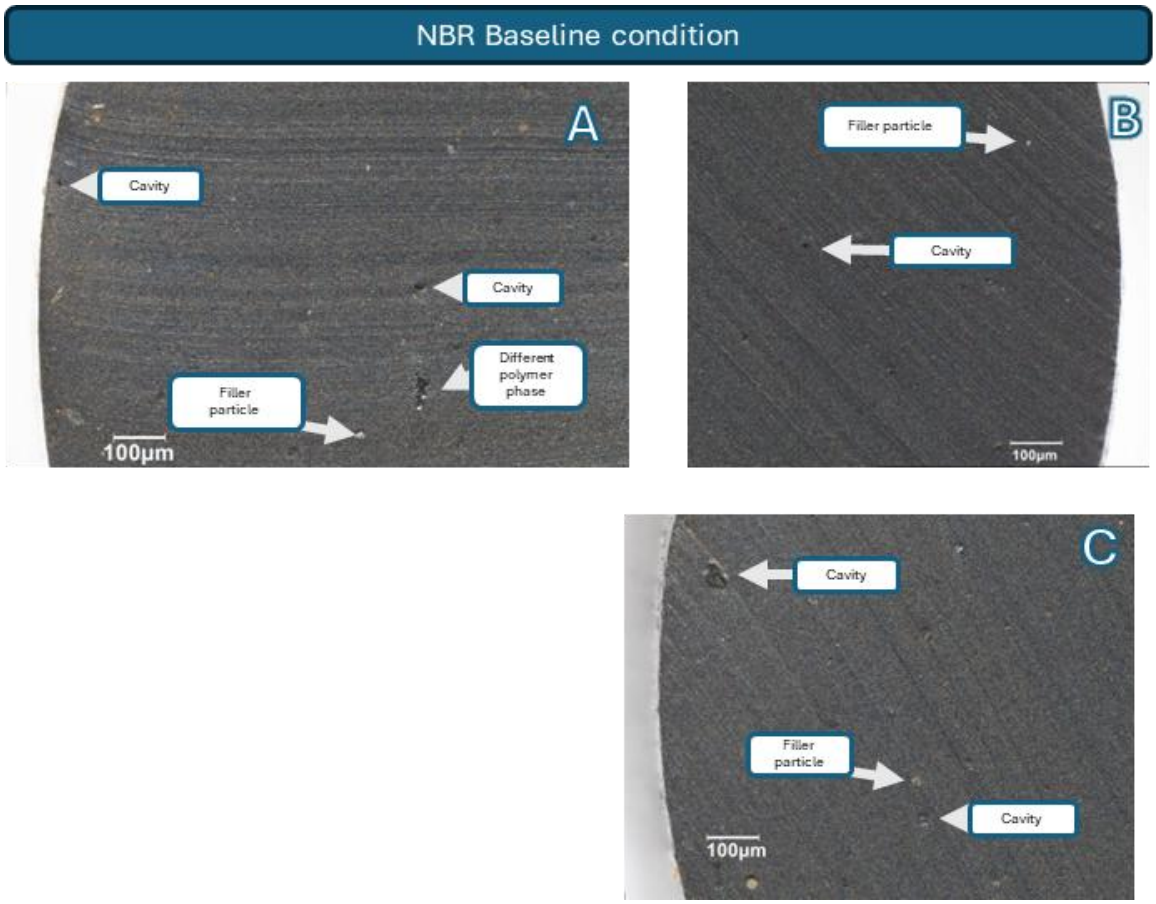


Figure 37: Images obtained from cross section of the NBR O-rings analyzed prior to exposure to hydrogen gas.

Similarly, Figures 38A-C show micrography images obtained from cross sections of intact EPMD-based O-ring samples. Figure 38 A shows an example of high concentration of filler particles in the form of relatively large crystals with a lighter color than the polymer matrix. These crystals do not show a uniform distribution and are not visible on all of the images obtained. Hence, it is possible that this image could be an example of the natural irregularities caused by the manufacturing process used to create this specific EPDM formulation. Similarly, figure 38 B shows an example of another irregularity in the material in the form of voids within the polymer matrix. In this image we can observe the presence of cavities near the outside diameter of the sample. These cavities have a regular shape and

are not agglomerated or grouped together. In contrast, on the right of figure 38 B, toward the center of the O-ring cross section, we can observe a higher concentration of cavities in the polymer matrix. These voids have irregular shapes and do not follow the groves created when obtaining the specimen. Lastly, figure 38 C shows a more typical cross section of the EPDM O-rings analyzed. In this case, the groves created by the knife edge are more visible. However, the presence of crystals and voids through the matrix can also be observed. These inclusions in the polymer matrix are more evenly distributed.

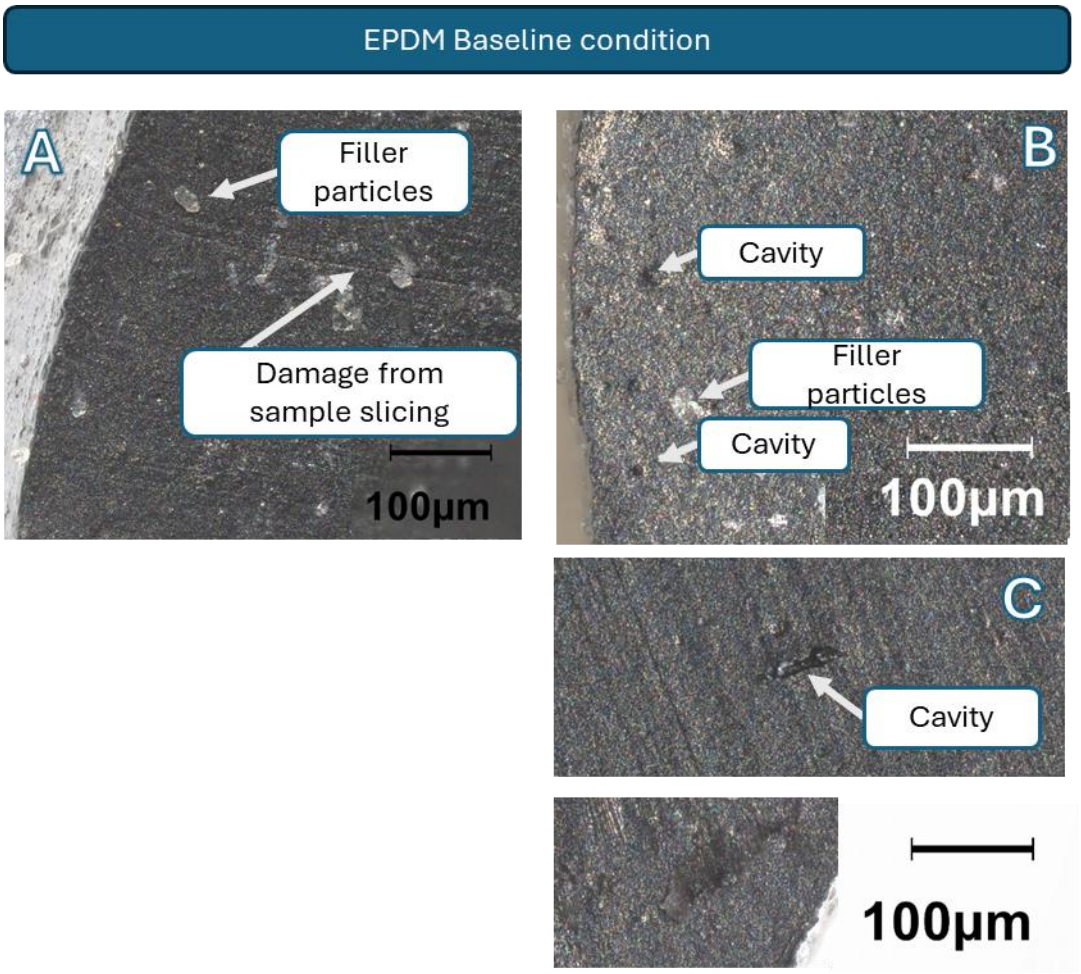


Figure 38: Cross sections obtained from EPDM O-ring samples before exposure to hydrogen gas highlighting main chracteristics of the material morphology.

Following this, image analysis software was used to crop a predetermined area of 0.34 mm^2 from all of the images obtained. Similarly, computational methods were used to perform a

threshold analysis limiting the objects of interest to the lower 10% of the gamma displayed, distinguishing the polymer material from voids in the matrix. Then, additional computational methods were employed to quantify characteristics of the surface analyzed. This analysis was performed to characterize the size, and concentration of material imperfections and voids observed on the material samples. Cross sections obtained from material samples before hydrogen exposure were used to establish a baseline for comparison against the specimens exposed to hydrogen gas. This information was used to support the results obtained through mechanical analysis and to qualify the degree of material degradation. Figure 39 shows a summary of the method used to process the images obtained for morphological analysis of the materials investigated. In this case, particles smaller than 15 μm^2 were omitted from the analysis in order to reduce the noise caused by the tearing other material during the slicing of the samples.

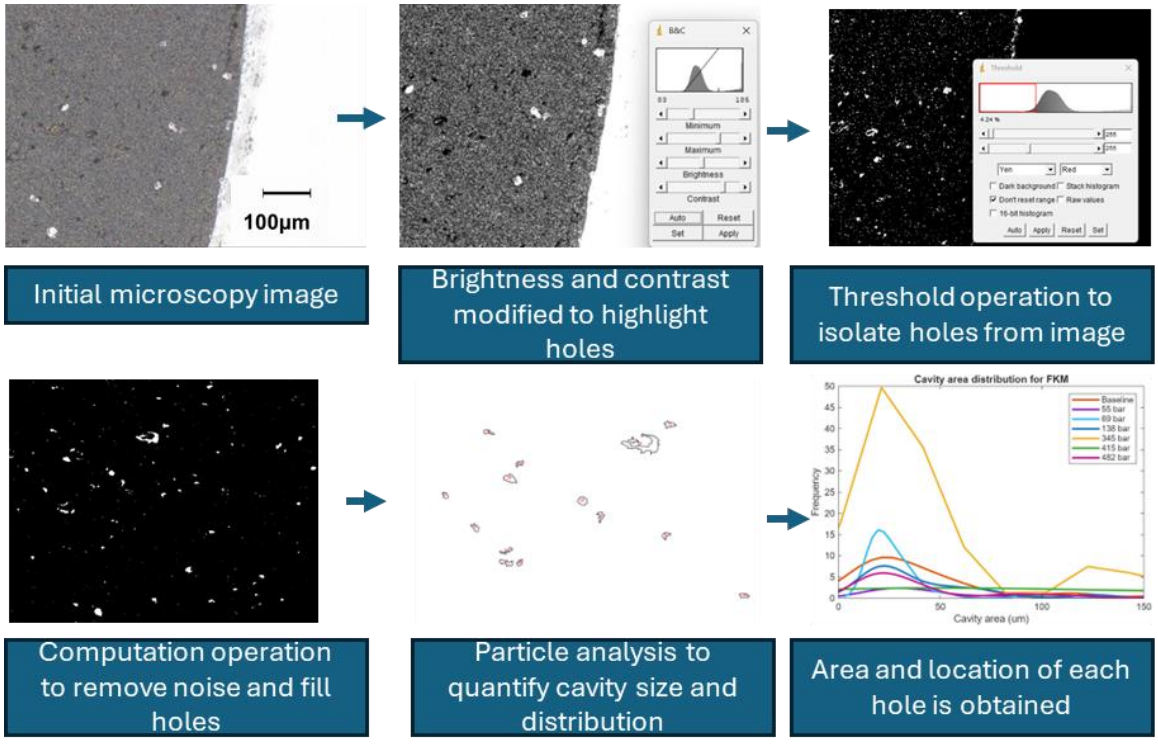


Figure 39: Schematic of the process used to analyze the quantity and distribution of the cavities present in the O-ring slices highlighting the main computational operations of the process.

These results were used to quantify the presence of voids within the polymer matrix of the materials selected. Figure 40 shows a comparison of the three materials selected prior to exposure to hydrogen gas. Figure 40 A shows a comparison of the average area for the cavities observed in the materials. From this comparison we can observe that the FKM displays the smallest defects while the NBR based material samples show larger holes. Nevertheless, the cavities observed are all comparable in size across the three materials. Similarly, figure 40 B shows a comparison of the fraction of the area analyzed occupied by cavities. In this case we can observe a similar trend with FKM displaying the least coverage while NBR has the highest coverage at 0.6%.

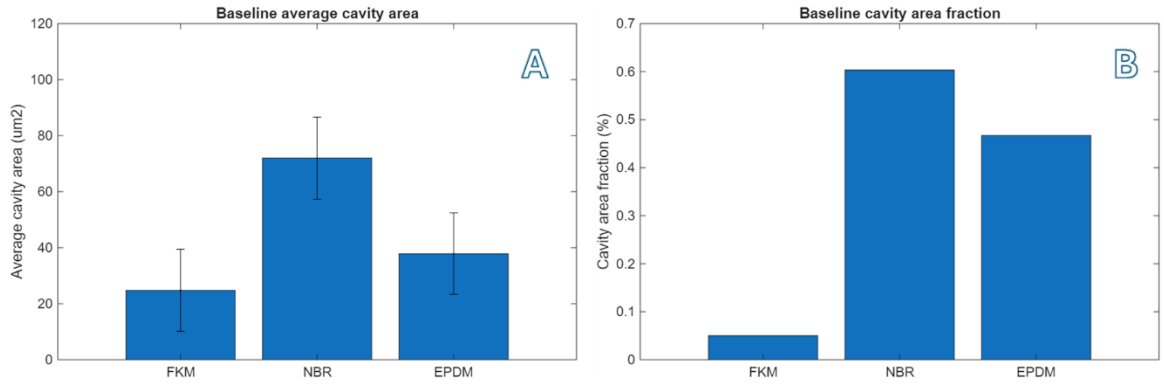


Figure 40: Quantified voids for baseline condition of the materials investigated

3.4 Conclusion

In this way, the characterization of mechanical properties and material morphology were characterized. The system designed for the controlled exposure of material samples to a hydrogen environment pressurized at varying levels was successfully employed in this study. In this regard, the pressure of the hydrogen gas was controlled using the selected control system between the selected experimental in a safe and consistent manner. Additionally, the automatic pressure monitoring logic implemented was successful in maintaining pressures up to 482 bar for the aging period of 200 hours without significant changes. Furthermore, the hydrogen detectors and the integrated safety interlocking mechanisms were successful in preventing hazards during operation. Periodical inspection of the tubing and fittings enhanced safety and guaranteed consistent aging conditions through this study.

Moreover, preventive maintenance of the fittings and seal elements employed in the reactor vessel were successful in preserving the integrity of the experimental system, avoiding deterioration of critical components and ensuring continued operation for further investigations.

Similarly, the methodology employed for the characterization of polymer materials prior to exposure to hydrogen gas was successful in determining key characteristics of the material samples. The tensile strength and hardness of the materials was determined to be within range according to the manufacturing specification and available literature. Similarly, changes in material relaxation were identified and characterized for a range of exposure pressure and deformation levels. Additionally, the imaging of the material samples provided useful data regarding the average cavity size and the fraction of the material surface they occupy. This information is valuable for comparison against material samples exposed to hydrogen gas and to establish a quantification of the material degradation caused on the polymer samples.

CHAPTER 4: EXPERIMENTAL RESULTS AND DISCUSSION

This section presents the results of the different tests and analysis performed on the different materials investigated after exposure to high pressure hydrogen gas. The material degradation is evaluated with respect to the measured changes in mechanical properties as well as the material morphology characterization performed through microscopic imaging. The changes to mechanical properties are quantified through measured changes in tensile strength, elongation at rupture, changes in relaxation behavior under tensile load, and changes in hardness. The changes to material morphology are quantified through measuring the size and distribution of cavities observed on the material before and after exposure to high pressure hydrogen gas. Furthermore, as a means to evaluate the significance of the changes observed, inferential statistical methods were conducted to compare the aged specimens to baseline parameters.

4.1 Tensile testing

As previously described, tensile strength is an important characteristic to take into consideration for materials design sealing applications. During operation, polymer sealing elements experience forces that deform the material [102]. Hence, understanding the limits of the materials becomes an important aspect for the design of sealing components. Nevertheless, in the case of hydrogen applications, these limits may be affected by operating parameters, material interactions, or other factors. In this way, a comparison of how materials react was constructed by analyzing the tensile strength and maximum deformation of polymer materials exposed to hydrogen gas at different pressure levels.

The material specimens were tested following the completion of exposure time under high pressure hydrogen. Each specimen was loaded on the testing apparatus, and a continuous deformation was applied until rupture. The tensile strength for each specimen was calculated using the specimen cross section thickness as previously described. Following this, the calculated strength of the exposed samples was normalized with respect to the tensile strength measured before hydrogen exposure. The following sections present the results of this analysis for the three polymer-based O-ring materials investigated

4.1.1 FKM material

The changes to tensile strength of the FKM samples exposed to hydrogen gas are shown in figure 41 A. Similarly, the changes to the maximum deformation are shown in figure 41 B. The maximum force measured decreased approximately 10 % following exposure to pressurized hydrogen gas, with no significant difference between pressure levels. In contrast, the maximum deformation of the material does not appear to have been affected by exposure to hydrogen gas.

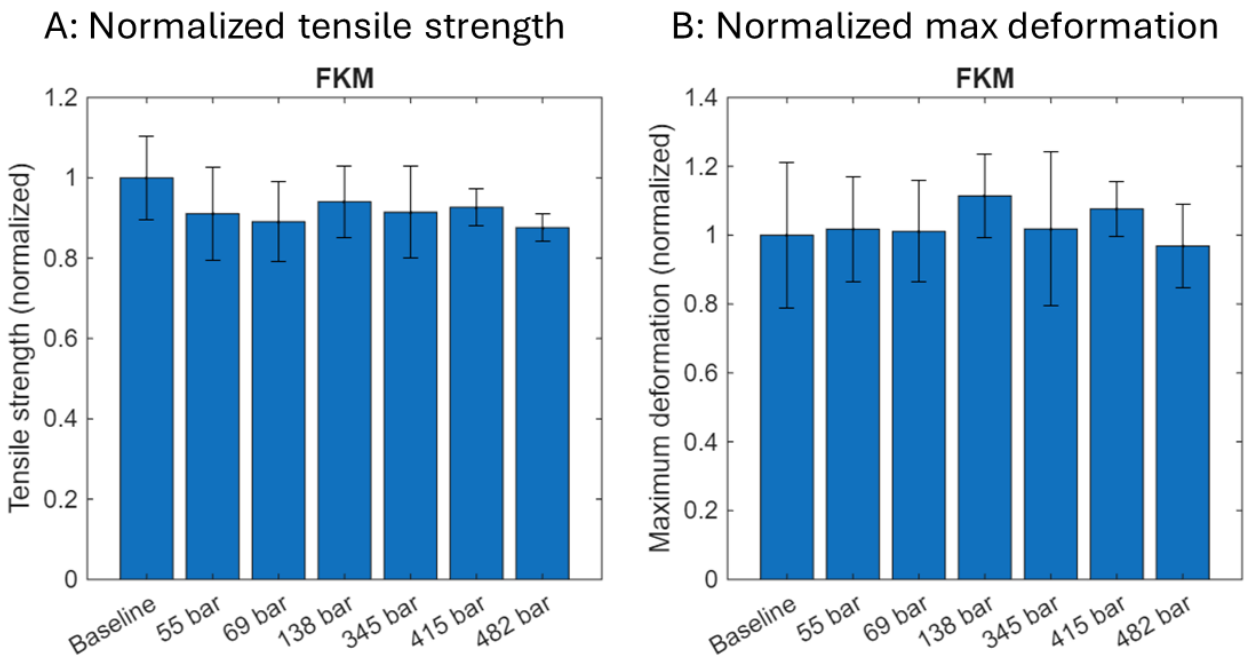


Figure 41: Bar plot showing the tensile strength (A) and maximum deformation (B) calculated for FKM samples exposed to hydrogen gas at different pressures.

The data for baseline tensile strength and maximum deformation are shown with a unit value. In this case, the tensile strength of the material is slightly diminished by exposure to hydrogen gas as shown on table 4. At an exposure pressure of 55 bar, the FKM material tested showed a decrease in tensile strength of 8.9% while a decrease of 10.9% was measured for samples exposed to a pressure of 69 bar. The change with respect to the baseline tensile strength for the FKM material exposed to 138 bar showed a decrease of 6%, 345 showed a decrease of 8.5%, and 415 bar showed a decrease of 7.3%. In contrast, the greatest change

with respect to the baseline of 12.4 % was observed for the material exposed to a pressure of 482 bar.

Table 3: Summary of the calculated tensile strength and maximum deformation observed on FKM samples after exposure to hydrogen gas at different pressure levels.

Exposure pressure (bar)	**Tensile strength (normalized)**	**Tensile strength (variance)**	**Max deformation (normalized)**	**Max deformation (variance)**
0	1.000	0.105	1.000	0.211
55	0.911	0.115	1.018	0.153
69	0.891	0.099	1.011	0.148
138	0.940	0.089	1.114	0.122
345	0.914	0.115	1.018	0.224
415	0.927	0.047	1.076	0.078
482	0.876	0.033	0.969	0.121

4.1.2 NBR material

In a similar way, the results for the tensile strength analysis of NBR were obtained and processed. Figure 42 A shows a comparison of the tensile strength measured for NBR samples after exposure to hydrogen gas at different pressure levels. Similarly, figure 42 B shows the maximum deformation observed. For this material, the tensile strength of the samples exposed to pressures higher than 69 bar shows an increase of approximately 10% while the material exposed to 55 bar shows an increase of only 1.8%. However, the aging pressure conditions did not seem to cause noticeable effects in the case of the maximum deformation observed.

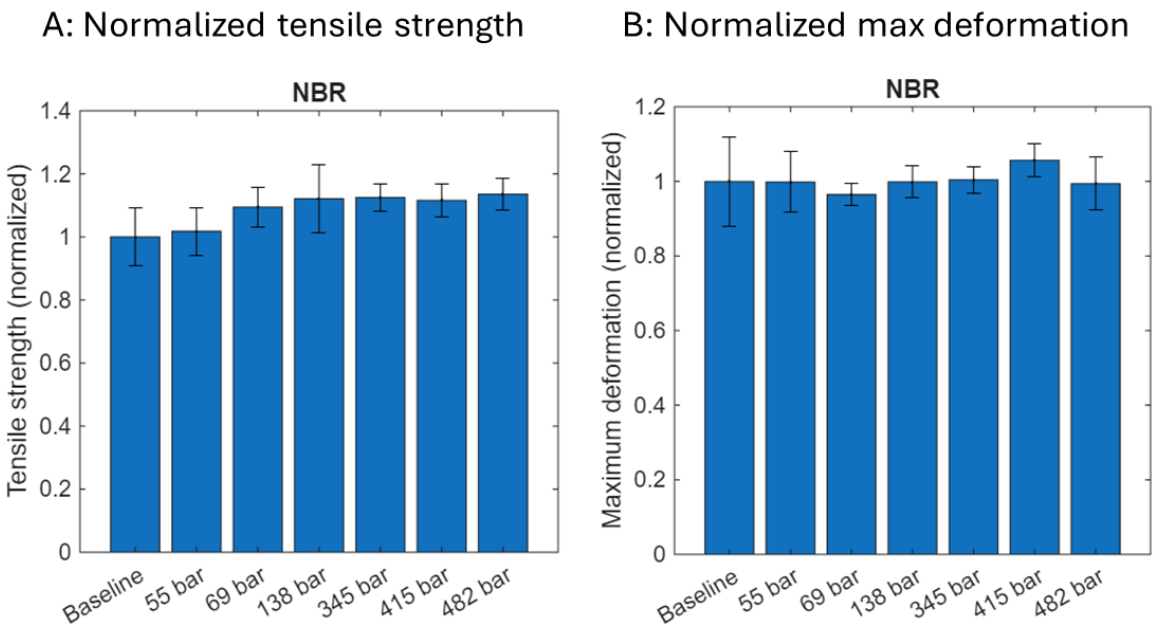


Figure 42: Comparison of the tensile strength and maximum deformation observed for NBR materials exposed to hydrogen gas at different pressure levels.

When compared to the baseline results, the sample aged at a pressure of 55 bar shows a relatively small increase in tensile strength which cannot be considered statistically significant. However, the sample exposed to 69 bar shows the largest increase in tensile strength of 9.4%. Following this, the samples exposed to 138 bar and 345 bar show an increase of 12.1% and 12.5% respectively; the samples exposed to 415 bar showed an increase of 11.6%; the sample aged at 482 bar showed an increase of 13.6%. On the other hand, the maximum deformation of the NBR material tested showed no statistically significant change for the selected pressure levels. Table 5 shows a summary of these changes.

Table 4: Summary of the calculated tensile strength and maximum deformation observed on NBR samples after exposure to hydrogen gas at different pressure levels.

Exposure pressure (bar)	**Tensile strength (normalized)**	**Tensile strength (variance)**	**Max deformation (normalized)**	**Max deformation (variance)**
0	1.000	0.092	1.000	0.120
55	1.018	0.075	1.018	0.082
69	1.094	0.062	1.094	0.030
138	1.121	0.107	1.121	0.043
345	1.125	0.043	1.125	0.035
415	1.116	0.052	1.116	0.045
482	1.136	0.050	1.136	0.071

4.1.3 EPDM material

Lastly, figure 43 A shows a comparison of the tensile strength measured for EPDM samples after exposure to hydrogen gas at different pressure levels. Similarly, figure 43 B shows the maximum deformation observed. In a similar trend as the NBR material, the tensile strength the EPDM samples investigated showed an increase with higher exposure pressure. For the samples aged at 55 bar the tensile strength increased 5.2%; for samples aged at 69 bar the tensile strength increased by 19.1%; for samples aged at 138 bar the tensile strength increased by 9.1%; for samples aged at 345 bar the tensile strength increased by 4.8%; for samples aged at 415 bar the tensile strength increased by 7.2%; for samples aged at 482 bar the tensile strength increased by 9.6%.

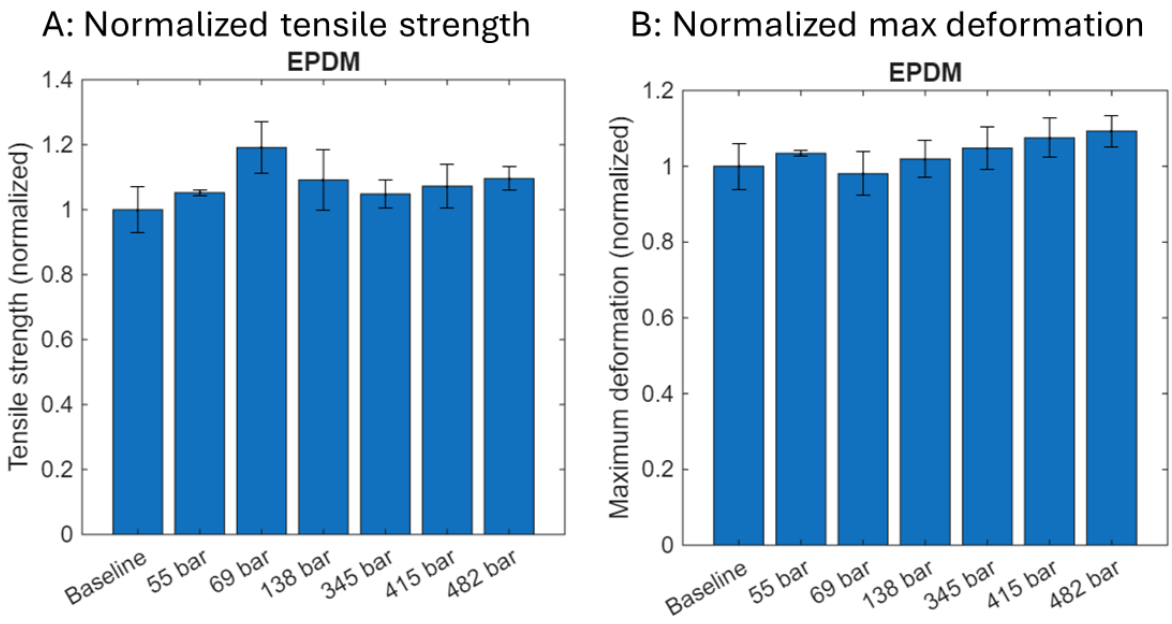


Figure 43: Comparison of the tensile strength and maximum deformation observed for EPDM materials exposed to hydrogen gas at different pressure levels.

In contrast to the other materials tested, EPDM showed an increase in the deformation measured at rupture. The samples exposed to 55 bar and 69 bar showed a change in maximum deformation of 3.4% and 1.9% respectively. However, the samples exposed to 138 bar and higher pressures show a trend on increasing maximum elongation. The O-ring samples exposed to 138 bar show an increase in maximum deformation of 4.8%; the samples exposed to 345 bar show an increase in maximum deformation of 7.5%; the samples exposed to 482 bar show an increase in maximum deformation of 9.3%. Table 6 shows a summary of the changes in tensile strength and maximum deformation measured for the EPDM O-ring material investigated.

Table 5: Summary of the calculated tensile strength and maximum deformation observed on NBR samples after exposure to hydrogen gas at different pressure levels.

Exposure pressure (bar)	**Tensile strength (normalized)**	**Tensile strength (variance)**	**Max deformation (normalized)**	**Max deformation (variance)**
0	1.000	0.070	1.000	0.060
55	1.052	0.009	1.034	0.007
69	1.191	0.079	0.981	0.058
138	1.091	0.092	1.019	0.049
345	1.048	0.043	1.048	0.057
415	1.072	0.067	1.075	0.052
482	1.096	0.037	1.093	0.042

4.1.4 Material comparison

From the analysis of the tensile strength of the samples exposed to pressurized hydrogen gas we can observe that the tensile strength and maximum deformation of the analyzed O-ring material samples were affected by exposure to hydrogen gas at the different pressure levels selected. Nevertheless, a decrease in tensile strength for the FKM based material tested was observed for the aged samples, while for the NBR and EPDM materials tested, the maximum force recorded at rupture increased for exposure pressures 69 bar and higher. Similarly, the materials showed different changes in maximum elongation after being exposed to pressurized hydrogen gas. Figure 44 A shows a comparison between the tensile strength exhibited by the materials. Similarly, figure 44 B shows a comparison of the deformation of rupture measured for the three different materials exposed at varying pressure levels.

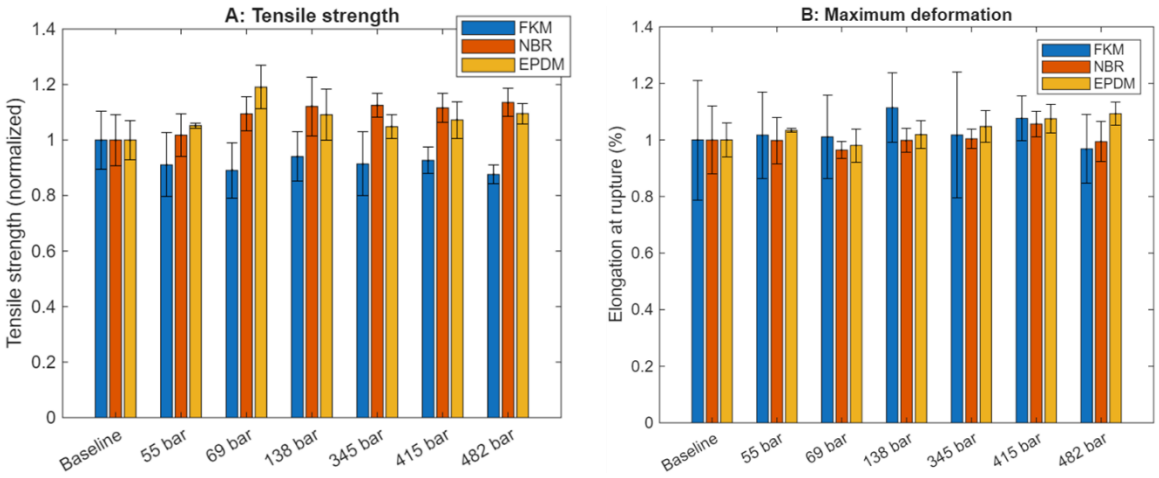


Figure 44: Material comparison of the effects of hydrogen exposure on tensile strength (A) and maximum deformation (B) calculated for the materials tested.

From this mechanical analysis we can appreciate the changes caused by exposure to hydrogen gas to the materials investigated. In this case, the tensile strength of the FKM-based O-rings was reduced for all of the aging pressures. However, this reduction was less severe for the samples exposed to 138 bar. In contrast, the NBR and EPDM based O-rings showed an increase in tensile strength for the samples exposed to 69 bar and higher. In this regard, the samples exposed to 69 bar showed a greater increase in tensile strength when compared to all other material conditions. Furthermore, the changes in tensile strength do not display a linear relationship with exposure pressure. These results could indicate the competing effects between material swelling due to hydrogen dissolution and the internal stresses generated by high pressure exerted by the gas accumulated in cavities and the material free volume. Analogously, the elongation at rupture for the materials investigated did not display a linear dependency with respect to the exposure pressure. In the case of the FKM material analyzed, the maximum deformation was recorded for the samples exposed to 138 bar while the lowest value was recorded for the samples aged at 482 bar. Similarly, the NBR and EPDM material did not display a linear relationship with the aging pressure. Both materials show a decrease in maximum elongation for an aging pressure of 69 bar, followed by an increase for the exposure pressures between 138 bar and 415 bar. For the samples exposed to 482 bar, NBR shows a sudden decrease in maximum elongation while EPDM

continues a rising trend. In this way, through the tensile testing of the different polymer materials we can observe differences in their response to hydrogen exposure.

4.2 Relaxation analysis

Continuing with the aim of characterizing the material changes, a tensile relaxation analysis was performed after the material samples were exposed to pressurized gas. As previously described, the O-ring samples were loaded on the testing fixture, and a known deformation was applied. Then, the maximum and minimum force for the deformation were recorded. The change tension measured was then normalized with respect to the highest force measured at that deformation level. This process was repeated for a total of seven equally spaced deformation levels. This data was then used to compare the changes as a function of the pressure at which the samples were aged. Similarly, the normalized tensile relaxation data was used to compare the magnitude of the changes to mechanical properties between the different polymer-based materials investigated. The following sections present a summary of the results obtained for the three polymer-based O-ring materials investigated.

4.2.1 FKM material

Figure 45 shows a comparison of the relaxation behavior of the FKM samples exposed to hydrogen gas at different pressure levels when subjected to the varying levels of deformation. From this figure we can appreciate that under for the 70mm deformation, the samples exposed to different pressure conditions show a wide scattering in the average tension calculated for the different aging pressures. Similarly, we can appreciate how as a result of exposure to hydrogen gas the material shows a different tensile response for identical deformation steps. In this case, the samples exposed to 345 bar show a smaller force for all the deformation steps when compared to the other aging conditions.

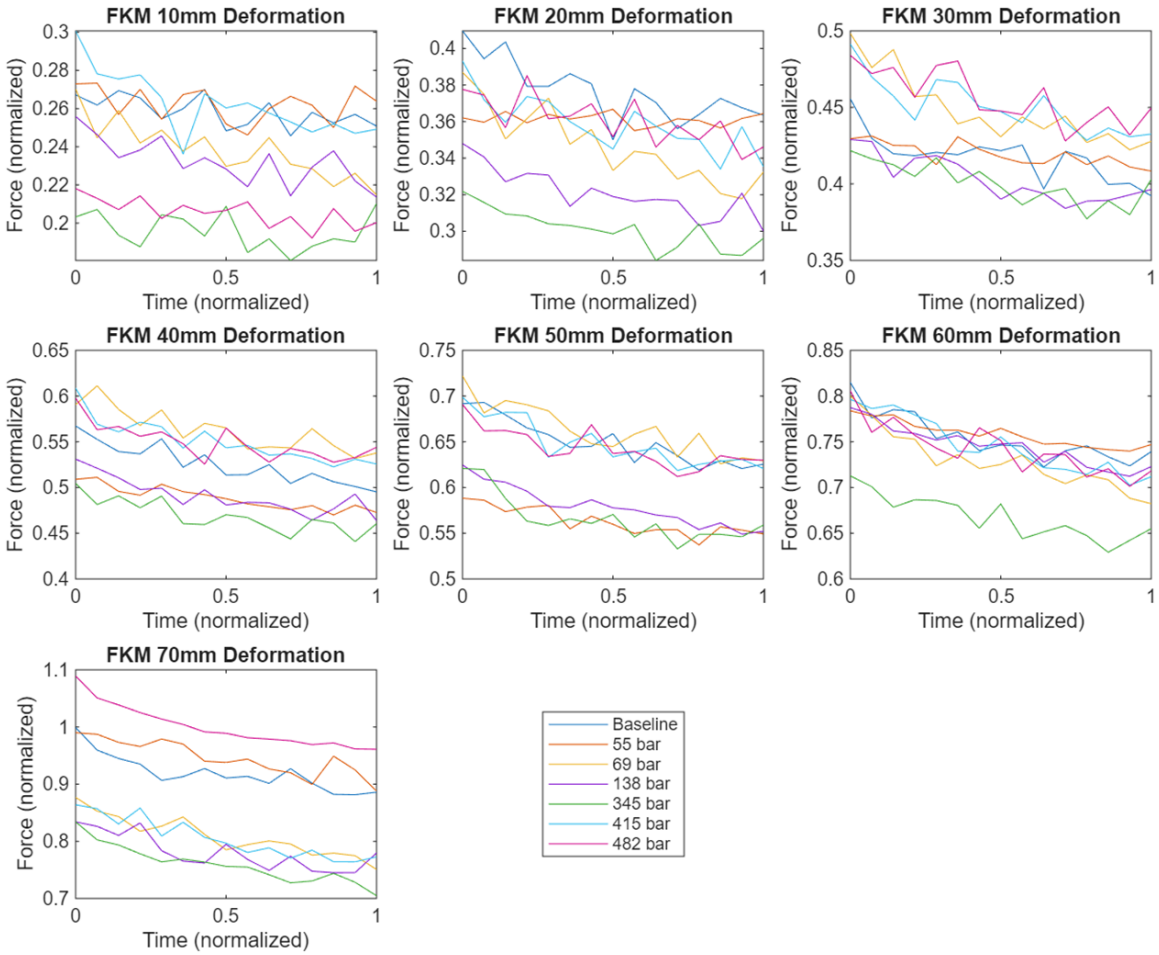


Figure 45: Tensile relaxation at different deformation levels for the FKM material samples exposed to hydrogen gas at different pressure levels.

Similarly, from figure 46 we can observe the differences in the relaxation modulus at a deformation level of 40 mm. In this case, the exposure to hydrogen gas at a pressure of 55 bar causes the material to relax a lower percentage of the initial tension when compared to the other exposure conditions. Furthermore, the samples exposed to 55 bar show a smaller rate of change in the tension measured, highlighting changes in stiffness to the material.

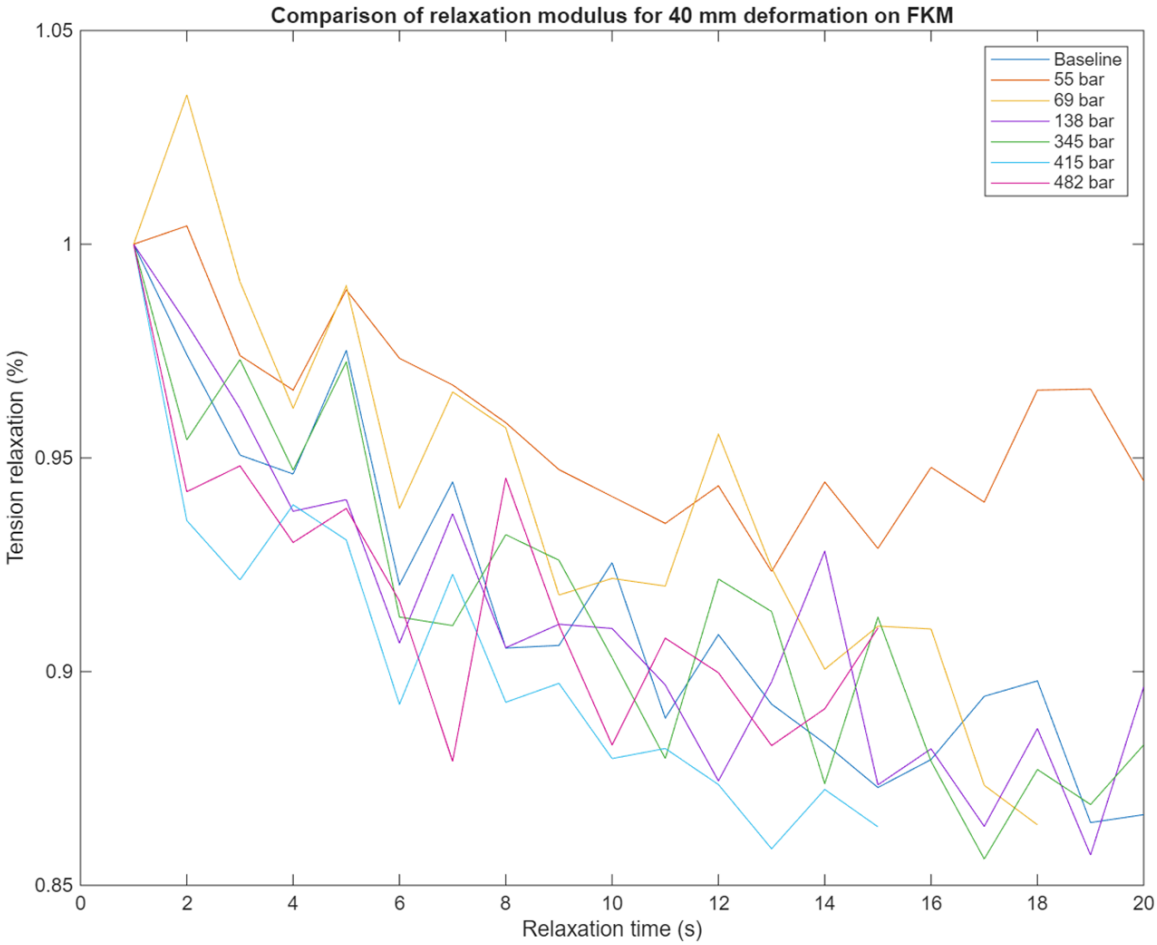


Figure 46: Fraction of force drop as a function of sample deformation for FKM samples exposed to hydrogen gas pressurized at different levels.

Another important aspect from this analysis is the change in measured force over time, at the lowest deformation level, the tension in the material does not show a large reduction during the relaxation period. In contrast, at higher deformation levels, the material shows a greater reduction in tension after the relaxation period elapsed. Figure 47 shows a comparison of the tensile relaxation of the FKM samples exposed to different pressure levels. From this figure we can appreciate the scatter in the relaxation of the material samples for the low deformation levels, particularly at a deformation of 10mm. in this case, the FKM material before exposure to hydrogen gas shows a drop of 9.5% with respect to the tension measured at the start of the relaxation period. In contrast, the samples exposed to

415 bar showed a relaxation of 17.1%. Similarly, the samples exposed to 55 bar showed a much smaller relaxation of 2.5% to 5.5% for most of the deformations applied. On the other hand, for the larger deformation levels such as 60mm and 70mm, the exposure pressure appears to have a less pronounced effect on the tensile relaxation behavior of the material. Furthermore, from this figure we can appreciate that the samples exposed to 69 bar presented the greatest relaxation for the 10mm, 20mm, and 30mm deformation with 19.6%, 18.3%, and 15.2% respectively. In contrast, the samples exposed to 138 and 345 bar showed the largest relaxation for the 70mm deformation with 15.6% and 16.1% respectively. In this case, the relaxation percentage of the material does not show a linear relationship with the exposure pressure. Instead, a sharp decline is observed between the baseline condition and the samples exposed to 55 bar followed by an increasing trend for the samples exposed to pressures between 138 bar and 145 bar.

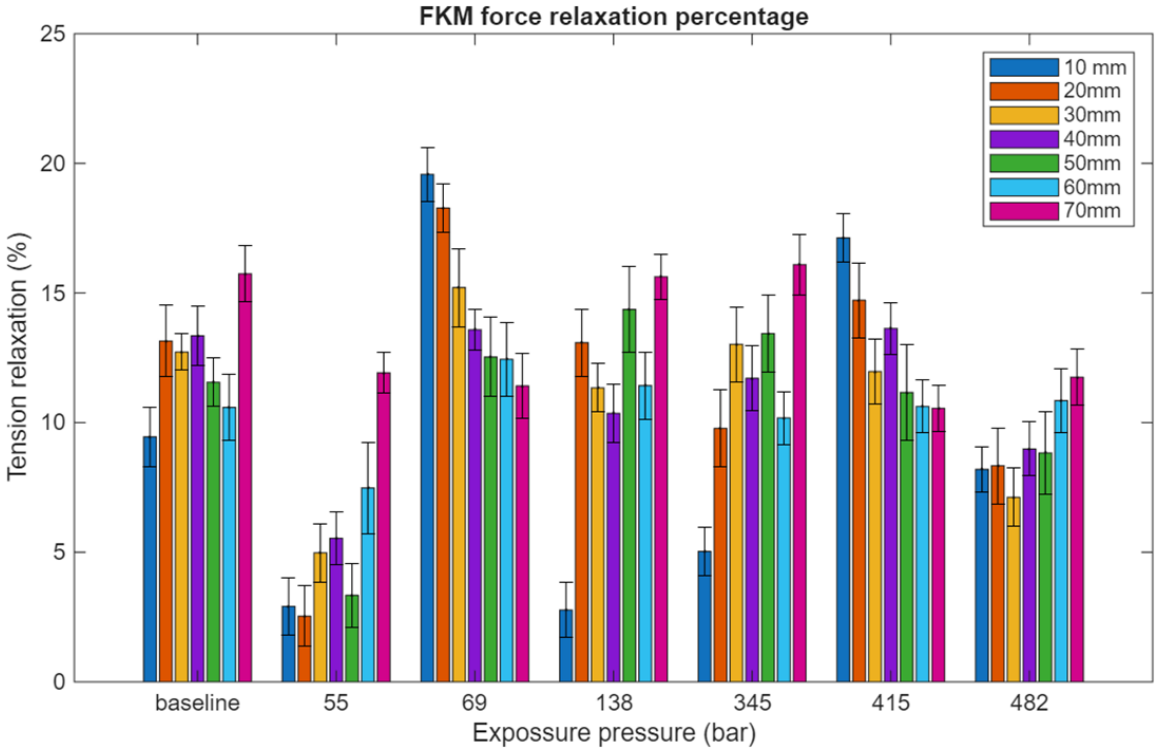


Figure 47: Comparison of the tension relaxation percentage for the different deformation levels as a function of the pressure the FKM-based material was exposed to.

4.2.2 NBR material

In a similar way, the NBR-based material samples were analyzed to determine changes to the tensile relaxation of the material. Figure 48 shows a summary of the relaxation behavior of the material aged through exposure to pressurized hydrogen gas for varying levels of deformation. In contrast to FKM, the NBR-based material analyzed shows less scattering between the samples aged at different pressure levels. Furthermore, from this analysis we can appreciate how the samples exposed to hydrogen gas at a pressure of 138 bar show a higher force for equivalent deformations when compared to the other material conditions. In this way, the changes with respect to the baseline condition in the force measured for different deformation levels indicate changes in stiffness on the material as a consequence of exposure to hydrogen gas.

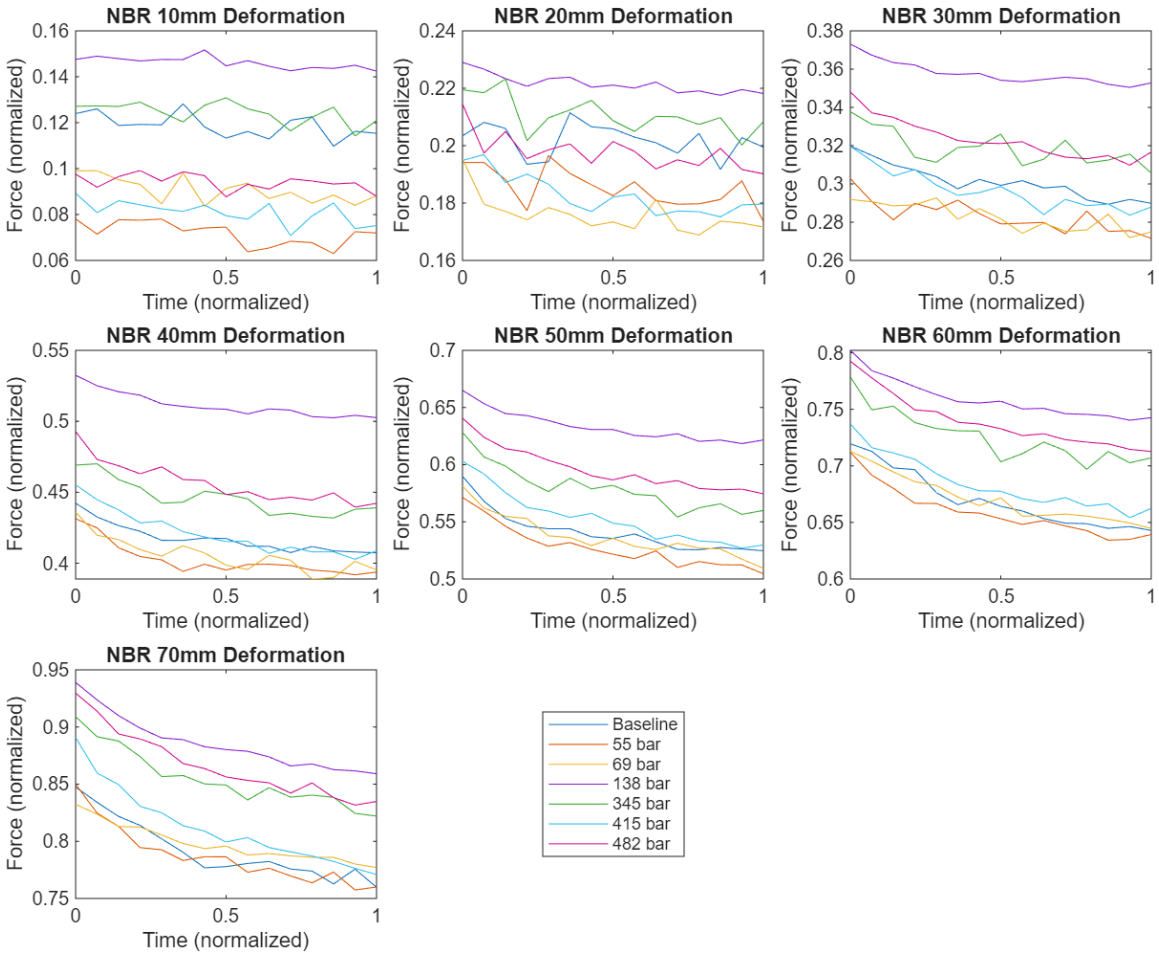


Figure 48: Tensile relaxation at different deformation levels for the NBR material samples exposed to hydrogen gas at different pressure levels.

Similarly, figure 49 shows a comparison of the elastic modulus for the NBR material samples under a deformation of 40mm. From this figure we can observe the changes in stiffness caused by exposure to hydrogen gas. In this case, the exposure pressure of 138 bar results in a lower percentage of force relaxation as well as a reduced rate of change in the tension measured. Together with the results shown in figure 48, these outcomes suggest an increased stiffness for these material samples. In contrast, for the NBR material, exposure to hydrogen gas at a pressure of 415 bar and 482 bar resulted in a larger percentage of force change due to material relaxation as well as a sharper decline over time. In this way, the aging of the NBR material samples resulted in changes to material stiffness and the relaxation

modules of the material. Nevertheless, these changes are not monotonic, suggesting competing effects between material swelling and other physical mechanisms.

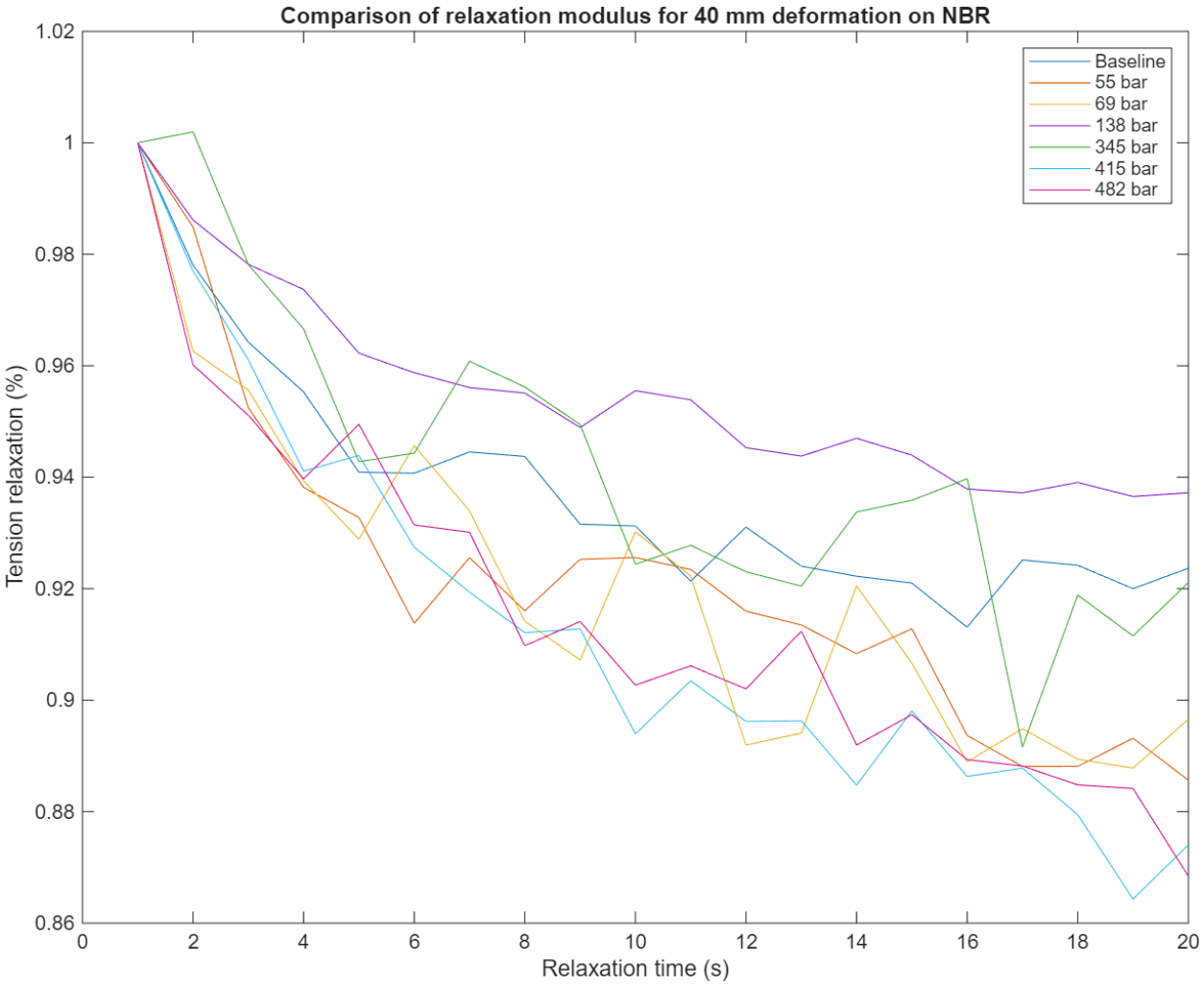


Figure 49: Comparison of elastic modulus

Similarly, Figure 50 shows the tension relaxation of the samples tested as a function of the deformation applied. In this case the tested NBR material follows a similar pattern to the previously described FKM based O-rings. At an exposure pressure of 138 bar the relaxation of the material ranges between 0.6 % and 9.0 %. In contrast, at an aging pressure of 482 bar the material relaxation varies between 10.2 % and 13.2 %. In this case we can observe that for this exposure level the relaxation of the material shows increased stability when

compared to the other material conditions. Lastly. From this figure we can observe the non-monotonic changes to material relaxation as a function of material exposure pressure. For this material, exposure to pressures of 55 bar and 69 bar have the effect of increasing the material relaxation when compared to the baseline. In contrast, this trend changes after an exposure pressure of 138 bar, where material relaxation increases along with the aging pressure before stabilizing.

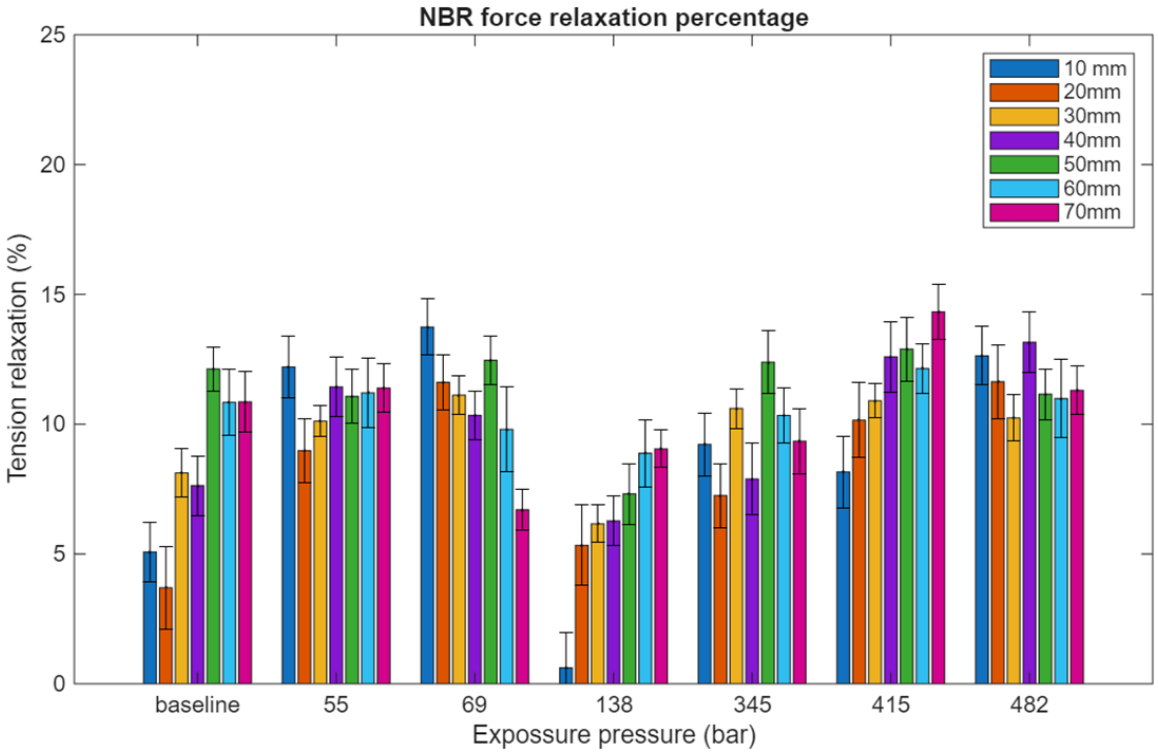


Figure 50: Comparison of the tension relaxation percentage for the different deformation levels as a function of the pressure the NBR-based material was exposed to.

4.2.3 EPDM material

Lastly, the EPDM-based O-ring samples were analyzed in the same manner as previously described. Following this, the raw data was processed to compare the effects of the different aging pressure levels selected. In this case, the different EPDM material samples also show changes in the tensile deformation behavior as a result of exposure to hydrogen gas. Mirroring the results obtained for the other materials, EPDM shows a scatter in the tension measured for different material conditions at equivalent deformation levels. In this case, the

material samples exposed to an aging pressure of 138 bar shows a higher force measured for the deformation of 20 mm to 60 mm. However, the case of the 10mm and 70 mm deformation levels, the material exposed to 69 bar shows a stiffer response to deformation compared to the other material conditions. Figure 51 shows a summary of the tensile relaxation behavior for the EPDM material samples analyzed at varying deformation levels.

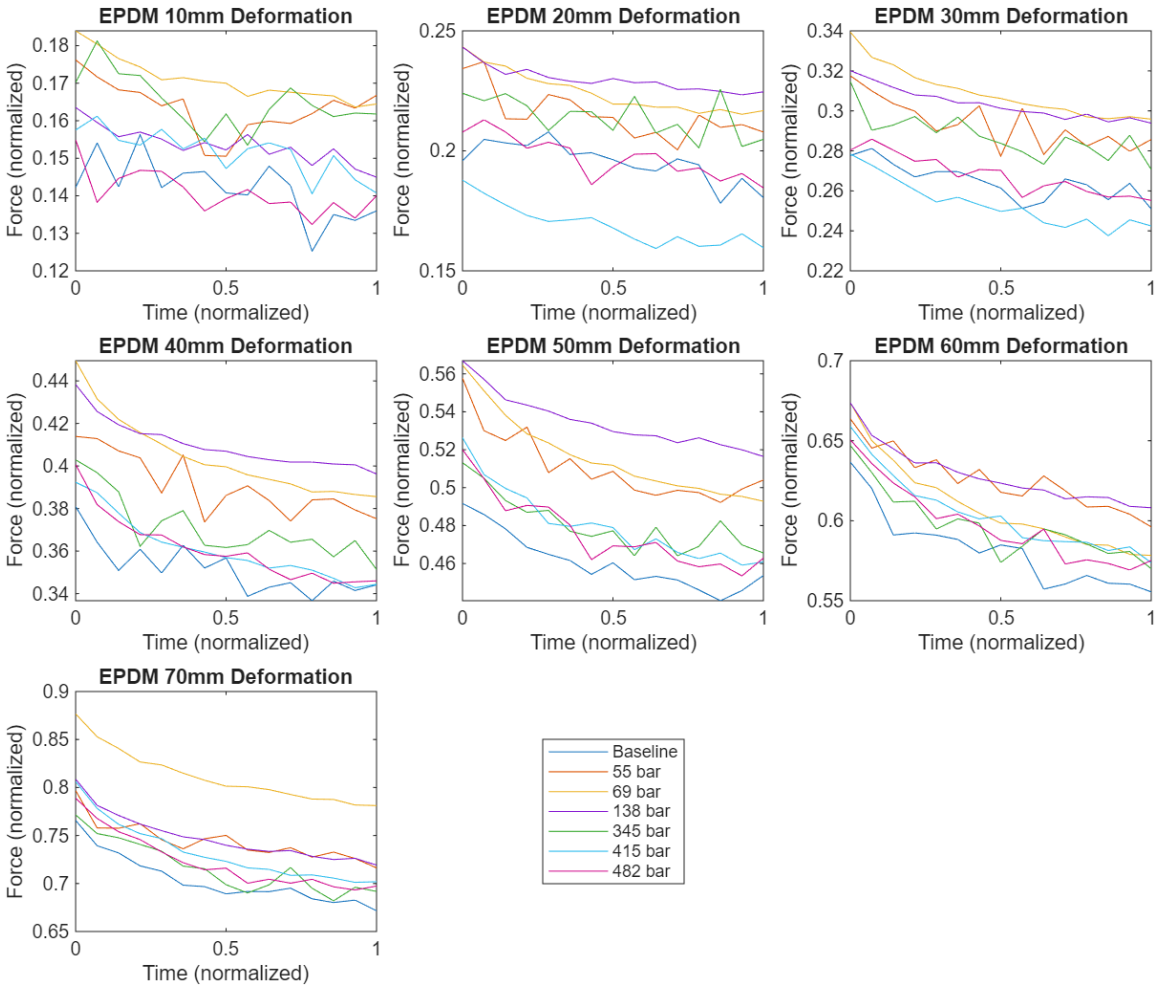


Figure 51: Tensile relaxation at different deformation levels for the EPDM material samples exposed to hydrogen gas at different pressure levels.

Similarly, figure 52 shows a comparison of the relaxation modulus of the EPDM materials exposed to hydrogen gas at different pressure levels subjected to a deformation of 40 mm. In this case, after normalizing each relaxation line to facilitate comparison, we can observe the difference between the effects caused by the aging pressures of 55 bar and 69 bar. For

EPDM, the lowest exposure level of 55 bar caused a material response with the least percentage of force dissipated and the slowest rate of change. These results suggest that at a low pressure, the infiltration of hydrogen molecules and the dislocation of polymer chains increases the stiffness of the material. In contrast the exposure levels of 69 bar and 482 bar displayed similar responses to the applied deformation. These two material aging conditions resulted in the largest percentage of force dissipated through relaxation as well as the fastest change over time, suggesting a decrease in material stiffness. In this way, the results obtained hint at a non-monotonic change in stiffness as a result of exposure to varying pressure levels.

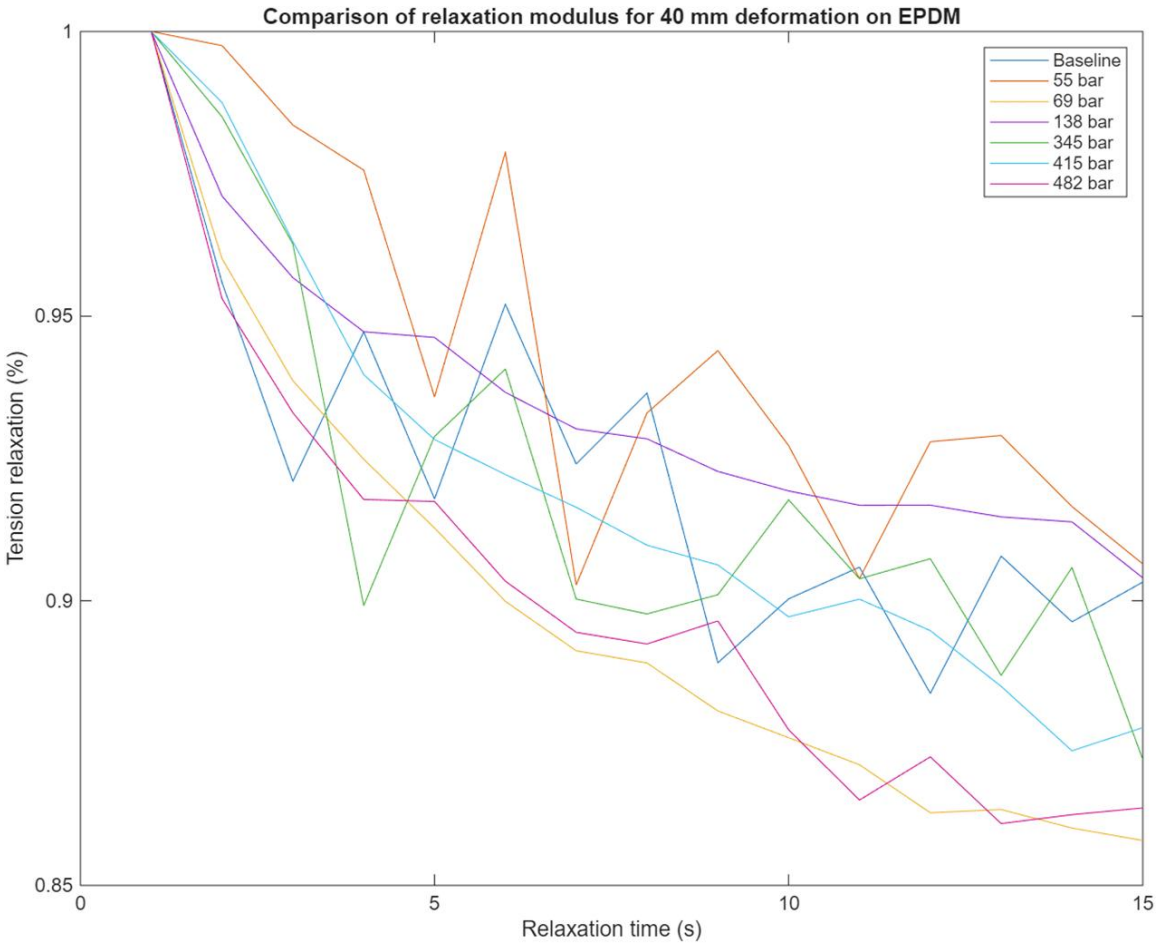


Figure 52: Fraction of force drop as a function of sample deformation for EPDM samples exposed to hydrogen gas pressurized at different levels.

Lastly, figure 53 shows a comparison of the tensile relaxation for the EPDM material tested as a function of the deformation applied. In this case the EPDM samples also show a greater scatter in the relaxation percentage for smaller deformation levels when compared to the 70 mm deformation applied. Similarly, by observing the effects of increased aging pressure for each deformation level we can appreciate the non-linearity of the changes.

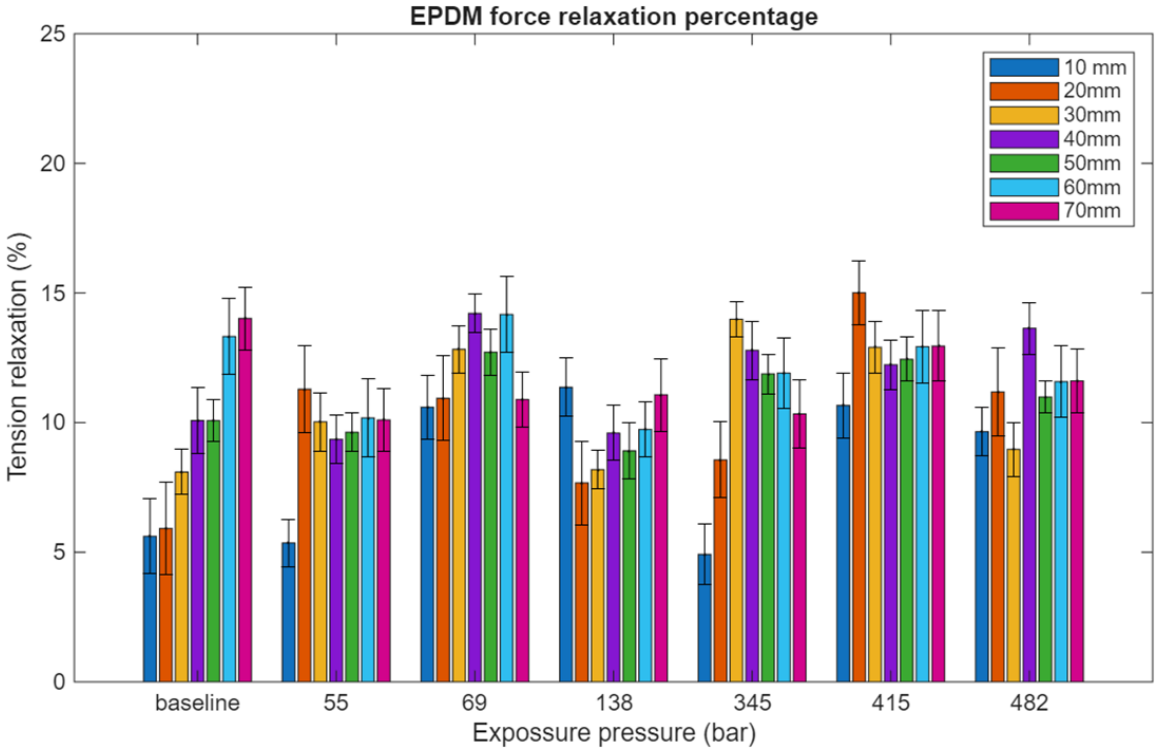


Figure 53: Comparison of the tension relaxation percentage for the different deformation levels as a function of the pressure the EPDM-based material was exposed to.

4.2.4 Material comparison

Figure 54 shows a comparison of the tensile relaxation percentage for each deformation level grouped according to the aging pressure to which the material samples were exposed to. In this case, the exposure to hydrogen gas at a pressure of 55 bar has different effects on the materials. From this figure we can observe how the NBR material displays a more uniform relaxation response when compared to the other two materials tested. Furthermore, from this comparison, the magnitude of the force relaxation of each material can be compared. In the case of deformations of less than 60 mm FKM displays a smaller

percentage of relaxation compared to EPDM and FKM. Nevertheless, at a deformation of 70 mm FKM displays a larger drop. These results serve to highlight the material dependency on hydrogen induced degradation as well as the non-monotonic response as a function of the exposure pressure.

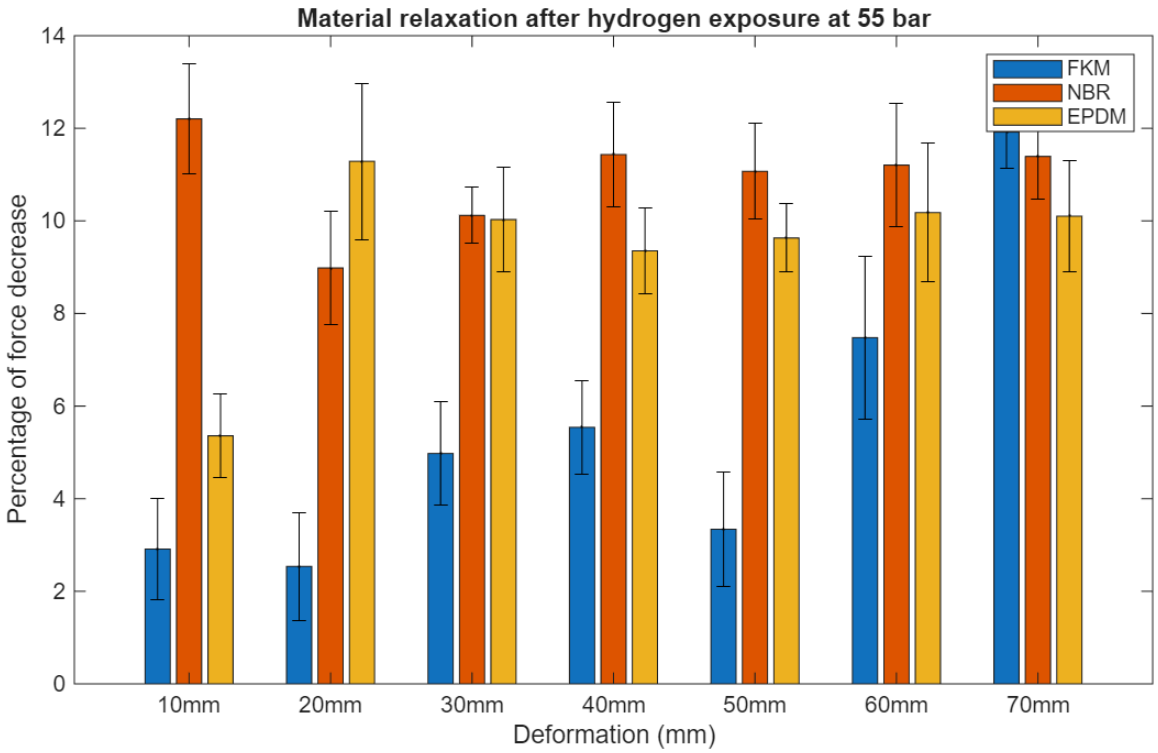


Figure 54: Comparison of the tension relaxation percentage for the different materials exposed to hydrogen environment at 55 bar and subjected to varying deformation levels.

4.3 Hardness measurement

As previously described, the material O-ring samples were sliced at multiple locations of the circumference. The hardness of the cross section was then analyzed to determine changes in hardness caused as a result of material interactions with hydrogen gas. This measurement serves to illustrate the changes to wear resistance that the materials undergo due to hydrogen assisted degradation. In this way, the analysis of the changes in hardness associated with exposure to hydrogen gas can be used to determine changes to wear resistance on polymer-based materials. Furthermore, determining the relation between hardness changes and pressure is essential for the design of components in dynamic

applications, where polymer materials are expected to be affected by predictable wear in a predictable manner. Hence, the hardness of the materials analyzed was measured after exposing the samples to hydrogen gas at different pressure levels. The following sections present a summary of the changes to shore A hardness measured for the three polymer-based O-ring materials investigated.

4.3.1 FKM material

Figure 55 shows the changes in shore A hardness for the FKM material samples for the different exposure pressures investigated. In this case, the hardness shows a significant decrease after exposure to hydrogen gas. The measured hardness for the samples exposed to 55 bar had an average shore A measurement of 72.0. Following this sharp decline, the samples exposed to 69 bar, 138 bar, and 345 bar showed values of 73.6, 73.6, and 73.9 respectively. Finally, the samples exposed to 482 bar showed a hardness value of 72.2. While these results do not display a linear dependency with respect to exposure pressure, they mirror the findings of the tensile and relaxation studies performed. In this case, the material degradation is highest for the exposure pressures of 55 bar and 482 bar, with the intermediate exposure levels showing a condition closest to the baseline at the exposure pressure of 345 bar. In this way, these results highlight the competing effects between material swelling and internal stress generated by the pressure gradient.

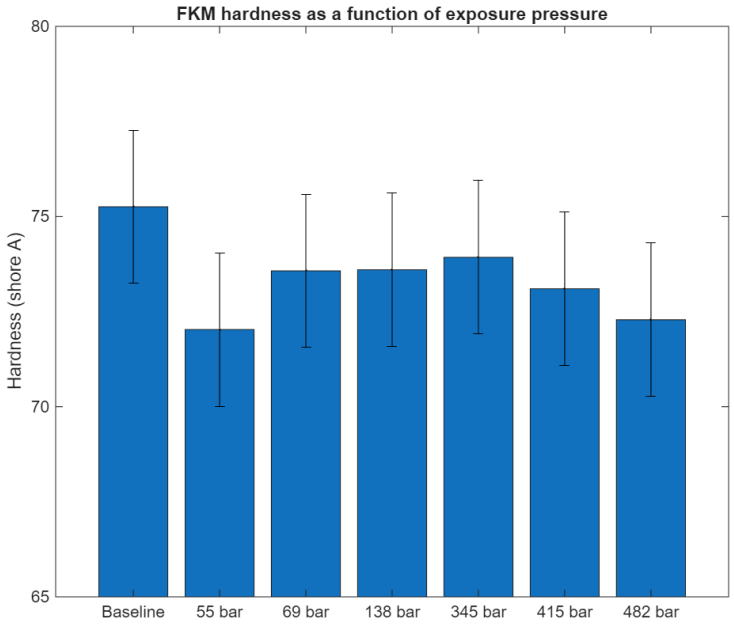


Figure 55: Shore A hardness measured for the FKM material samples as a function of the exposure pressure

4.3.2 NBR material

Similarly, the NBR based material was analyzed to determine changes to hardness as a function of the aging pressure. Figure 56 shows a comparison of the shore A hardness measured for the different pressure levels investigated. In this case, the material showed a reduced effect when compared to FKM. Only the samples exposed to 55 bar showed a significant change, showing a hardness shore A of 70.9. In contrast, the rest of the samples showed an average of 72.4, deviating minimally from the calculated baseline average of 73.0. In this case, the exposure pressure of 55 bar shows a sharp decline with respect to the baseline condition followed by intervals of increasing and decreasing hardness.

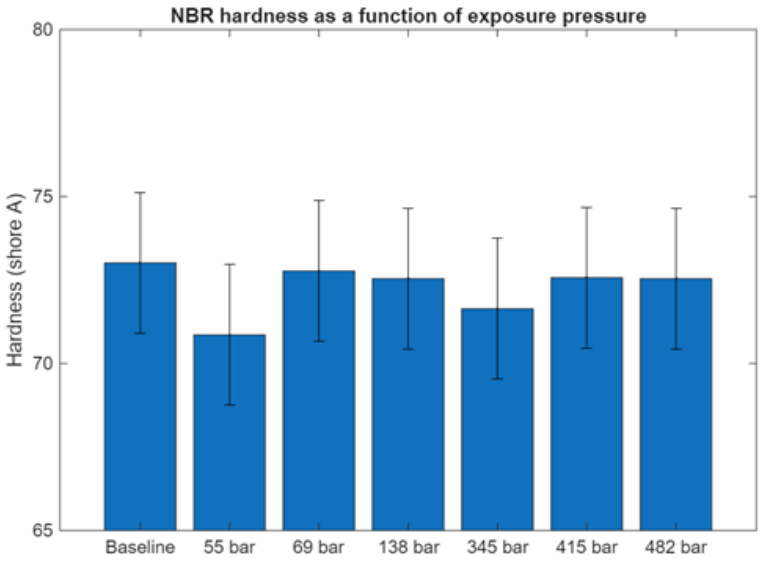


Figure 56: Comparison of the shore A hardness measured for the NBR samples exposed to different pressure levels

4.3.3 EPDM material

Lastly, the EPDM based material samples were analyzed in the same manner. In this regard, EPDM shows the greatest decrease in measured hardness for all of the pressure levels investigated. The samples exposed to 55 bar and 69 bar showed a measurement of 68.9 and 68.4 respectively, marking a sharp decline from the baseline average of 73.1. Similarly, the samples exposed to 138 show a hardness of 70.4, demonstrating an increase with respect to the lower exposure pressure but a clear decrease from the baseline. Similarly, the samples exposed to 345 bar, 415 bar, and 482 bar showed a shore A hardness of 68.8, 68.2, and 68.1 respectively. Figure 57 shows a comparison of the shore A hardness measured for the samples exposed to hydrogen gas at different pressure levels. Once again, the hardness of EPDM does not display a linear relationship with the aging pressure. In its place, we can observe distinct segments in which the hardness decreases as a function of pressure. However, a higher value is observed for the exposure pressure of 138 bar when compared to

the other material conditions. These results could be indicative of the competing effects of hydrogen dissolution in the material and the internal stresses that this generates.

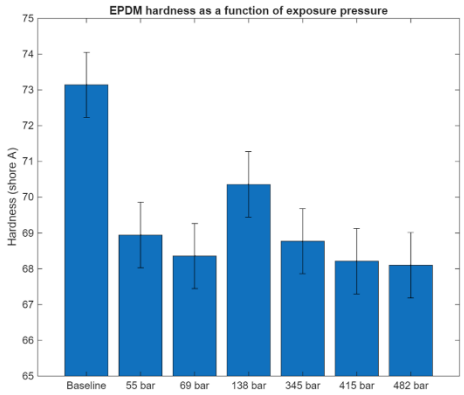


Figure 57: Measured shore A hardness for the EPDM based material samples exposed to hydrogen gas at different pressure levels.

4.3.4 Material comparison

In order to facilitate the comparison between the different materials, the shore A hardness value for the samples was normalized with respect to the baseline average calculated for each material prior to exposure to hydrogen gas. Figure 58 shows a comparison of the changes in the measured for the three materials investigated. In this case we can observe how the exposure pressure of 55 bar has a negative effect on the three polymers selected. However, the hardness of the EPDM material is the most affected by hydrogen exposure, showing the greatest decrease with respect to the baseline condition for all of the aging pressure levels. Following this, the NBR material tested shows the least material degradation for the aging pressures if 415 bar and 482 bar when compared to FKM and NBR.

Furthermore, the NBR material tested shows the smallest decrease with respect to the baseline condition for all of the aging pressures.

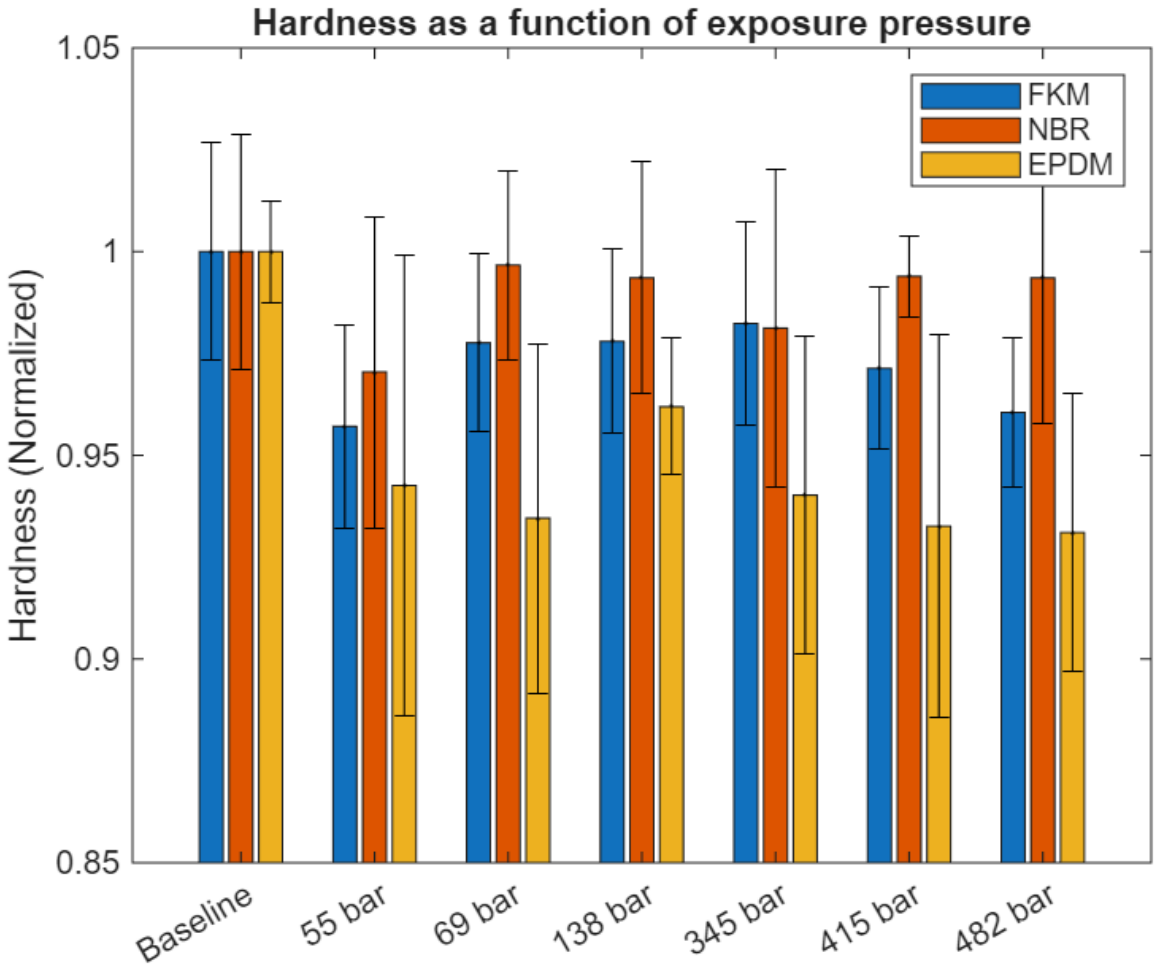


Figure 58: Shore A hradness measurement normalized with respect to the baselline average for the three materials investigated as a function of the expossure pressure.

4.4 Material imaging

While the data obtained through mechanical analysis of the materials investigated provides valuable information regarding how interaction with hydrogen gas affects different polymers, it is not enough to explain these changes. In this regard, microscopic imaging of cross sections obtained from the samples studied provides insight into structural changes that could explain the observed changes in mechanical properties. To this end, slices from the material samples exposed to hydrogen gas were obtained and imaged. The following

sections provide a summary of the results obtained for the three polymer-based materials tested.

4.4.1 FKM material

Figure 59 shows three images obtained from different O-ring samples representing the typical conditions observed for the exposure pressures of 55 bar, 69 bar, and 138 bar respectively. From this image we can observe the high concentrations of filler particles observed in the baseline conditions. However, in this case, the material presents an increased number and size of cavities as the exposure pressure increases. Tiles A through C show small cavities and shadows formed around filler particles. These features were typical for the samples aged at a pressure of 55 bar and appear with a relatively low frequency. Similarly, tiles D-F shows cross sections of material samples exposed to 69 bar. In this case, the cavities appear with a darker color and larger size, thus being easier to identify. Lastly, tiles G-I shows examples of the samples exposed to 138 bar. In this case, the cavities have edges that are more defined and appear in higher numbers.

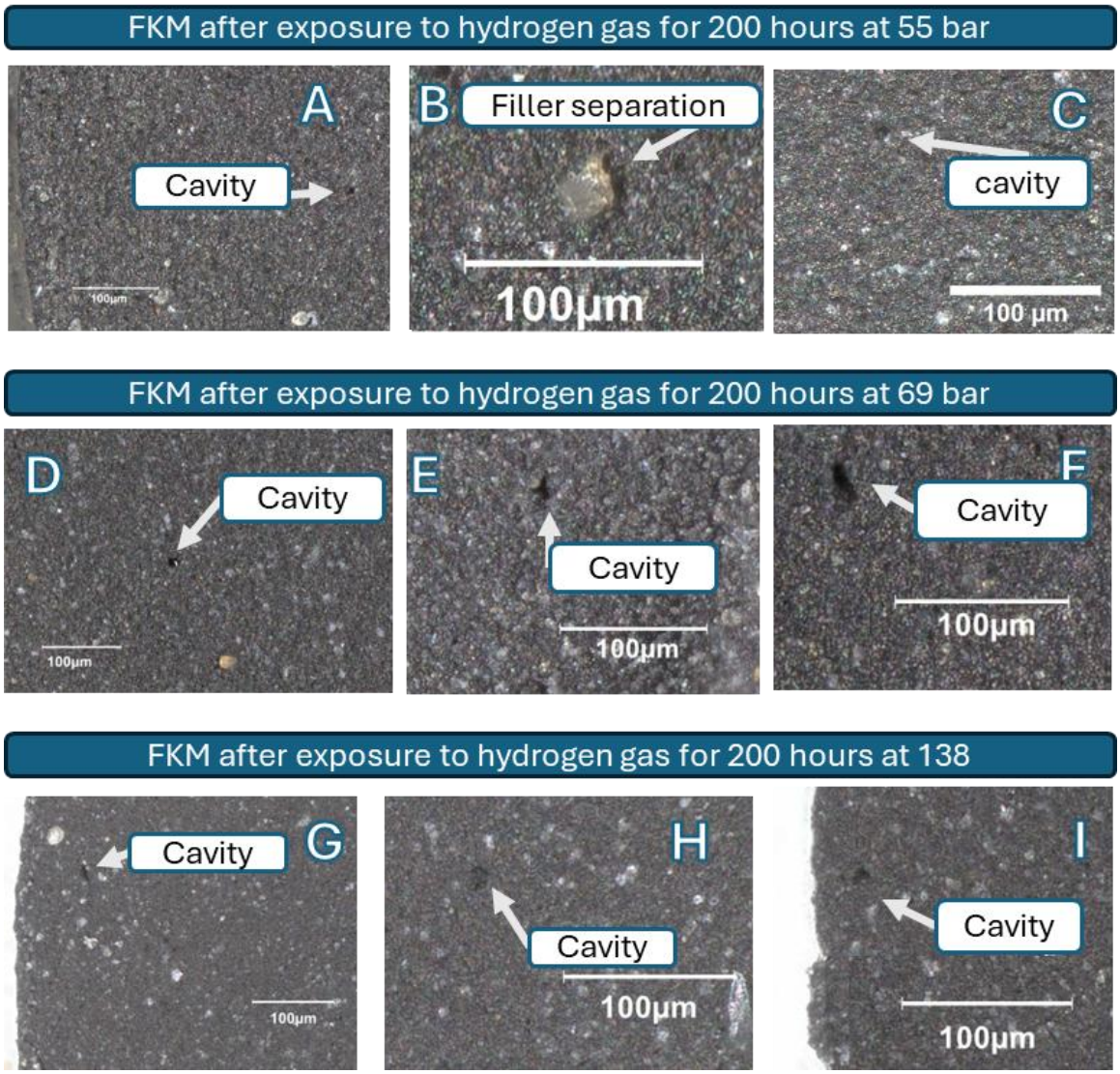


Figure 59: Microscopic images obtained from FKM O-ring samples exposed to hydrogen gas at 55 bar 69 bar and 138 bar respectively highlighting the main defects observed.

Similarly figure 60 shows cross sections typical for the samples exposed to hydrogen at pressures of 345 bar, 415 bar, and 482 bar. Tiles A-C show cress sections of samples exposed to 345 bar. In this case, the samples display cavities of different sizes through the imaged area. Following this tiles D-F show samples exposed to 415 bar. In this case, the sample displays an increase in the number of defects near the edge of the specimen. Tile D shows a field of cavities with varying sizes while tile F shows an accumulation of filler particles with voids between them. In contrast, tile E shows cavities distributed through the specimen

cross section. Lastly, tiles G-I show typical cross sections of samples exposed to 482 bar. In this case, the number and size of cavities is higher when compared to the other material conditions. Particularly, tile H displays the most numerous and largest cavities observed for the FKM samples.

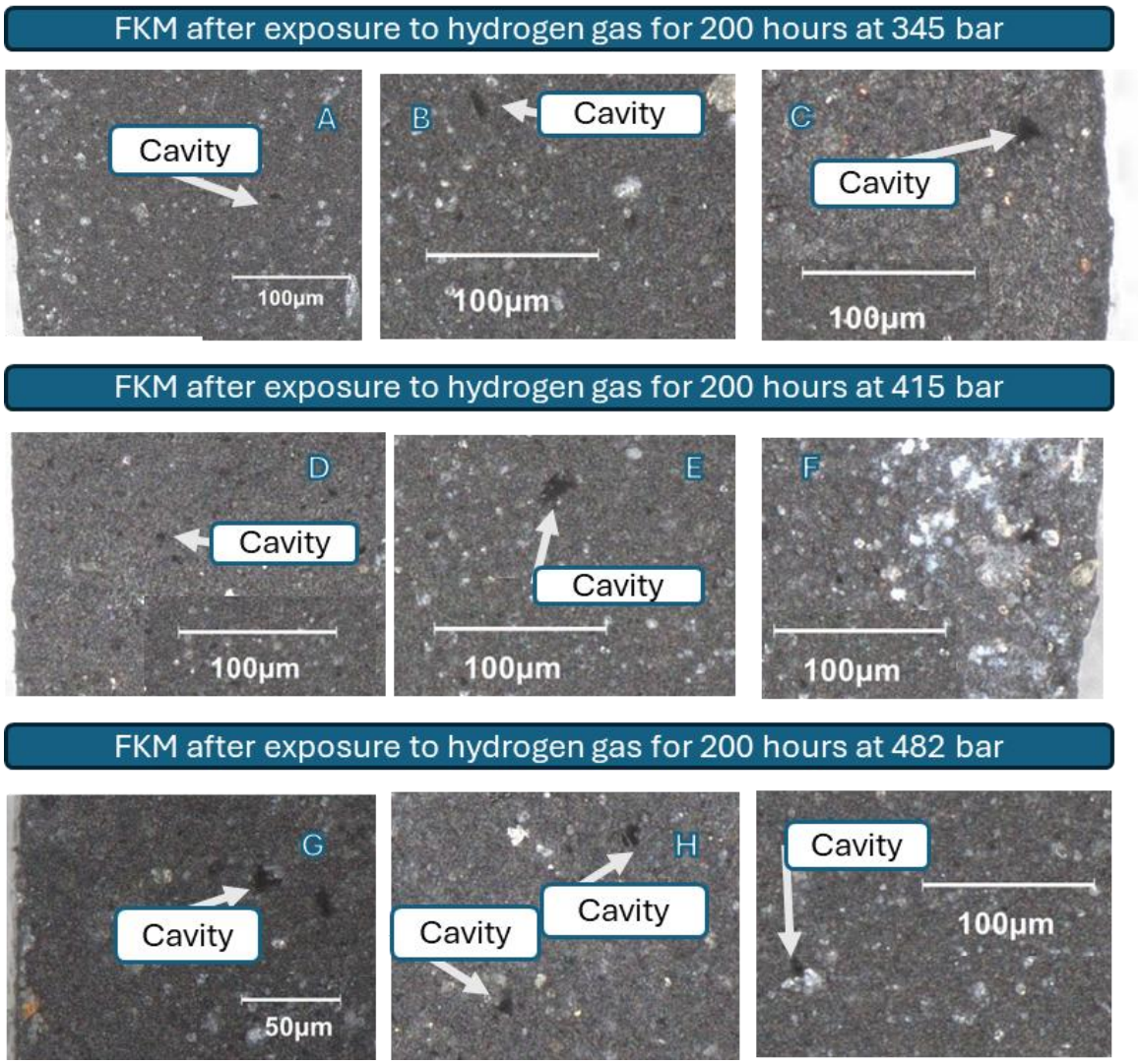


Figure 60: Microscopic images obtained from FKM O-ring samples exposed to hydrogen gas at 345 bar 415 bar and 482 bar respectively highlighting the main defects observed.

Following the imaging of material samples, computational methods were used to calculate the average area of the cavities observed as well as the fraction of the total area covered by these defects. The information obtained from the analysis of different images was then used

to quantify the changes observed as a consequence of the effects of exposure to hydrogen gas at varying pressure levels. Figure 61 A shows the average cavity area calculated from multiple cross sections at the different aging pressure levels investigated. In this case, the material displays the largest cavities when exposed to a pressure of 69 bar. Following the trend observed with the mechanical analysis of the material, the average cavity size decreases for an exposure pressure of 138 bar steadily increasing as a function of the aging pressure. Interestingly, the standard deviation of the cavity size at an exposure pressure of 415 bar and 69 bar reflect the variability on the calculated area due to larger defects observed for these material conditions. Similarly, figure 61 B shows the calculated area fraction occupied by cavities. In this case the percentage of the cross section occupied by defects appears to increase as a result of exposure to hydrogen gas at the investigated pressures of 69 bar and higher. Furthermore, the calculated area fraction increases along with the aging pressure. Nevertheless, the largest fraction is observed by an exposure pressure of 345 bar at 0.32 %. These results continue showing evidence of competing effects between swelling of the material due to hydrogen permeation and the internal stresses generated by the pressure gradient inside the polymer matrix.

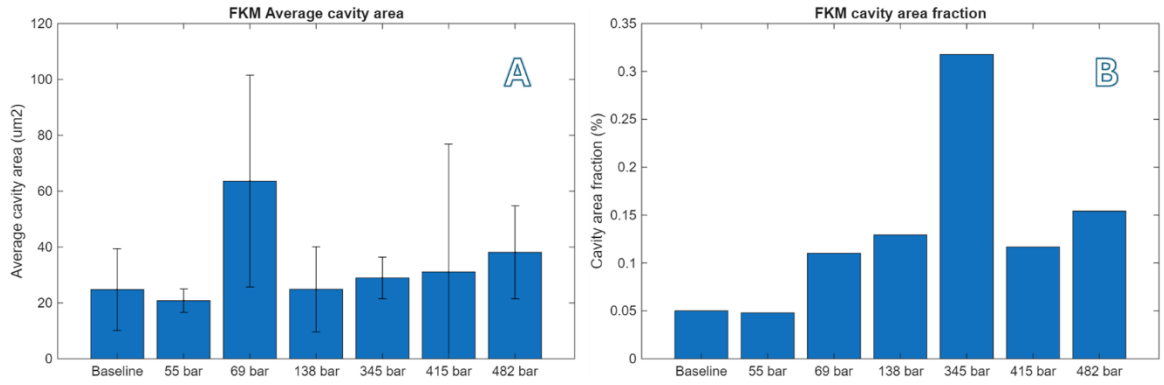


Figure 61: Results of the image analysis for quantification of voids for FKM material

4.4.2 NBR material

Following this trend, the samples obtained from NBR-based O-rings were also imaged and analyzed. Figure 62 shows typical cross sections from NBR samples exposed to 55 bar, 69 bar, and 138 bar. In this case we can appreciate the lower concentration of filler particles

when compared to the FKM based samples. Tiles A-C show typical features observed for NBR samples exposed to 55 bar. IN this case, we can observe well defined cavities with circular edges. Similarly, tiles D-F shows examples of the material exposed to 69 bar. In this case, the cavities appear in greater numbers through the cross section. Furthermore, the variability in size and shape of the defects increases for this exposure pressure. Lastly, tiles G-I show typical features observed in NBR samples exposed to 138 bar. In this case, the cavities appear with lower frequency compared to the samples aged at a pressure of 69 bar. However, the outer edge of the imaged cross sections showed an increased number and type of defects such accumulation of filler particles on tiles G and H and an instance of different polymer phases on tile I.

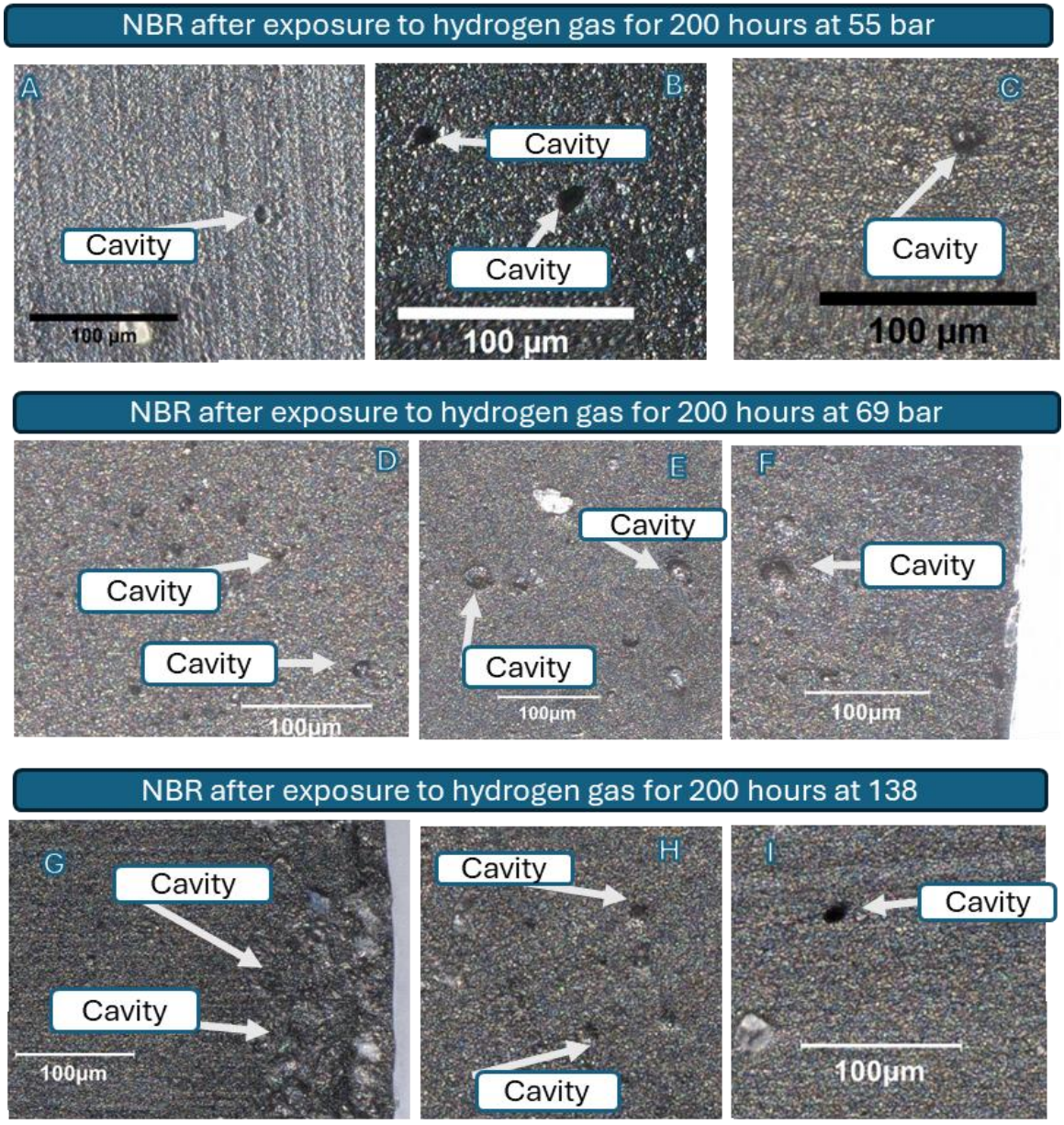


Figure 62: Microscopic images obtained from NBR O-ring samples exposed to hydrogen gas at 55 bar 69 bar and 138 bar respectively highlighting the main defects observed.

Following this, figure 63 shows typical cross sections of the NBR samples exposed to hydrogen gas at higher pressures. Tiles A-C show the typical features observed on the samples aged at a pressure of 345 bar. In this case we can observe further instances of separation between acrylonitrile and butadiene phases of the material. Furthermore, the variability of the size and concentration of the cavities increases when compared to lower

exposure pressures. Similarly, tiles D-F show further instances of phase separation. However, in this case, the darker polymer material shows blistering and cracks which are likely to be caused by the effects of hydrogen gas permeation. Lastly, tiles G-I show examples of NBR material samples exposed to hydrogen gas at a pressure of 482 bar. In this case, the material shows extreme instances of blistering through both material phases, highlighting the damage caused by hydrogen gas dissolution and the subsequent depressurization.

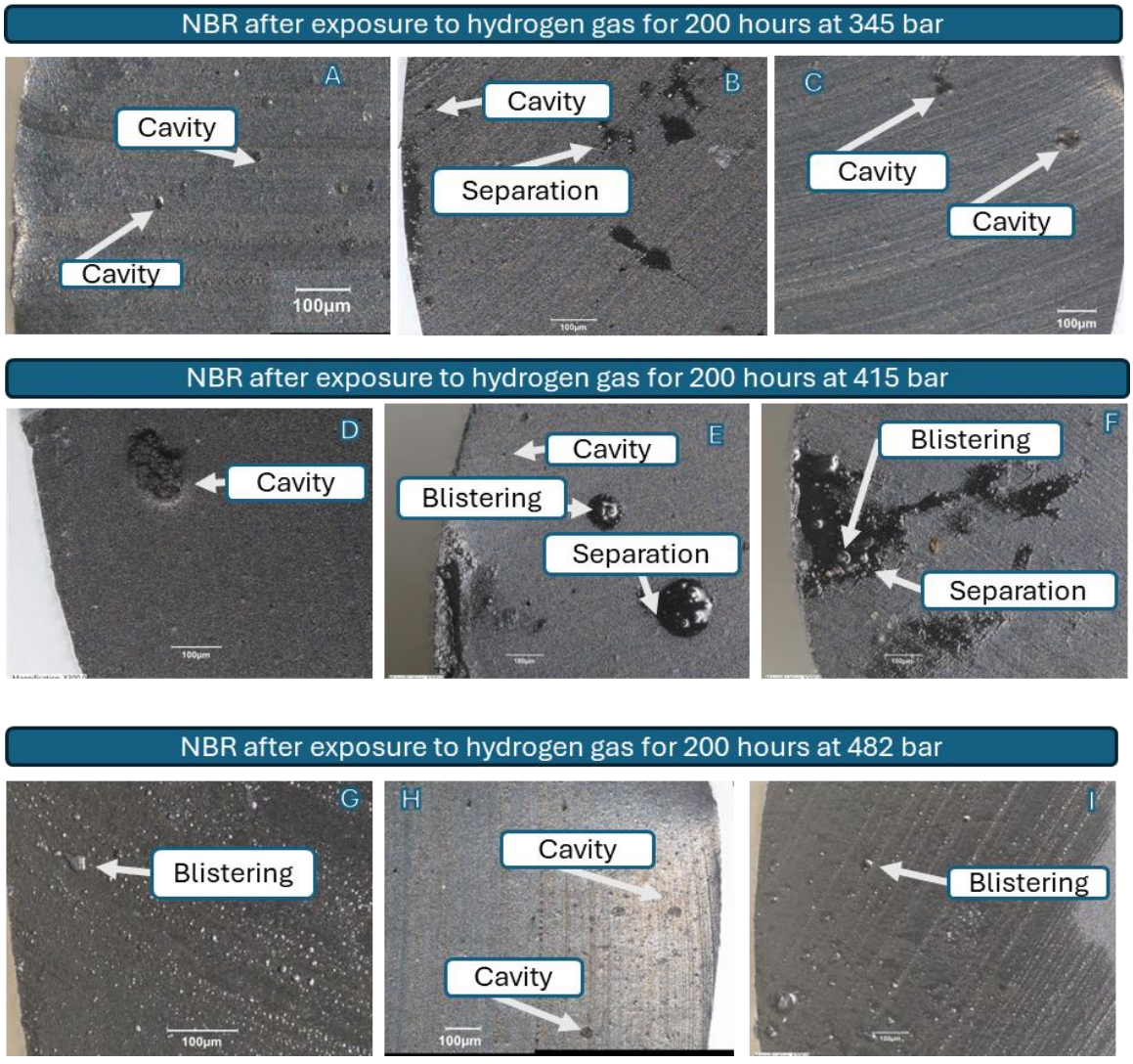


Figure 63: Microscopic images obtained from NBR O-ring samples exposed to hydrogen gas at 345 bar 415 bar and 482 bar respectively highlighting the main defects observed.

Following the imaging of the NBR material sample cross sections obtained. The previously described computational analysis was utilized to calculate the average area of the cavities observed as shows on figure 64 A. For this material, the largest defects, with an average size of 234 um^2, were observed after exposure to a pressure of 415 bar in a hydrogen gas environment. Similarly, the material exposed to 345 bar shows relatively large cavities with an average size of 141 um^2. Additionally, figure 64 B shows the calculated area fraction covered by the defects imaged. In this case, the material shows the largest coverage of 1.69 % and 1.56 % for aging pressures of 345 bar and 415 bar respectively. In this way, these results suggest that the competing effects of material swelling and the internal stresses generated by the pressure gradient inside the polymer matrix inhibit the formation or enlargement of existing cavities at a pressure 482 bar, where the material exhibits an average cavity area of 54.1 um^2 and a defect area fraction of 0.71 %.

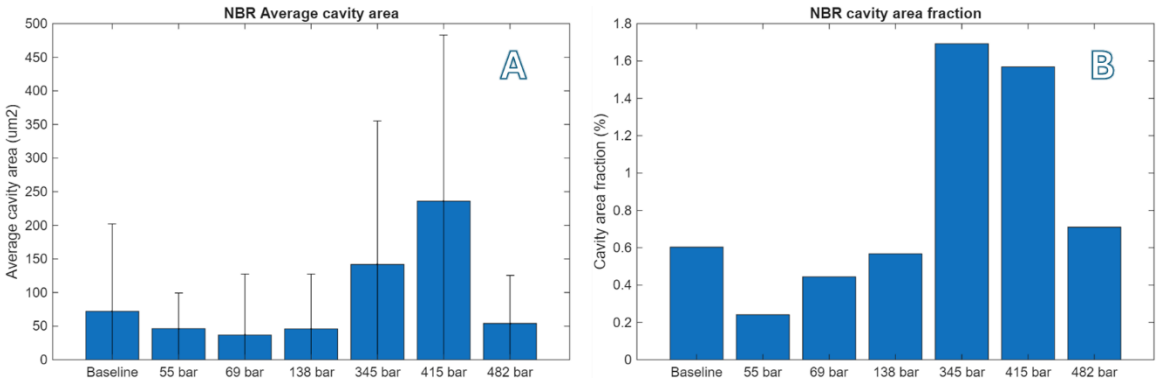


Figure 64: Results of the image analysis for quantification of voids for NBR material.

4.4.3 EPDM material

Likewise, figure 65 shows typical cross sections obtained from EPDM samples exposed to hydrogen gas. Tiles A-C show examples of material samples aged at a pressure of 55 bar. In this case, the material displays filler particles of a relatively large size as well as cavities with a circular, well-defined edge. Similarly, tiles D-F show typical cross sections of the EPDM samples exposed to 69 bar. In this case, the material shows an elevated number in cavities as well as an increase in the variability of their size. Furthermore, tiles E and F display cavities surrounding filler particles, suggesting accumulation of hydrogen gas at interstitial sites,

leading to blistering and the loss of mechanical properties. Lastly, tiles G-I show examples of the features observed on samples exposed to hydrogen gas at 138 bar. In this case the material displays agglomerations or groups of cavities.

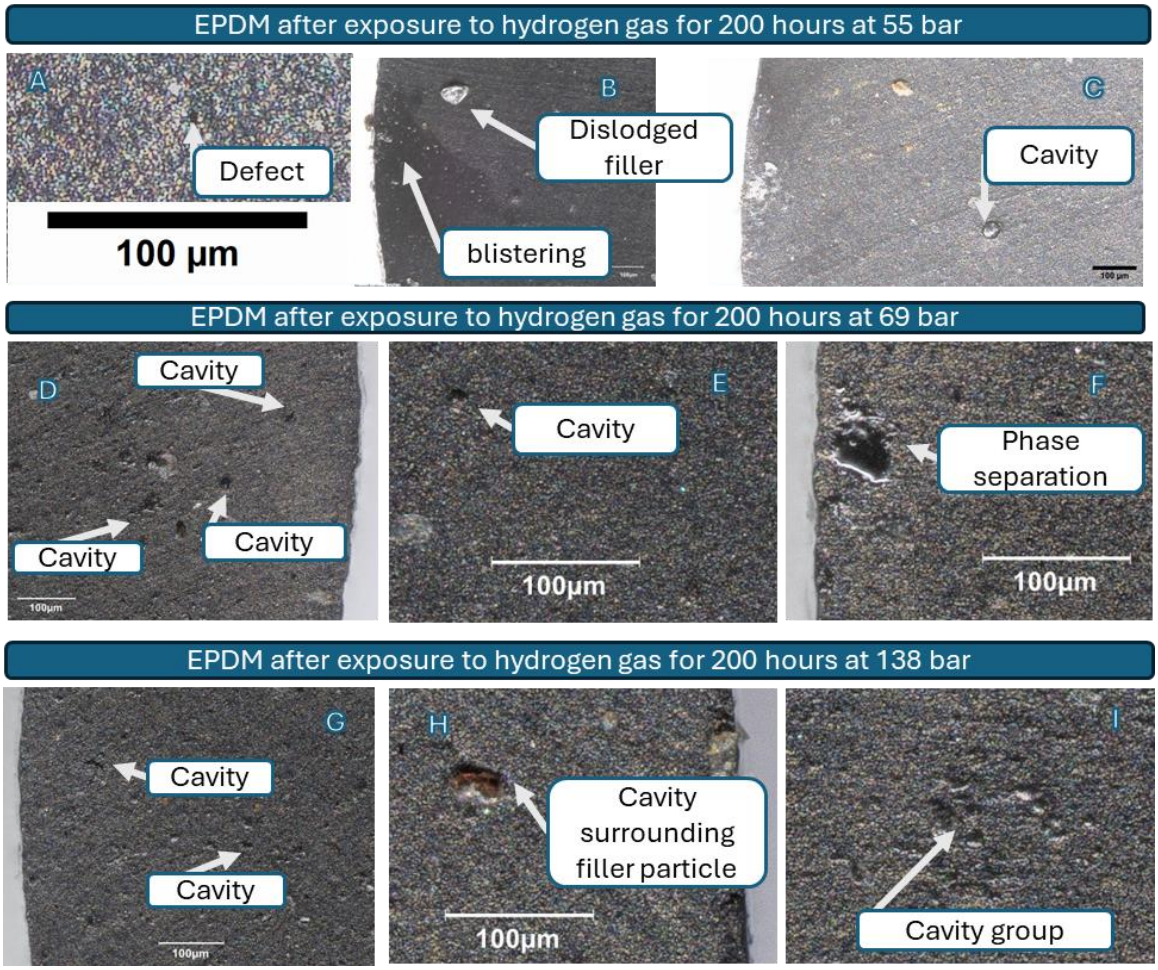


Figure 65: Microscopic images obtained from EPDM O-ring samples exposed to hydrogen gas at 55 bar 69 bar and 138 bar respectively highlighting the main defects observed.

Additionally, figure 66 shows some of the typical features observed on the cross sections obtained from EPDM material aged at higher pressures. Tiles A-C show images obtained from samples aged at 345 bar. In this case we can observe an accumulation of filler particles along with a large cavity. Similarly, an increased number in cavities as well as variability in their size can be observed. Following this, tiles D-F show features observed on samples aged at 415 bar. From these images we can observe a pronounced number of cavities with a large

size. Furthermore, some of these voids have well-defined edge suggesting the formation of a bubble or blister through gas inclusion. Lastly, tiles G-I show examples of the EPDM material exposed to hydrogen gas at 482 bar. In this case, the cavities are smaller when compared to lower pressures. However, these voids also appear to have a more uniform distribution through the O-ring cross-section.

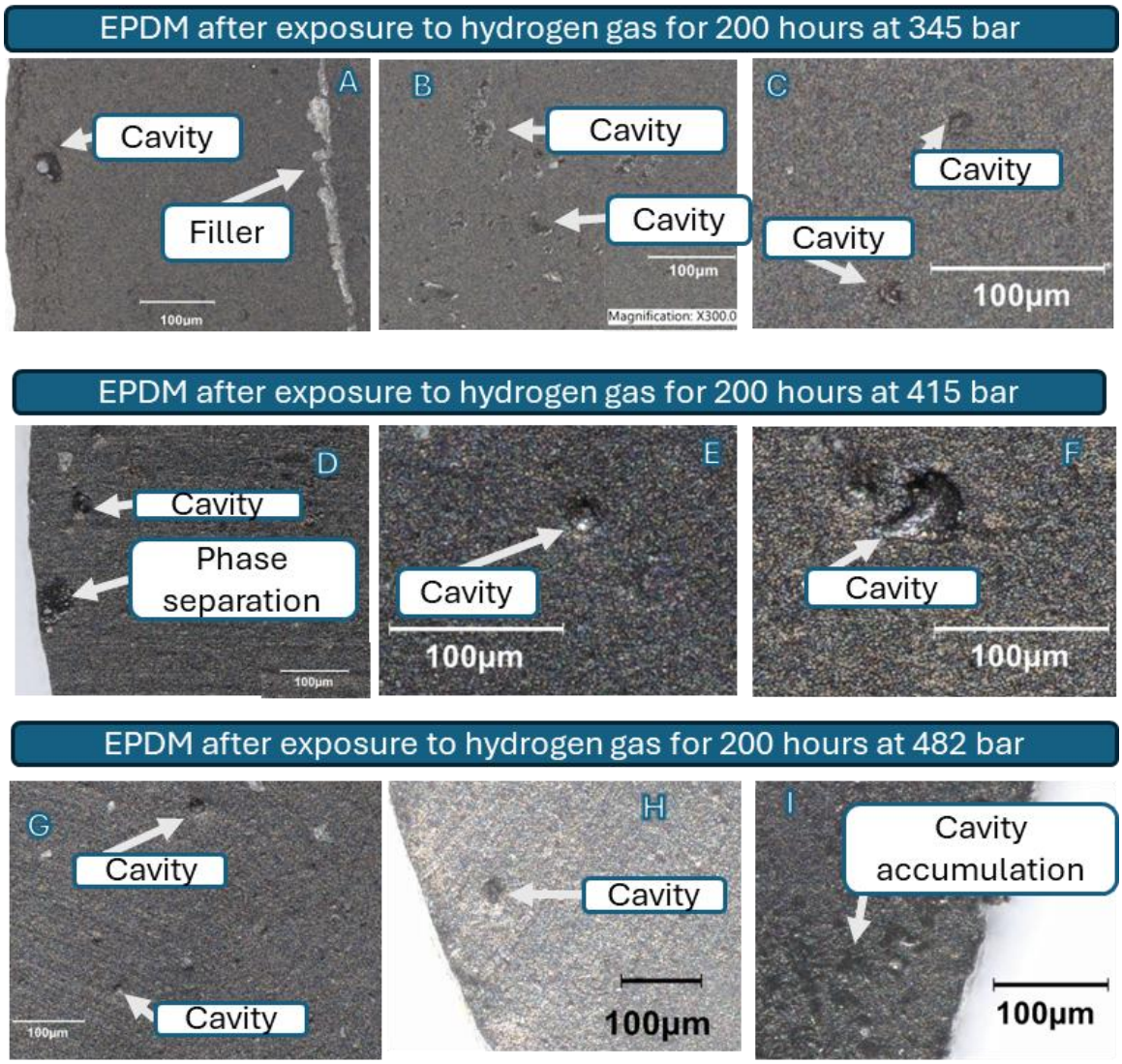


Figure 66: Microscopic images obtained from NBR O-ring samples exposed to hydrogen gas at 345 bar 415 bar and 482 bar respectively highlighting the main defects observed.

After collecting images from multiple sections of the different EPDM samples, the computational analysis previously described was carried out. Figure 67 shows a plot of the

average cavity area and the area fraction occupied by these defects. Figure 66 A highlights the presence of larger defects through the specimen cross section, as shown in figure 67 F and H, through the elevated value of standard deviation. Furthermore, the highest average defect size observed for EPDM occurs at an aging pressure of 55 bar with an area of 86.6 μm^2. Nevertheless, the average cavity area remains lower than 100 μm^2 and shows a decreasing trend between 55 bar and 138. For the aging pressures of 69 bar and 138 bar the average defect size are 59.2 μm^2 and 28.9 μm^2 respectively. Following this, the exposure pressures of 345 bar and 415 show an increasing trend with average cavity sizes of 51.9 μm^2 and 57.2 μm^2 respectively. Lastly, the material exposed to a hydrogen environment at a pressure of 482 bar showed a reduced average defect size of 27.2 μm^2. Additionally, figure 67 B shows a comparison of the area fraction covered by cavities as measured for the EPDM samples exposed to hydrogen gas. In this case the exposure pressures of 55 bar, 138 bar and 482 bar show a cavity area fraction of 0.4 %, 0.37%, and 0.36% respectively. These values are lower than the baseline area fraction of 0.47 %. In contrast, the exposure pressures of 69 bar, 315 bar and 415 bar show a cavity area fraction higher than the baseline at 0.73 %, 0.59 % and 0.64 % respectively.

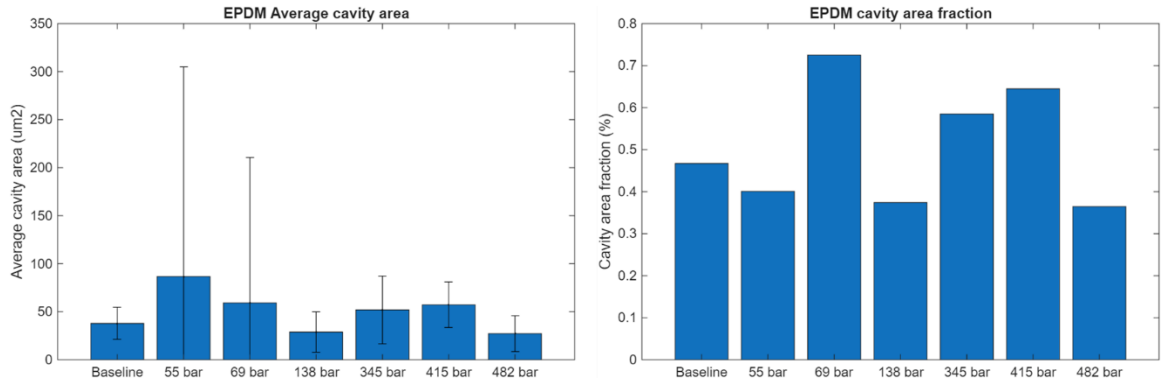


Figure 67: Results of the image analysis for quantification of voids for EPDM material.

4.4.4 Material comparison

The information collected through the image analysis of the different materials was used to construct a comparison of the effects of hydrogen gas pressurized at different levels. Figure 68 A shows comparison of the average cavity size normalized with respect to the bassline

condition for the three polymer-based materials. In this figure we can observe that the largest departure from the baseline does not occur at the same exposure pressure for the three materials. In this case, the FKM is most affected by an ageing pressure of 69 bar, showing an average defect size of 2.56 times the average calculated for the baseline. Similarly, the EPDM based material investigated shows the greatest degradation for an exposure pressure of 55 bar with cavities 2.29 times as large as the average calculated for the material prior to hydrogen exposure. In contrast, the NBR material shows the largest defects after exposure to hydrogen gas at a pressure of 415 bar, where the average defect size calculated is 3.27 times that of the baseline condition.

Similarly, figure 68 B shows a comparison of the average area fraction covered by defects as calculated for multiple material specimen cross sections. In this case, the FKM material showed a greater increase in the area covered by defects. While the size of the cavities did not increase, this was caused by an increase in their numbers. In contrast, the defect coverage EPDM material was the least affected by hydrogen exposure with exception of the 69 bar pressure level, where NBR shows less coverage. These results highlight the differences between the ways the materials are affected by hydrogen gas, specifically, the difference between which pressure level causes the most significant degradation can be observed.

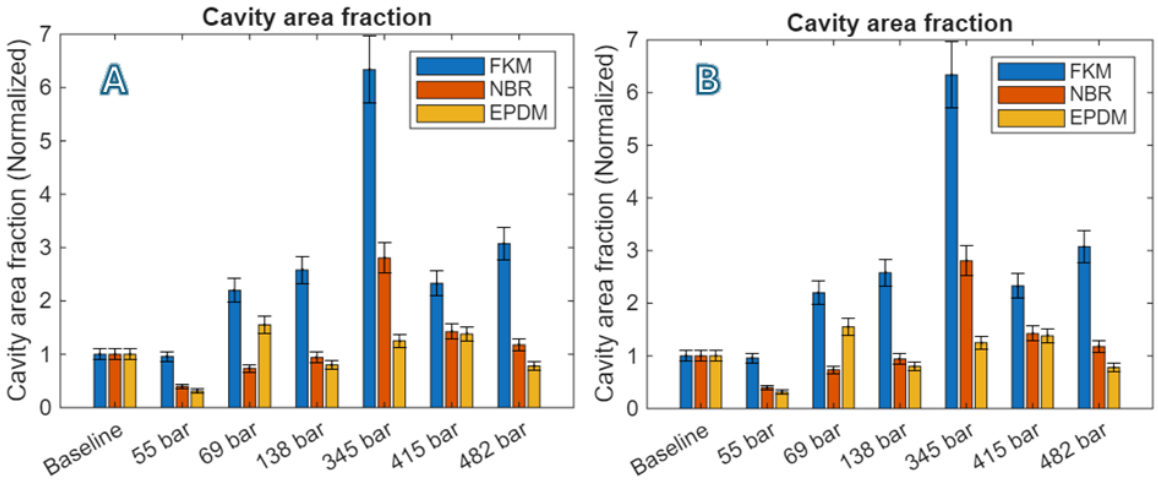


Figure 68: Comparison of the average cavity area (A) and cavity area fraction (B) observed on the different material samples exposed to hydrogen gas at different pressure levels.

4.5 Conclusion

Multiple findings were obtained through the mechanical analysis performed on the materials samples exposed to a hydrogen environment. Firstly, changes in the tensile strength of the materials selected for multiple exposure pressure levels were measured and characterized over multiple samples. Similarly, the tensile relaxation behavior of the O-ring samples investigated was analyzed to determine the effect of hydrogen infiltration on the deformation response of the materials. This information was used to evaluate changes in stiffness of the polymer matrix between the different materials. Additionally, the shore A hardness of multiple cross section specimens was used to evaluate changes in wear resistance of the polymers as a function of the aging pressure. This information was then used to determine the changes to mechanical properties as a result of hydrogen exposure as well as to evaluate pressure-dependency of these changes. Additionally, imaging of the material samples produced valuable data on the enlargement of defects naturally existing within the material as well as the production of cavities due to interactions with hydrogen gas. The information gained through this study is then useful in establishing a comparison between the materials investigated.

CHAPTER 5: CONCLUDING REMARKS AND CONTRIBUTIONS

5.1 Research objectives and outlined findings

Polymer materials are formed by long carbon chains that form cross-linked networks [66]. For these materials, the cross-linking of the chains maintains the rigidity of the structure and heavily influences mechanical properties. Nevertheless, these cross-link bonds can be affected by chemical and mechanical processes such as the interactions with hydrogen observed gas molecules permeate the polymer. In this process, hydrogen molecules move through the polymer matrix occupying voids between the chains and exerting forces on them. These forces result in the dislocation of polymer chains, rupture of cross-linking bonds, and overall restructuring of the material [57]. In this regard, the free volume of the material becomes an important parameter influencing hydrogen assisted material degradation. Similarly, the infiltration of hydrogen molecules through the polymer matrix has a plasticizing effect, leading to changes in the mechanical properties of the material [66]. In this case, the presence of hydrogen molecules between the polymer chains reduced the molecular friction between carbon chains. This effect along with the scission of cross-linking bonds then leads to enhanced molecular mobility [66]. These combined processes then can lead to the expansion of the polymer matrix and the creation of larger voids and defects, thus affecting mechanical properties such as tensile strength and hardness. The extent of this plasticization effect is influenced by the ability of the gas molecules to diffuse through the polymer matrix as well as by the pressure gradient created by this diffusion. Figure 69 shows a schematic representation of this plasticization effect on polymer networks. While the plasticization of the polymer matrix leads to softening of the material, the rearrangement of the structure and the stresses generated by the pressure gradient can result in binding of the carbon chains. These competing effects can then lead to softening and hardening in polymers.

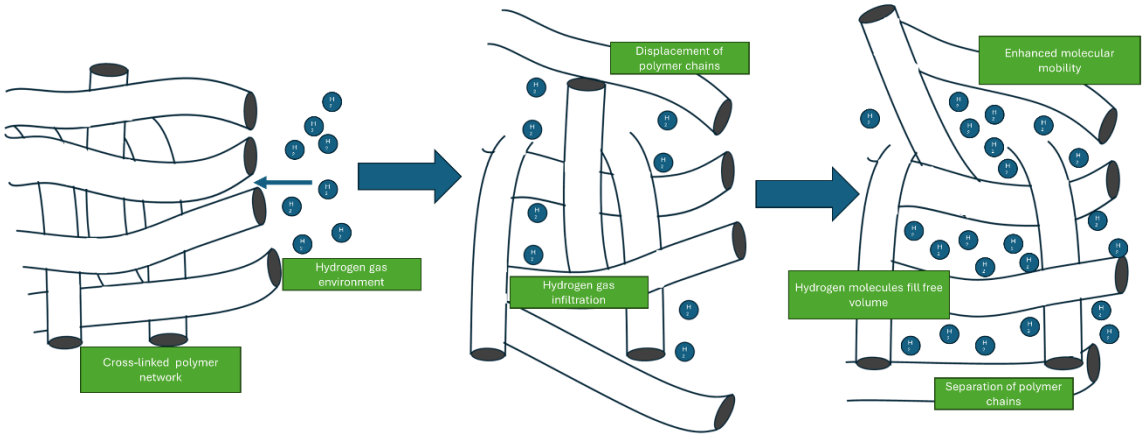


Figure 69: Schematic representation of plasticizing effect on polymers produced by hydrogen gas infiltration.

The objectives of this research are to investigate and characterize the changes to mechanical properties of general-use commercial polymer formulations as a result of exposure to pressurized hydrogen gas. Similarly, the changes to material morphology as a result of exposure to pressurized hydrogen gas were investigated. The pressure-dependent behavior of these changes was also investigated by comparing the material degradation caused by exposure of the material samples to varying pressure levels. Lastly, the differences in how the different materials present hydrogen assisted material degradation were investigated. The following chapter consolidates the experimental results to provide an understanding of the way the observed changes relate to mechanisms influenced by interactions between the polymer materials and hydrogen gas. The following section presents the conclusions reached based on the experimental results obtained from this study.

Objective 1: Investigate the effects of hydrogen exposure on mechanical properties of commercial polymer compounds commonly used for sealing components.

In this study, different experimental techniques were employed to investigate the effects of exposure to pressurized hydrogen gas on three commercial polymer materials, commonly used for the fabrication of sealing components. These polymer compounds were FKM fluoroelastomer, Acrylonitrile Butadiene Rubber (NBR), and Ethylene Propylene Diene

Monomer (EPDM). The mechanical properties of these materials were characterized before and after exposure to hydrogen gas at pressures ranging between 55 bar and 482 bar. The aging period was maintained at a constant duration of 200 hours for all tests. Similarly, the exposure temperature was maintained constant at 21 C for the different experiments in order to reduce the influence of temperature-dependent effects. The mechanical characterization tests included tensile strength, relaxation behavior, and maximum elongation, as well as measurement of material hardness. Through the different types of analysis performed on the three types of materials it is possible to understand the effects that exposure to pressurized hydrogen gas causes. The following conclusions were reached regarding the effects of hydrogen assisted material degradation on the mechanical properties of the polymer compounds investigated

1. The FKM material showed changes to mechanical properties due to the exposure to a pressurized hydrogen environment. A decrease in tensile strength of 8.9% and 10.1% was observed for exposure pressures of 55 and 69 bar, respectively. Furthermore, a similar reduction in tensile relaxation was observed for an aging pressure of 55 bar with respect to the baseline condition. Additionally, the investigated FKM material exhibited changes in the relaxation modulus and differences in the tensile response at identical deformation levels after exposure to hydrogen gas. Lastly, the shore A hardness of material samples obtained from the O-ring samples showed a significant decrease in specimens aged through hydrogen interactions.
2. The NBR material showed an increase in the tensile strength caused by exposure to hydrogen gas. After exposure to a hydrogen environment at a pressure of 415 bar and 482 bar the tensile strength of the NBR samples increased by 11.6% and 13.6%, respectively. Similarly, the NBR material investigated showed identical deformation levels in the tensile response after exposure to pressurized hydrogen gas. The relaxation modulus of the material and the percentage of force dissipated through relaxation also showed a change because of interactions between the polymer and

the hydrogen gas molecules. However, the material hardness did not display a significant change except for the aging pressures of 55 bar and 345 bar.

3. The EPDM material showed an increased tensile strength as a result of exposure to pressurized hydrogen gas. In this case, the tensile strength increased by 5 % after exposure to hydrogen gas pressurized at 69 bar when compared to the baseline condition. The tensile deformation response to identical deformation levels also saw an increased force value for samples exposed to 69 bar and 138 bar, when compared to the samples not exposed to hydrogen gas. Additionally, the percentage of force relaxation for the EPDM O-rings tested changed after exposure to hydrogen gas. Together, these materials suggest a change in stiffness as a result of interactions between the polymer and hydrogen gas. Furthermore, the EPDM material displayed a significant decrease in material hardness for all of the exposure pressures.

The effects of exposure to hydrogen gas, changes to mechanical properties in the materials selected have been identified and characterized. These changes in mechanical properties are assumed to be induced by the permeation of the hydrogen gas and the plasticization effect it has over the polymer matrix. In this way, the results from this study contribute to the understanding of interactions between polymer materials and hydrogen gas.

Objective 2: Image and characterize the changes to material morphology in commercial polymer compounds caused by hydrogen exposure.

Following the mechanical analysis of the studied samples, material imaging and computational methods were used to characterize the average cavity size and their concentration on cross sections obtained from the O-ring samples exposed to pressurized hydrogen gas. The results from material imaging suggest material-dependent competing effects between swelling due to hydrogen dissolution and the stresses produced by the pressure gradient, limiting the mobility of the polymer chains. In this case, each of the materials displayed larger and more numerous cavities at different pressure levels. Nevertheless, the three materials showed a tendency to be affected by hydrogen induced material degradation.

1. In the case of the FKM, samples exposed to 69 bar showed the greatest change in the average cavity size. At this exposure pressure the average change in area was 63.6 μm^2. Compared to the baseline condition that displayed cavities with an average area of 24.8 μm^2, this corresponds to an increase of 2.56 times. Similarly, after exposure to hydrogen gas, at a pressure of 345 bar, the FKM material showed an increase in the area fraction covered by cavities and defects from 0.05 % at the baseline condition to 0.32 %. These results reflect the increase in the free volume contained within the polymer matrix because of interactions from hydrogen gas. In this regard, the displacement of polymer matrix presents itself through the enlargement of existing cavities as well as through the creation of voids around filler particles and additives.
2. For the NBR material investigated, the average cavity area and the cavity area fraction observed for the material showed non-monotonic behavior with an increasing trend up to an exposure pressure of 415 bar and a sudden decrease for the exposure pressure 482 bar. In this case, the NBR material was most affected by an aging pressure of 415 bar, where the largest cavities with an average area of 235.9 μm^2 were observed. Compared to the baseline cavity area of 72 μm^2, the defects observed after exposure to 415 bar are 3.28 times as large. Tentatively, this is attributed to the displacement of the polymer matrix due to hydrogen absorption. Furthermore, after exposure to hydrogen gas at a pressure of 415 bar, the material shows an increased area fraction covered by effects from 0.6 % at the baseline condition to 1.57 %. This increase in defect coverage, along with an increase in average defect size hints at the enlargement of existing cavities and to the formation of new defects due to the displacement of polymer molecules. Additionally, after exposure to pressures of 345 bar and higher the O-ring samples displayed severe instances of phase separation between the rubber components. The areas affected by this phenomena displayed an increased number of defects in the form of bubbles and imperfections. These findings further highlight the plasticizing effect caused by the infiltration of hydrogen molecules through the free volume of the polymer matrix.

3. Following this trend, the EPDM material analyzed showed a similar pattern of increase in the cavity average area an increase in the area fraction covered by defects on the cross sections obtained from the material samples exposed to hydrogen gas. In this case, the average cavity area increased from 37.8 μm^2 to 86.7 μm^2 after being subjected to a hydrogen environment at 55 bar. This change corresponds to an enlargement of 2.29 times with respect to the baseline condition. Similarly, the area covered by defects increased from 0.46 % to 0.73 % after exposure to hydrogen gas. Additionally, samples exposed to a 55 bar and 69 bar displayed a few instances of defects significantly larger than the average size. These defects were not observed for the other aging conditions. Furthermore, the presence of these defects did not affect the mechanical properties of the material. Hence, the enlargement and formation of these void defects are tentatively attributed to displacement of the polymer matrix caused by the plasticizing effect of hydrogen gas.

The imaging of cross-section specimens obtained from the O-ring samples exposed to hydrogen gas contributes to our understanding of the interactions between polymers and hydrogen gas. Specifically, the enlargement of existing cavities and the proliferation of new defects were observed for all of the materials analyzed. Furthermore, evidence of the plasticization effect of hydrogen infiltration in polymers was observed for the NBR material analyzed. The characterization of the average defect size for the different material conditions analyzed provides a better understanding of macroscopic effects of hydrogen infiltration. Additionally, the characterization of the area fraction covered by defects in the different materials analyzed provides insight into the matrix displacement caused by the hydrogen molecules. In this way the results of this study contribute to the understanding of material compatibility for hydrogen applications.

Objective 3: Investigate the pressure dependent behavior of hydrogen assisted material degradation for polymer exposed to different pressure levels

Analysis of material samples exposed to a wide range of pressure levels reveals important information about the non-linearity of the changes in mechanical properties and material morphology as a function of aging pressure.

1. The FKM material investigated displayed a non-monotonic change to mechanical properties as a function of the exposure pressure. FKM samples showed a decrease in tensile strength for exposure pressures of 55 bar and 69 bar. Additionally, the greatest deviation in tensile strength from the baseline condition occurred on the samples exposed to hydrogen gas at a pressure of 69 bar. Similarly, the largest average cavity size was observed after exposure for this exposure pressure. In contrast, the samples exposed to 138 bar and higher show a relative increase in tensile strength. This trend of a decrease in mechanical properties followed by a relative increase and a downward trend is mirrored by the results obtained through the measurement of shore A hardness on cross section samples the material. Figure 70 shows a summary of the changes to the FKM material as a function of aging pressure normalized with respect to the values calculated prior to the hydrogen aging process. From this figure we can observe the sharp initial decrease in mechanical properties accompanied by an enlargement of existing cavities at exposure pressures of 55 bar and 69 bar. The non-monotonic behavior of the material is highlighted by an increase in the surface covered by cavities with a size comparable to the defects observed prior to hydrogen exposure. Together, these results indicate the creation of new voids in the polymer due to the plasticization and cavitation effects of infiltration of hydrogen gas. Nevertheless, the changes to mechanical properties for samples exposed to pressures of 138 bar, 345 bar, and 415 bar are less severe that those observed at lower pressures. These results could be interpreted as a consequence of the competing effects of plasticization and the underpinning of the polymer matrix by the stresses generated by the pressure gradient.

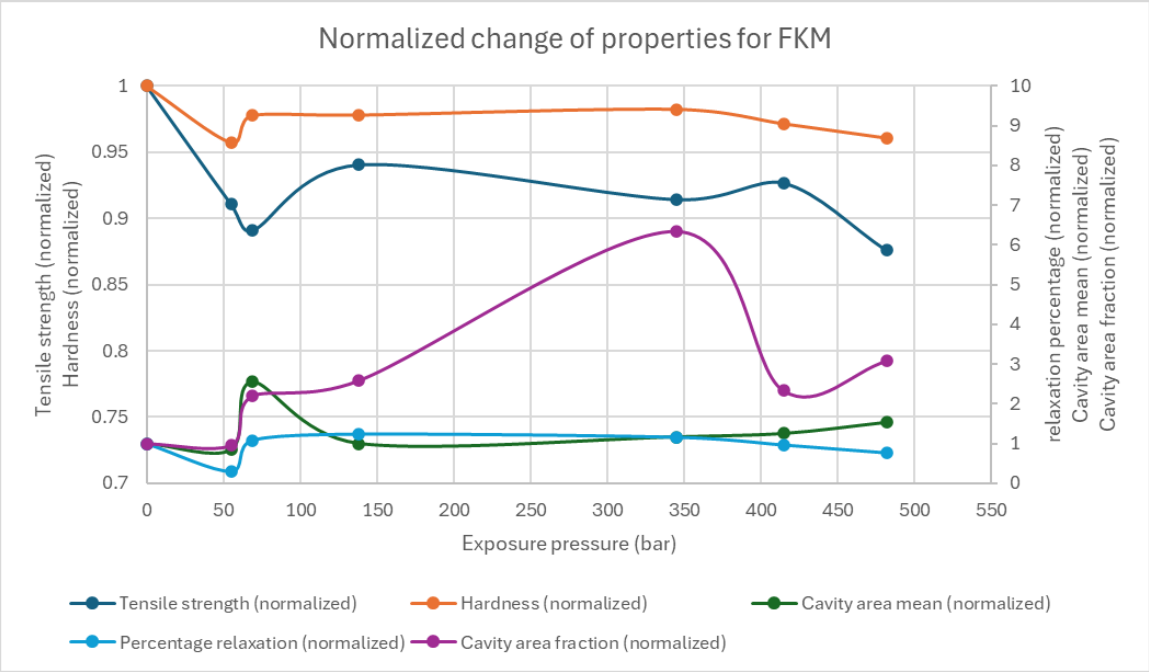


Figure 70: Summary of changes measured for FKM material as a function of aging pressure.

2. In contrast, the NBR material investigated displayed an increase in the tensile strength of the O-ring samples along with increased exposure pressure. This trend is marked by a sharp increase for samples exposed to a pressure of 69 bar followed by a stabilized tensile strength for aging pressures up to 482 bar. Similarly, the material's shore A hardness follows a similar trend, although with a smaller deviation with respect to the baseline condition. In contrast, the tensile relaxation for a deformation of 50 mm shows an initial decrease for exposure pressures of 55 bar and 69 bar followed by an increase in the percentage of force dissipated for samples aged at a pressure of 415 bar. Similarly, the cavity area mean and the fraction of material covered by defects display large increase with respect to the baseline condition for samples exposed to 415 bar before a sudden decrease for samples exposed to 482 bar. The non-monotonic nature of these changes is tentatively attributed to the competing effects of plasticization by infiltration of hydrogen. At most of the pressure levels investigated, the mechanical properties of the material are affected by interactions with hydrogen. However, at high pressures the plasticization effect promotes phase separation and the formation of defects on the acrylonitrile phase of

the rubber as shown in Chapter 4. Nevertheless, the formation of these defects does not seem to influence the mechanical properties of the material to a great extent. Figure 71 shows a summary of the changes observed for the NBR material normalized with respect to the baseline conditions.

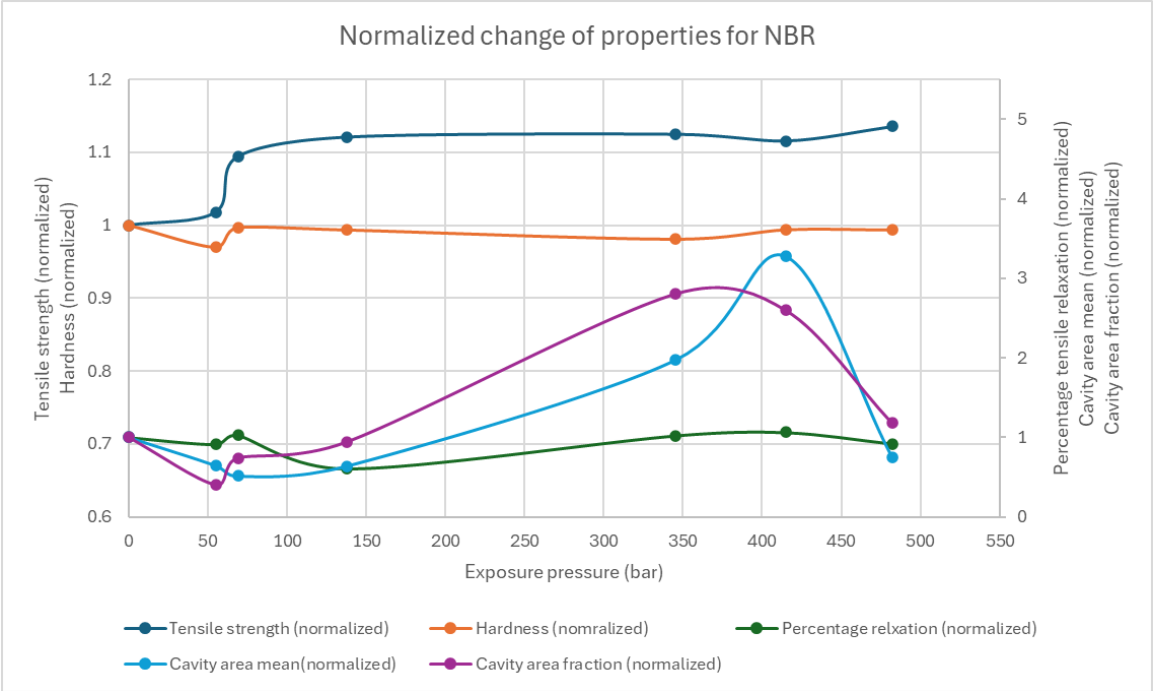


Figure 71: Summary of changes measured for NBR material as a function of aging pressure.

3. Lastly, the EPDM material showed a non-monotonic response in material degradation as a function of the aging pressure. In this case, while there is a general change in mechanical properties with respect to the baseline condition, the samples exposed to hydrogen gas at a pressure of 138 bar mark a change in the observed trends. For aging pressures of 55 bar and 69 bar the tensile strength of the material shows an increasing trend as aging pressure increases. However, the samples exposed to 138 bar show a sudden decrease in tensile strength relative to lower exposure pressures. This relative increase is then followed by a small increment in tensile strength as aging pressure increases. This trend is mirrored by the shore A hardness measured for the material. Samples exposed to 55 bar and 69 bar show a decreasing trend in hardness. Nevertheless, the samples exposed to 138 bar show a

sudden increase followed by a different decreasing trend for higher exposure pressures. Similarly, the material relaxation behavior of samples exposed to 55 bar and 69 bar show an increase in the force dissipated with respect to the baseline conditions. However, the samples exposed to 138 bar show lower relaxation than those not exposed to hydrogen gas. Moreover, the calculated cavity area mean and the percentage of the surface covered by these defects shows a larger increase for the exposure pressure of 69 bar compared to the closer aging pressures of 55 bar and 138 bar. Following this, the size and concentration of defects in the material cross section display a steady increase between the exposure pressures of 138 bar and 415 bar before displaying a sudden decrease for the highest aging pressure of 482 bar. The changes in the trends displayed suggest competing effects between plasticization and matrix underpinning. At the low range of exposure pressures covering 55 bar and 69 bar the material seems to undergo significant changes due to the small pressure gradient acting on the polymer matrix allowing high molecular mobility enhanced by plasticization. In contrast, at the exposure pressure of 138 bar, the forces holding the polymer chains in place overcome the plasticization effect of hydrogen molecules, allowing the material to retain a greater fraction of its original properties. This switch on the governing mechanism is observed again on the material relaxation and the results of image analysis between the exposure pressures of 415 bar and 482 bar. In this case, the samples exposed to 415 bar show changes in properties of a magnitude comparable to that observed in the samples aged at 55 bar. In contrast, the samples exposed to 482 retain a material relaxation and cavity area fraction closer to that observed in the baseline conditions for the material. Nevertheless, the effects of the increased pressure gradient cause a change in tensile strength and the mean cavity size. Figure 72 shows a summary of the changes observed for the EPDM material investigated as a function of the aging pressure.

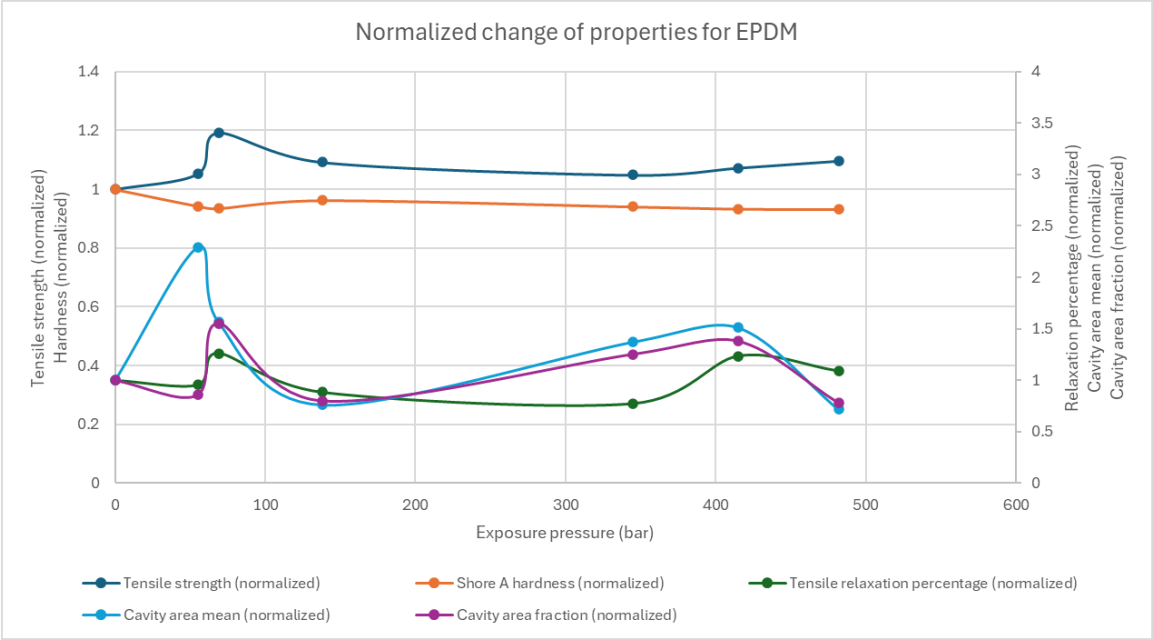


Figure 72: Summary of changes measured for EPDM material as a function of aging pressure.

Various observations were made through the analysis and comparison of the effects of hydrogen gas exposure across a wide range of pressures. The materials investigated displayed significant changes when exposed to hydrogen gas at relatively low pressures of 55 bar and 69 bar. In contrast, an exposure pressure of 138 bar had less noticeable effects on the three materials tested. In this case, the non-monotonic nature of the changes in mechanical properties along with the observed changes in material morphology were highlighted. Furthermore, by relating changes in mechanical properties to the presence of material defects, this study contributes a unique perspective that allows for understanding of the competing effects of plasticization due to hydrogen dissolution and the internal stresses generated by the pressure gradient that restrict the mobility of the polymer matrix. In this way, this study contributes to the understanding of material compatibility with hydrogen gas.

Objective 4: Investigate the differences in the presentation of hydrogen induced material degradation on different materials exposed to identical conditions

The data collected in this study were also used to compare the performance of the polymer-based materials following the characterization of changes. To facilitate the comparison among materials with different properties and characteristics, the mechanical and morphological properties of the samples exposed to hydrogen gas were normalized with respect to the baseline conditions for each material. In this way, this study allows for a comparison of material degradation as a result of hydrogen induced aging and rapid gas decompression under identical conditions. In this regard, Table 6 and Table 7 present a ranked comparison of the changes observed for each of the characterization methods utilized. In this case, the materials were ranked based on the percentage of deviation from the baseline conditions for the different properties analyzed. The material with the least change was ranked as ‘good’ while the material with the most deviation was labelled ‘bad’. The material ranking was divided into two distinct categories according to exposure pressure: Low pressure (55 bar, 69 bar, 138 bar) and high pressure (345 bar, 415 bar, 482 bar) to account for the changes in behavior at different pressure levels. From this ranking we can observe that for low pressure applications the most suitable material is NBR as it is able to retain its properties after exposure to hydrogen gas to a greater extent that the other two materials. Similarly, the FKM material investigated displayed the greatest deviation from baseline conditions at the low aging pressures. In contrast, for the samples exposed to high-pressure the materials show more variability regarding their ability to retain properties. In this case, the three materials show a mixture of positive and negative changes as a result of interactions with hydrogen.

Table 6: Comparison of the performance of materials exposed to low pressure

Low pressure

Material	Tensile strength	Material relaxation	Material hardness	Cavity size	Cavity coverage
FKM	Bad	Bad	Mid	Bad	Bad
NBR	Mid	Good	Good	Good	Good
EPDM	Good	Mid	Bad	Mid	Mid

Table 7: Comparison of the performance of materials exposed to high pressure

High pressure

Material	Tensile strength	Material relaxation	Material hardness	Cavity size	Cavity coverage
FKM	Bad	Good	Mid	Mid	Bad
NBR	Good	Mid	Good	Bad	Mid
EPDM	Mid	Bad	Bad	Good	Good

As described in Chapter 3, each of the materials selected has a distinct molecular structure with specific characteristics that grant them different advantages and disadvantages for operation with hydrogen gas. Additionally, commercially available, general use polymers were selected for this study in order to reflect real world components and applications. Hence, the properties of the materials utilized in this investigation were enhanced through the use of filler particles and additives. These materials have been developed for use in industrial applications over many years of research to develop compounds that are able to fulfil technological needs in a cost effective and reliable manner. In this way, the results of this research present information that can be applied in practical scenarios. Furthermore,

by comparing three different materials, this research contributes a useful perspective for material selection and component development that can be employed in industrial and scientific applications.

5.2 Limitations and future work

While important information about the effects of exposure to pressurized hydrogen gas on polymers has been successfully obtained, several areas of improvement have been identified through the completion of this investigation. Hence, the following section describes the limitations encountered as well as recommendations on research that could be pertinent to addressing knowledge gaps to enhance the long-term viability of hydrogen systems.

The experimental system used for the exposure of material samples to hydrogen environment was successful in creating the aging conditions necessary for this study. Nevertheless, several limitations were introduced by the design of the system as well as other factors. In this case, the range of pressure employed in this research provides a comprehensive range as it pertains to different applications such as low-pressure pipelines to high pressure storage tanks. Nevertheless, limitations in time and the cost of hydrogen gas meant that multiple gaps within this range were not investigated. The non-monotonic nature of the changes observed means that investigating more pressure levels could yield important information regarding changes to the materials. Furthermore, by investigating higher pressures it would be possible to address understand how the competing effects of the pressure gradient and the plasticization of the polymer matrix due to hydrogen infiltration evolve. Similarly, the exposure period employed in this study follows the example of other researchers as well as theoretical calculations to ensure that the martial samples were affected by hydrogen assisted degradation. Nevertheless, further investigation is necessary to understand how these changes progress over time. In this regard, it would be useful to investigate the effects of exposure to hydrogen for different durations. This would be important for determining the viability of polymer for long-term applications. Additionally, by understanding how material degradation progresses over a long period of time, it would be possible to predict the service life of components, providing recommendations for preventive maintenance practices and enhancing the reliability and safety of hydrogen systems. In contrast, by studying hydrogen induced material degradation over shorter periods of time it would be possible to understand the sequence of structural and chemical changes that eventually cause the degradation of mechanical properties. Lastly, the results of this study do

not reflect the temperature-dependent changes to materials that arise from interactions with hydrogen. While the aging system had the capacity to test over a range of temperatures, this capability was not employed. Hence, the introduction of different temperatures to the experimental matrix would yield important information about the mechanisms involved in material degradation. In this regard, further investigation regarding the interactions between polymer materials and hydrogen is necessary in order to fully understand the underling mechanisms and develop materials with adequate properties.

Additionally, the equipment used for the characterization of the material samples also introduced a unique set of constraints. In this case, the machine used for the tensile analysis of the O-ring samples was constructed according to establish industrial practices and standards. Furthermore, the design of this equipment allowed for different types of tests to be performed on the material samples. However, the utilization of a load cell with a range closer to the forces observed would provide results with higher accuracy. Similarly, by employing a higher frequency for data collection it would be possible to identify changes in the relaxation behavior that this research might have overlooked. Following this, the microscope used for the characterization of material morphology was able to provide useful images and measurements of the defects in the material samples. Nevertheless, limitations in time and availability of the equipment meant that a limited amount of specimens were analyzed. Additionally, by imaging only slices of the O-ring samples, it was impossible to know the volume of the cavities. In this way, the use of micro-tomography to characterize the changes to material morphology would be beneficial. This technology employs radiation to generate a volumetric scan of the material, making it possible to quantify the total number of defects through the material samples rather than a few characteristic slices. Similarly, the computational methods employed in this analysis were limited to well established, basic processing methods. While these methods are reliable and relatively easy to implement, they tend to be slow and involve extensive steps that must be taken with care to prevent influencing the results. In this case, the use machine learning and artificial intelligence would result beneficial in shortening the time required, thus allowing for other types of analysis.

REFERENCES

[1] R. R. Kaur and A. Luthra, "Population growth, urbanization and electricity - Challenges and initiatives in the state of Punjab, India.," *Energy Strategy Reviews,* vol. 21, pp. 50-61, 2018.

[2] A. G. Nitivattananon, V. Abbas and M. Sabir, "Green waste to biogas: Renewable energy possibilities for Thailand's green markets.," *Renewable and Sustainable Energy Reviews,* vol. 16, no. 7, pp. 5423-5429, 2012.

[3] I. D. Williams and B. Michael, "Autogeddon or autoheaven: Environmental and social effects of the automotive industry from launch to present," *Science of The Total Environment,* vol. 858, no. 3, 2023.

[4] N. Kapilan, K. Nithin and K. Chiranth, "Challenges and opportunities in solar photovoltaic system," *Materials Today: Proceedings,* vol. 62, no. 6, pp. 3538-3543, 2022.

[5] A. Olabi, E. Khaled, O. Khaled, A. A. Mohammad, R. Hegazy, W. Tabbi, M. M. Hussein and T. S. Enas, "Renewable energy systems: Comparisons, challenges and barriers, sustainability indicators, and the contribution to UN sustainable development goals," *International Journal of Thermofluids,,* vol. 20, no. 100498, 2023.

[6] M. MOMIRLAN and T. VEZIROGLU, "The properties of hydrogen as fuel tomorrow in sustainable energy system for a cleaner planet.," *International Journal of Hydrogen Energy,* vol. 30, no. 7, pp. 795-802, 2005.

[7] R. R. Barth, K. L. Simmons and C. W. San Marchi, "Polymers for hydrogen infrastructure and vehicle fuel systems," *United States,* p. https://doi.org/10.2172/1104755, 2013.

[8] A. Leon, Hydrogen Technology, 10.1007/978-3-540-69925-5., 2008.

[9] W. Balasooriya, C. Clute, B. Schrittesser and G. Pinter, "A Review on Applicability, Limitations, and Improvements of Polymeric Materials in High-Pressure Hydrogen Gas Atmospheres.," *Polymer Reviews,* no. doi:10.1080/15583724.2021.1897997, pp. 1-36, 2021.

[10] M. Hasankhani, J. v. Engelen, S. Celik and J. C. Diehl, "Unveiling complexity of hydrogen integration: A multi-faceted exploration of challenges in the Dutch context," *Journal of Cleaner Production,* vol. 434, no. 139927, 2024.

[11] Koohi-Fayegh, M. A. Rosen and Seama, "The prospects for hydrogen as an energy carrier: an overview of hydrogen energy and hydrogen energy systems," *Energy, Ecology and Environment,* vol. 1, no. 1, pp. 10-29, 2016.

[12] F. Ustolin, N. Paltrinieri and F. Berto, "Loss of integrity of hydrogen technologies: A critical review," *International Journal Of Hydrogen Energy,* vol. 45, no. 43, pp. 23809-23840, 2020.

[13] L. Thibaut, K. Maroua, S. Quentin and R. Aurore, "Biomass-to-hydrogen: A review of main routes production, processes evaluation and techno-economical assessment," *Biomass and Bioenergy,* vol. 144, no. 105920, 2021.

[14] E. Norman, V. Maestre, A. Ortiz and I. Ortiz, "Steam electrolysis for green hydrogen generation. State of the art and research perspective," *Renewable and Sustainable Energy Reviews,* vol. 202, 2024.

[15] J. Z. Guo, Y. hu, Z. Zheng, C. Mao, J. Jaroniec, M. Qiao and T. Shizhang Ling, "Direct seawater electrolysis by adjusting the local reaction environment of a catalyst.," *Nature Energy,* vol. 8, pp. 1-9, 2023.

[16] S. Satyapal, J. Petrovic, C. Read, G. Thomas and G. Ordaz, "The U.S. Department of Energy's National Hydrogen Storage Project: Progress towards meeting hydrogen-powered vehicle requirements.," *Catalysis Today,* vol. 120, no. 3-4, pp. 246-256, 2007.

[17] M. S. Abdellatif, Z. H. Raad, K. H. Ahmed, T. Hussein, M. Armin, F. I. Haytham, R. P. Amit and H. M. Amin, "Hydrogen energy systems: Technologies, trends, and future prospects," *Science of The Total Environment,,* vol. 939, no. 173622, 2024.

[18] H. Barthelemy, M. Weber and F. Barbier, "Hydrogen storage: Recent improvements and industrial perspectives," *International Journal of Hydrogen Energy,* vol. 42, no. 11, pp. 7254-7262, 2017.

[19] N. Balzani and A. Vincenzo, Energy For a Sustainable World, Wiley-VCH, 2011.

[20] Clean Energy Group, "The Drawbacks of Liquid Hydrogen," July 2025. [Online]. Available: https://www.cleanegroup.org/wp-content/uploads/Hydrogen-Liquefaction-Fact-Sheet.pdf. [Accessed 28 October 2025].

[21] M. BOUOUDINA, D. GRANT and G. WALKER, "Review on hydrogen absorbing materials—structure, microstructure, and thermodynamic properties," *International Journal of Hydrogen Energy,* vol. 31, no. 2, pp. 177-182, 2006.

[22] WHA International INC, "Top Industrial Uses of Hydrogen, and the Need for Industrial Hydrogen Safety," WHA International INC, 21 September 2023. [Online]. Available: https://wha-international.com/hydrogen-in-industry/. [Accessed 15 October 2024].

[23] O. M. Virginia, "Chart: Which countries are leading the green hydrogen race?," Canary Media, 02 February 2024. [Online]. Available: https://www.canarymedia.com/articles/hydrogen/chart-which-countries-are-leading-the-green-hydrogen-race. [Accessed 16 October 2024].

[24] Z. Fu, L. Lu, C. Zhang, Q. Xu, X. Zhang, Z. Gao and J. Li, "Fuel cell and hydrogen in maritime application: A review on aspects of technology, cost and regulations," *Sustainable Energy Technologies and Assessments,* vol. 57, no. 103181, 2023.

[25] V. Nguyen and L. Blum, "5 - Reversible fuel cells," in *Compendium of Hydrogen Energy*, Woodhead Publishing, 2016, pp. 115-145.

[26] S. Manpreet, S. Manish, K. Safaraliev, M. Singh, K. Odinaev, I. Menaem and A. Abdel, "Advancements and challenges of fuel cell integration in electric vehicles: A comprehensive analysis," *International Journal of Hydrogen Energy,* vol. 88, pp. 1386-1397, 2024.

[27] M. A. Habib, G. A. Abdulrahman, A. B. Alquaity and N. A. Qasem, "Hydrogen combustion, production, and applications: A review," *Alexandria Engineering Journal,* vol. 100, pp. 182-207, 2024.

[28] A. Campari, F. Ustolin, A. Alvaro and N. Paltrinieri, "A review on hydrogen embrittlement and risk-based inspection of hydrogen technologies," *International Journal of Hydrogen Energy,* vol. 48, pp. 35316-35346, 2023.

[29] B. Schrittesser, G. Pinter, T. Schwarz, Z. Kadar and T. Nagy, "Rapid Gas Decompression Performance of elastomers - A study of influencing testing parameters," *Procedia Structural Integrity,* vol. 2, pp. 1774-1754, 2016.

[30] M. G. Gado, "Green hydrogen: A key energy carrier replacing fossil fuels across multiple sectors," *Renewable and Sustainable Energy Reviews,* vol. 230, no. 116683, 2026.

[31] R. Dutton, "Materials degradation problems in hydrogen energy systems," *International Journal of Hydrogen Energy,* vol. 9, no. 1-2, pp. 147-155, 1984.

[32] A. Ishkov, O. Zhdaneev, K. Romanov, E. Koloshkin, S. Nastich, V. Egorov, A. Arabey, A. Mikhalev and V. Lopatkin, "Hydrogen degradation of materials and changes in the operation mode of compressor station equipment as factors of increased risks and costs during transportation of hydrogen-containing gas through main gas pipelines," *International Journal of Hydrogen Energy,* vol. 130, pp. 147-155, 2025.

[33] A. Islam, T. Alam, N. Sheibley, K. Edmonson, D. Burns and M. Hernandez, "Hydrogen blending in natural gas pipelines: A comprehensive review of material compatibility and safety considerations," *International Journal of Hydrogen Energy,* vol. 93, pp. 1429-1461, 2024.

[34] S. Dong-Ho and K. Seong-Jong, "Effect of hydrogen charging on the wear resistance of CrN-coated Al alloy for hydrogen valve of fuel cell electric vehicles,," *International Journal of Hydrogen Energy,* vol. 89, pp. 279-292, 2024.

[35] H. Zakaria, V. Robin, T. Finger, D. Christian, G. Bjarnhéðinn, C. D. Augusto, A. Tariq and N. J. Arackal, "A comprehensive review on the compatibility of polymeric materials for hydrogen transportation and storage," *International Journal of Hydrogen Energy,* vol. 192, 2025.

[36] G. Jia, M. Lei, M. Li, W. Xu, R. Li, Y. Lu and M. Cai, "Hydrogen embrittlement in hydrogen-blended natural gas transportation systems: A review," *International Journal of Hydrogen Energy,* vol. 48, no. 82, pp. 32137-32157, 2023.

[37] S. Castagnet, J.-C. Grandidier, M. Comyn and G. Benoît, "Effect of long-term hydrogen exposure on the mechanical properties of polymers used for pipes and tested in pressurized hydrogen," *International Journal of Pressure Vessels and Piping,* vol. 89, pp. 203-209, 2012.

[38] H. Kotake, R. Matsumoto, S. Taketomi and N. Miyazaki, "Transient hydrogen diffusion analyses coupled with crack-tip plasticity under cyclic loading," *International Journal of Pressure Vessels and Piping,* vol. 85, no. 8, pp. 540-549, 2008.

[39] G. Xiaoming, C. Honghao, Z. Chilou, X. Caiyi, P. Wei, Z. Tao, M. Jinkun, L. Hongpeng, Z. Yimeng and C. Guohua, "A review of safety risk management strategies for hydrogen refueling stations," *Renewable and Sustainable Energy Reviews,* vol. 226, no. Part B, 2026.

[40] R. Alfasfos, J. Sillman and R. Soukka, "Lessons learned and recommendations from analysis of hydrogen incidents and accidents to support risk assessment for the hydrogen economy," *International Journal of Hydrogen Energy,* vol. 60, pp. 1203-1214, 2024.

[41] H. Wang, Z. Tong, G. Zhou, C. Zhang, H. Zhou, Y. Wang and W. Zheng, "Research and demonstration on hydrogen compatibility of pipelines: a review of current status and challenges," *International Journal of Hydrogen Energy,* vol. 47, no. 66, pp. 28585-28604, 2022.

[42] C. López, S. Pacheco-Álvarez and A. Jaques, "Prediction of permeation-related hydrogen losses in pipelines based on machine learning," *Energy Reports,* vol. 13, pp. 5266-5280, 2025.

[43] M. H. Klopffer and B. Flaconneche, "Transport Properties of Gases in Polymers: Bibliographic Review," *Oil & Gas Science and Technology,* vol. 56, no. 3, pp. 223-244, 2001.

[44] E. H. Daniel and L. C. Stuart, "Chapter I.2.2 - Polymers: Basic Principles," in *Biomaterials Science (Third Edition)*, Academic Press, 2013, pp. 64-79.

[45] R. M. Barrer, "Some Properties of Diffusion Coefficients in Polymers," *The Journal of Physical Chemistry,* vol. 61, no. 2, pp. 178-189, 1957.

[46] R. J. Pace and A. Datyner, "Statistical mechanical model of sorption and diffusion of simple penetrants in polymers," *Polymer Engineering & Science,* vol. 20, no. 1, pp. 51-58, 1980.

[47] R. Yadav, M. Singh, D. Shekhawat, S.-Y. Lee and S.-J. Park, "The role of fillers to enhance the mechanical, thermal, and wear characteristics of polymer composite materials: A review," *Composites Part A: Applied Science and Manufacturing,* vol. 175, no. 107775, 2023.

[48] J. Jung, C. Lee, U. Baek, M. Choi and J. Bae, "Filler Influence on H2 Permeation Properties in Sulfur-CrossLinked Ethylene Propylene Diene Monomer Polymers Blended with Different Concentrations of Carbon Black and Silica Fillers," *Polymers,* vol. 14, no. 3, p. 592, 2022.

[49] J. Jung, C. Lee, M. Son, J. Lee, U. Baek, K. Chung, M. Choi and J. Bae, "Filler Effects on H2 Diffusion Behavior in Nitrile Butadiene Rubber Blended with Carbon Black and Silica Fillers of Different Concentrations," *Polymers,* vol. 14, no. 4, p. 700, 2022.

[50] C. Zhou, L. Xianhui, Z. Yiran and H. Zhengli, "A comprehensive review of hydrogen-induced swelling in rubber composites," *Composites Part B: Engineering,* vol. 275, no. 111342, pp. 1359-8368, 2024.

[51] J. Yamabe and S. Nishimura, "20 - Hydrogen-induced degradation of rubber seals, Volume 2," in *Gaseous Hydrogen Embrittlement of Materials in Energy Technologies*, Woodhead Publishing, 2012, pp. 769-816.

[52] R. A. Middaugh and C. A. Goudey, "The dimensional change of polymers under high hydrostatic pressure," *Proceedings of OCEANS '93,* vol. 1, pp. I149-I154, 1993.

[53] J. K. Jung, I. G. Kim, S. K. Jeon, K.-T. Kim, U. B. Baek and S. H. Nahm, "Volumetric analysis technique for analyzing the transport properties of hydrogen gas in cylindrical-shaped rubbery polymers," *Polymer Testing,* vol. 99, no. 107147, 2021.

[54] X. Lei, X. Jin and K. D. Prodip, "Chapter 2 - Fuel cell fundamentals," in *Fuel Cells for Transportation*, Woodhead Publishing, 2023, pp. 29-72.

[55] M. Okumuş, F. Janssen and Ł. Figiel, "Modelling and experimental study of hydrogen permeation in polymer composites: Effects of fibre agglomeration and orientation," *Composites Part A: Applied Science and Manufacturing,* vol. 199, no. 109213, 2025.

[56] G. Theiler, N. C. Murillo, K. Halder, W. Balasooriya, A. Hausberger and A. Kaiser, "Effect of high-pressure hydrogen environment on the physical and mechanical properties of elastomers,," *International Journal of Hydrogen Energy,,* vol. 58, pp. 389-399, 2024.

[57] The U.S. Department of Energy, , "Hydrogen program plan," The U.S. Department of Energy, 2024.

[58] W. Kuang, B. Arey, A. Dohnalkova, L. Kovarik, B. Mills, N. Menon, R. Seffens and K. Simmons, "Multi-scale imaging of high-pressure hydrogen induced damage in EPDM rubber using X-ray microcomputed tomography, helium-ion microscopy and transmission electron microscopy," *International Journal of Hydrogen Energy,* vol. 48, no. 23, pp. 8573-8587, 2023.

[59] M. Yang, S. Yasin, Q. Chen, W. Peng, Z. Lv, Z. Qi and J. Shi, "Suppressing high pressure hydrogen blistering in NBR via Zn-based MOF vulcanization: Microstructural and mechanical insights," *International Journal of Hydrogen Energy,* vol. 181, no. 151810, pp. 0360-3199, 2025.

[60] U.S. Department of Energy, "Physical Hydrogen Storage," U.S. Department of Energy, [Online]. Available: https://www.energy.gov/eere/fuelcells/physical-hydrogen-storage. [Accessed 20 Jan 2026].

[61] Office of Energy Efficiency & Renewable Energy, "Hydrogen Storage," [Online]. Available: https://www.energy.gov/eere/fuelcells/hydrogen-storage. [Accessed 15 August 2024].

[62] H. Li, X. Cao, Y. Liu, Y. Shao, Z. Nan, L. Teng, W. Peng and J. Bian, "Safety of hydrogen storage and transportation: An overview on mechanisms, techniques, and challenges," *Energy Reports,* vol. 8, pp. 6258-6269, 2022.

[63] R. P. Gangloff and B. P. Somerday, Gaseous Hydrogen Embrittlement of Materials in Energy Technologies, Elsevier, 2016.

[64] Z. Jin, Y. Su, L. Hong, M. Liu, W. Li and C. Zhang, "Review of Decompression Damage of the Polymer Liner of the Type IV Hydrogen Storage Tank," *Polymers,* vol. 15, no. 10, p. 2258, 2023.

[65] S. Kulkarni, C. K., W. Kuang, N. Menon, B. Mills, A. Soulami and K. Simmons, "Damage evolution in polymer due to exposure to high-pressure hydrogen gas," *International Journal of Hydrogen Energy,* vol. 46, no. 36, pp. 19001-19022, 2021.

[66] B. Gentilleau, M. Bertin, F. Touchard and J.-C. Grandidier, "Stress analysis in specimens made of multi-layer polymer/composite used for hydrogen storage application: Comparison with experimental results.," *Composite Structures,* vol. 93, no. 11, pp. 2760-2767, 2011.

[67] M. Zaghdoudi, A. Kömmling, M. Böhning and M. Jaunich, "Ageing of elastomers in air and in hydrogen environment: A comparative study," *International Journal of Hydrogen Energy,* vol. 63, pp. 207-216, 2024.

[68] F. Zhang, R. Yang and a. D. Lu, "Investigation of Polymer Aging Mechanisms Using Molecular Simulations: A Review," *Polymers,* vol. 15, no. 8, p. 1928, 2023.

[69] S. A. Ghafri, "Hydrogen liquefaction: A review of the fundamental physics, engineering practice and future opportunities," *Energy & Environmental Science,* vol. 15, pp. 2690-2731, 2022.

[70] A. Züttel, "Materials for hydrogen storage," *Materials Today,* vol. 6, no. 9, pp. 24-33, 2003.

[71] W. Vielstich, A. Lamm and H. A. Gasteiger, Handbook of Fuel Cells: Fundamentals, Technology, Applications, Wiley, 2003.

[72] R. Grenoble and T. Gates, "Hydrogen Permeability of Polymer Matrix Composites at Cryogenic Temperatures," *American Institute of Aeronautics and Astronautics.*

[73] Fraunhofer IFAM, "Solid Hydrogen Carriers," *White paper,* 2024.

[74] T. Tian, W. Xuansheng, S. Keke, L. Fang, W. Jiali, Z. Xiaoying, L. Shengting, C. Wei, S. Yufei, L. Jinping and L. Guang, "Boosting hydrogen storage performance of MgH2 by efficient V2O3/C catalyst," *Journal of Alloys and Compounds,* vol. 1010, no. 178333, 2025.

[75] J. F. Stampfer, C. E. Holley and J. F. Suttle, "The Magnesium-Hydrogen System," *Journal of the American Chemical Society,* vol. 82, no. 14, pp. 3504-3508, 1960.

[76] Y. Shang, C. Pistidda, G. Gizer, T. Klassen and M. Dornheim, "Mg-based materials for hydrogen storage," *Journal of Magnesium and Alloys,* vol. 9, no. 6, pp. 1837-1860, 2021.

[77] M. Alfè and D. Pozzo, "Hydrogen dissociation and diffusion on transition metal (=Ti, Zr, V, Fe, Ru, Co, Rh, Ni, Pd, Cu, Ag)-doped Mg(0001) surfaces," *International Journal of Hydrogen Energy,* vol. 34, no. 4, pp. 1922-1930, 2009.

[78] N. Eliaz and D. Eliezer, "An Overview of Hydrogen Interaction with Amorphous Alloys.," *Advanced Performance Materials,* vol. 6, pp. 5-31, 1999.

[79] N. Yang, J. Deng, C. Wang, Z. Bai and J. Qu, "High pressure hydrogen leakage diffusion: Research progress," *International Journal Of Hydrogen Energy,* vol. 50, no. A, pp. 1029-1046, 2024.

[80] Evolvedh20, "Molecular Hydrogen Size, Comparisson, and Scientific Insights," Evolvedh20, 08 February 2025. [Online]. Available: https://evolvedh2o.com/blogs/news/how-big-is-molecular-hydrogen. [Accessed 25 October 2025].

[81] Ministry of Education Government of India, "Hydrogen," Sathee, [Online]. Available: https://sathee.iitk.ac.in/article/chemistry/hydrogen/. [Accessed 25 October 2025].

[82] M. L. Martin and Petros Sofronis, "Hydrogen-induced cracking and blistering in steels: A review,," *Journal of Natural Gas Science and Engineering,,* vol. 101, no. 104547, 2022.

[83] W. H. Johnson, "On Some Remarkable Changes Produced in Iron and Steel by the Action of Hydrogen," *Proceedings of the Royal Society of London,* vol. 23, pp. 168-179, 1874.

[84] R. Hren, A. Vujanović, Y. V. Fan, J. J. Klemeš, D. Krajnc and L. Čuček, "Hydrogen production, storage and transport for renewable energy and chemicals: An environmental footprint assessment," *Renewable and Sustainable Energy Reviews,* vol. 173, no. 113113, 2023.

[85] M. Dadfarnia, P. Novak, C. Ahn, J. Liu, P. Sofronis, D. D. Johnson and I. M. Robertson, "Recent Advances in the Study of Structural Materials Compatibility with Hydrogen.," *Advanced Materials,* vol. 22, no. 10, pp. 1128-1135, 2010.

[86] H. Wipf, Hydrogen in Metals III, Properties and Applications, Springer-Verlag Berlin, 2014.

[87] H. k. D. H. Bhadeshia, "Prevention of Hydrogen Embrittlement in Steels," *ISIJ International,* vol. 56, pp. 24-36, 2016.

[88] V. R. Dominick, V. R. Donald and V. R. Matthew, "2 - Plastic Property," in *Plastic Product Material and Process Selection Handbook*, Elsevier, 2004, pp. 40-129.

[89] Morand Lambla, "21 - Reactive Processing of Thermoplastic Polymers," in *Comprehensive Polymer Science and Supplements*, Pergamon, 1989, pp. 619-642.

[90] M. M. H. Bhuiyan, N. Subedi and Z. Siddique, "Material compatibility in hydrogen infrastructure: Challenges, advances, and future prospects," *International Journal of Hydrogen Energy,,* vol. 190, no. 152138, 2025.

[91] K. Friedrich, "Polymer composites for tribological applications," *Advanced Industrial and Engineering Polymer Research,* vol. 1, no. 1, pp. 3-39, 2018.

[92] S. S. Kulkarni, Y. Shin, K. S. Choi and K. Simmons, "Investigation of desorption of hydrogen gas from polymer matrix using thermal desorption analysis and finite element modeling," *Polymer,* vol. 282, no. 126182, 2023.

[93] N. C. Menon, A. M. Kruizenga, K. J. Alvine, C. San Marchi, A. Nissen and K. Brooks, "Volume 6B: Materials and Fabrication," in *Behaviour of Polymers in High Pressure Environments as Applicable to the Hydrogen Infrastructure*, 2016.

[94] A. N. Gent, Engineering with Rubber: How to Design Rubber Components, Hanser, 2001.

[95] G. Kwatia, C. Ezeakacha and S. Salehi, "LITERATURE REPORT OF ELASTOMER SEALING MATERIALS AND CEMENT," University of Oklahoma, Norman, 2017.

[96] M. A. Wilson and A. L. Frischknecht, "High-pressure hydrogen decompression in sulfur crosslinked elastomers," *International Journal of Hydrogen Energy,* vol. 47, no. 33, 2022.

[97] S. Bohlul and M. Alimardani, "Revisiting the mechanism of rapid gas decompression failure in silica-reinforced NBR composites: Effect of interfacial phenomena," *Composites Communications,* vol. 50, no. 102009, 2024.

[98] Z. Major and W. Lang, "Characterization of the fracture behavior of NBR and FKM grade elastomers for oilfield applications.," *Engineering Failure Analysis,* vol. 17, no. 3, pp. 701-711, 2010.

[99] D. M. Hill, "Degradation of elastomers," in *Latex Dipping: Science and Technology*, Boston, De Gruyter, 2019, pp. 73-78.

[100] E. Boersheim, R. Clemens, V. Albrecht, D. Pudlo and D. L. Ganzer., "Experimental Investigation of Integrity Issues of UGS Containing Hydrogen," *Paper presented at the SPE Europec featured at 81st EAGE Conference and Exhibition,* 2019.

[101] A. Kömmling, M. Jaunich, M. Goral and D. Wolff, "Insights for lifetime predictions of O-ring seals from five-year long-term aging tests," *Polymer Degradation and Stability,* vol. 179, no. 109278, 2020.

[102] V. C. Chandrasekaran, "Rubber Properties for Functional Seal Requirements," in *Rubber Seals for Fluid and Hydraulic Systems*, Elsevier, 2010, pp. 7-22.

[103] M. B. Djukic, S. Zeravcic, V. Bakic, A. Sedmak and B. Rajicic, "Hydrogen damage of steels: A case study and hydrogen embrittlement model.," *Engineering Failure Analysis,* vol. 58, pp. 485-498, 2015.

[104] Y. Katz, N. Tymiak and W. W. Gerberich, "Nanomechanical probes as new approaches to hydrogen/deformation interaction studies," *Engineering Fracture Mechanics,* vol. 6, no. 68, p. 619–646, 2001.

[105] CHMC CSA ANSI, ""CHMC 2-19; Test Methods for Evaluating Material Compatibility in Compressed Hydrogen Applications Polymers," CSA Gas Standards (CSA/AM), Toronto, Canada, 2019.

[106] F. Hirotada, O. Hiroaki and N. Shin, "Degradation behavior of acrylonitrile butadiene rubber after cyclic high-pressure hydrogen exposure," *International Journal of Hydrogen Energy,* vol. 40, no. 4, pp. 2025-2034, 2015.

[107] T. Sreethu and N. Kinsuk, "Zinc oxide with various surface characteristics and its role on mechanical properties, cure-characteristics, and morphological analysis of natural rubber/carbon black composites," *Journal of Polymer Research,* vol. 28, no. 183, 2021.

[108] A. Coran, "Chapter 7 - Vulcanization," in *The Science and Technology of Rubber (Fourth Edition)*, Academic Press, 2013, pp. 337-381.

[109] K. Klajn, T. Gozdek and D. Bieliński, "Metal Organic Frameworks: Current State and Analysis of Their Use as Modifiers of the Vulcanization Process and Properties of Rubber," *Materials,* vol. 16, no. 7631, 2023.

[110] J. Li, B. Song and J. Kwon, "A Cycle Analysis of Flow and Thermal Parameters in the Hydrogen Charging System at the Pressure of 50 MPa," *Machines,* vol. 10, no. 461, 2022.

[111] Eriks Sealing Elements, , "o-ring info datasheets," 01 09 2006. [Online]. Available: https://o-ring.info/en/datasheets/viton/ERIKS%20-%20FKM514625.pdf. [Accessed 24 01 2026].

[112] Y. Shin, W. Kuang and K. L. Simmons, "Network stability of FKM rubber compounds under hydrogen pressure," *AIP Conference proceedings,* vol. 2884, no. 1, 2023.

[113] S. T. Semegen, "Rubber, Synthetic," in *Encyclopedia of Physical Science and Technology (Third Edition)*, Academic Press, 203, pp. 395-405.

[114] The American Society for Testing Materials International, "ASTM D2000-24 Standard Classification System for Rubber Products in Automotive Applications," ASTM International, West Conshohocken, PA, 2024.

[115] C. Chellappa, "9 - Rubber Lining for Nuclear Equipment," in *In Plastics Design Library, Anticorrosive Rubber Lining*, William Andrew Publishing, 2017, pp. 67-72.

[116] M. Liu, H. McDonald, A. Wallwork, G. Wilson, M. A. Bissett, I. A. Kinloch and L. Chen, "High-performance EPDM elastomer nanocomposites reinforced by graphene nanoplatelets for sealing applications against SF6(g) emissions," *Composites Part B: Engineering,* vol. 311, no. 113231, 2026.

[117] Parker O-Ring & Engineered Seals Division (OES) North America, "Evaluation of Parker Compound E0603-70," [Online]. Available: https://www.parker.com/content/dam/Parker-com/Literature/O-Ring-Division-Literature/e0603.pdf. [Accessed 26 01 2026].

[118] H. J. Fabris and W. G. Knauss, "5 - Synthetic Polymer Adhesives," in *Comprehensive Polymer Science and Supplements*, Pergamon, 1989, pp. 131-177.

[119] T. Yasin, S. Ahmed, F. Yoshii and K. Makuuchi, "Effect of acrylonitrile content on physical properties of electron beam irradiated acrylonitrile–butadiene rubber," *Reactive and Functional Polymers,* vol. 57, no. 2-3, pp. 113-118, 2003.

[120] H. Ono, H. Fujiwara and S. Nishimura, "Penetrated hydrogen content and volume inflation in unfilled NBR exposed to high-pressure hydrogen–What are the characteristics of unfilled-NBR dominating them?," *International Journal of Hydrogen Energy,,* vol. 43, no. 39, pp. 18392-18402, 2018.

[121] ERIKS sealing elements, "EPDM 75-compound 559187 Vulc-O-Ring - technical Data Sheet," ERIKS sealing elements, 2010.

[122] M seals, "NBR-B75 75a Soft Nitrile Butadiene Rubber MATERIAL DATA SHEET (Version 6.0 – 05.2022)," M seals-part of Diploma PLC, 2022.

[123] Polymax, "FKM (Viton) 75 ShA".

[124] F. Pérez-Ràfols, R. Larsson and A. Almqvist, "Modelling of leakage on metal-to-metal seals," *Tribology International,* vol. 94, pp. 421-427, 2016.

[125] ASTM International, "Standard Test Methods for Rubber O-Rings, ASTM Standard D1414-22," ASTM International, West Conshohocken, PA, 2022.

[126] ASTM International, "Standard test method for rubber property—durometer hardness (ASTM D2240-15R21)," ASTM International, West Conshohocken, PA, 2021.